Spring 2022

Mining-Contaminated Sediment and Metal Storage in Channel Deposits in Turkey Creek, Tri-State Mining District, Missouri and Kansas

Max Quinn Hillermann
Missouri State University, Hillermann573@live.missouristate.edu

MINING-CONTAMINATED SEDIMENT AND METAL STORAGE IN CHANNEL DEPOSITS IN TURKEY CREEK, TRI-STATE MINING DISTRICT, MISSOURI AND KANSAS

A Master's Thesis

Presented to

The Graduate College of

Missouri State University

In Partial Fulfillment

Of the Requirements for the Degree

Master of Science, Geography and Geology

By

Max Hillermann

May 2022

MINING-CONTAMINATED SEDIMENT AND METAL STORAGE IN CHANNEL DEPOSITS IN TURKEY CREEK, TRI-STATE MINING DISTRICT, MISSOURI AND KANSAS

Geography, Geology and Planning

Missouri State University, May 2022

Master of Science, Geography and Geology

Max Hillermann

ABSTRACT

The Joplin subdistrict, within the Tri-State Mining District (TSMD), was a major producer of lead (Pb) and zinc (Zn) ore between the 1880s to 1920s. Metalliferous mining wastes are still stored in the channel deposits of local streams raising environmental and health concerns. This study quantifies the volume, sediment size, and metal concentrations in channel bed, bar, bench, and chute deposits to quantify the spatial variability of contaminated sediment storage in Turkey Creek (119 km^2). Sample reaches (n=14) contained metal concentrations elevated above the Tri-State Mining District specific probable effects concentration at every site with mean concentrations in fine sediment (<2 mm) ranging from 229 to 996 mg kg^{-1} Pb and 4,946 to 5,819 mg kg^{-1} Zn. Mean concentrations in powdered coarse sediments (2 – 16 mm) ranged from 60 to 86 mg kg^{-1} Pb and 1,660 to 2,488 mg kg^{-1} Zn. Metal contamination levels were typically highest in the fine sediment fraction with the greatest metal concentrations observed near mining impaired sites. Regression modeling using distance downstream estimated that 127,000 kg Pb and 2,160,000 kg Zn are stored within a 18.8 km main channel segment of Turkey Creek. Fine sediment represented only 19% of in-channel sediment but stored the greatest mass of metal for both Pb and Zn representing 61% and 52% of total metal storage, respectively. Bar deposits stored the most Pb (69%) and Zn (74%).Volumetric storage of contaminated sediment (m^3/m channel length) was positively related to active channel width (R^2 = 0.97), bankfull width (R^2 = 0.96), distance downstream (R^2 = 0.74), slope (R^2 = 0.70), average bed depth (R^2 = 0.68), and drainage area (R^2 = 0.83). These geomorphic variables can be used to estimate the total sediment volume and mass as well as metal mass by reach for Turkey Creek. Metal concentrations and storage rates are still relatively high below remediated mine sites in the main channel and some tributaries.

KEYWORDS: mining contamination, Tri-State Mining District, sediment storage, metal storage, lead, zinc

MINING-CONTAMINATED SEDIMENT AND METAL STORAGE IN CHANNEL DEPOSITS IN TURKEY CREEK, TRI-STATE MINING DISTRICT, MISSOURI AND KANSAS

By

Max Hillermann

A Master's Thesis
Submitted to the Graduate College
Of Missouri State University
In Partial Fulfillment of the Requirements
For the Degree of Master of Science, Geography and Geology

May 2022

Approved:

Robert Pavlowsky, Ph.D., Thesis Committee Chair

Marc Owen, M.S., Committee Member

Xiaomin Qui, Ph.D., Committee Member

Julie Masterson, Ph.D., Dean of the Graduate College

ACKNOWLEDGEMENTS

I would like to thank my advisor Dr. Robert Pavlowsky for his continued support and guidance throughout this project. This thesis would not be possible without him. I would also like to thank my committee members Marc Owen and Dr. Xiaomin Qiu for their continued assistance throughout my research. More over, I would like to acknowledge the Ozarks Environmental and Water Resources Institute (OEWRI) for my research assistantship which made this research possible. My thanks also goes out to all the OEWRI members who helped me in the field including Michael Ferguson, Kayla Coonen, Shoukat Ahmed, Hannah Eades, and Brendan Ryan. I would also like to thank Steve Kemp (EPA) and Shane Cherry (HGL) who graciously gave me a tour of active remediation sites in the Tri-State Mining District.

The staff in the Department of Geography, Geology, and Planning at Missouri State were a big help to me including Deana Gibson and Tracy Carroll. I also thank Dr. Douglas Gouzie for his support with the advisement process and Dr. Toby Dogwiler for being a dedicated and inclusive department head. I would especially like to thank Dr. Melanie Carden-Jessen for being an absolute joy to work with as my supervisor during my teaching assistantship for Earth Science for Educators.

Lastly, I would like to thank for parents for their love and continued support throughout my education. Finally, I would like to thank my girlfriend, Emily Wilkinson, for her constant love and support.

TABLE OF CONTENTS

LIST OF TABLES

LIST OF FIGURES

INTRODUCTION

The effects of mining contamination on the environment are well documented throughout the world (Swennen et al., 1994; Nriagu, 1996; Lee et al., 2001). The processing of ore generates large amounts of mineral waste which typically contain high residual metal concentrations with grain sizes ranging from clay to fine-gravel (Wright, 1918). Processed wastes are stored in tailings piles and subsequently released to streams via weathering and erosion where it becomes mixed with natural channel sediments. After being deposited in channel bar deposits and floodplain soils, contaminated deposits can become secondary sources of contamination as remobilization occurs over time (Wolfenden and Lewin, 1977; Bradley and Cox, 1986; Moore et al., 1989; Walling et al., 1998; Miller and Orbock Miller, 2007; Davis, 2009). Further, contaminated sediment stored in channel deposits can pose a toxicity risk to aquatic ecology and human health (Luoma, 1983; Dickson et al., 2013). Heavy metals have lasting environmental impacts due to their long residency time in fluvial systems and the potential for uptake and bioaccumulation of toxic metals into flora and fauna (Skidmore, 1964; Beyer et al., 2004). Many studies across the world have focused on the spatial distribution and storage of contaminated mining sediment (Kim et al., 2003; Hürkamp et al., 2009; Byrne et al., 2010; Smith, 2016) while others have studied the effects of heavy metal contamination on the ecosystem (Beyer et al., 2004; Fernandes et al.; 2016; Venkateswarlu et al., 2016). This study will advance the understanding of the factors that control the spatial trends of mining metal storage in channel deposits of stream systems.

Anthropogenic changes to the landscape through mining and land clearing are commonly observed to alter the geomorphological characteristics of watersheds and the stream networks

that drain them. Mining activities generate large quantities of sediment which directly increase the sediment supply of adjacent streams as contaminated sediment enters the channel (Knighton, 1987). The combined mixture of sediments from natural and mining sources has been referred to in literature as "mining sediment" (James 2013; Pavlowsky et al., 2017). Land clearing can increase the volume and rate of surface runoff which leads to flashier floods with increased stream power that delivers more sediment to streams, increases flow energy, and forces channel adjustments (Jacobson, 1995; Jacobson and Gran, 1999; Panfil and Jacobson, 2001). Stream channels respond to these disturbances through erosion, widening, change in form, and increased sedimentation rates (Hammer, 1972; Trimble, 1983; Jacobson and Coleman, 1986; Jacobson, 1995; James and Lecce, 2013). However, streams often exhibit geomorphic features that indicate the effects of watershed disturbances (Lewin and Macklin, 1987; Jacobson, 1995; Royall et al., 2010). For example, streams with increased sediment supply often exhibit aggraded deposits that raise the bed elevation and increase the width of flood-prone areas (Knighton, 1989; Knighton, 1991; Ahmed et al., 2019). In general, channel deposits can indicate environmental changes through changes in slope, grain-size distribution, and bar size (Dietrich and Whiting, 1989; Wood-Smith and Buffington, 1996).

Sediment Storage

Once mining sediment has entered the channel, it becomes incorporated into the stream where a large contribution is stored in active channel and overbank floodplain deposits. Channel banks under stable conditions typically form to the height needed to contain the 1.5 - 2 year recurrence interval flood (Rosgen and Silvey, 1996; Simon et al., 2004; Pavlowsky et al., 2010; Owen et al., 2011). As the channel bed migrates back and forth laterally, it forms a sequence of

bars, pools, and riffles (Leopold et al., 1964). Bars form when bed material is scoured from the channel bed and deposited as higher accumulations in areas of lower velocity or flow separation (Hansen, 1967; Fujita and Muramoto, 1985). Benches, sometimes referred to as berms or shelves, are in-channel deposits that form on stable bar surfaces and are often covered to some extent by vegetation (Royall et al., 2010; Owen et al., 2011; Dean and Schmidt, 2013). They are more stable than channel bars, contain fine-grained sediment, and can represent an immature or developing floodplain. They form during periods of higher flow and remain in place for longer periods of time than bar and bed deposits (Royall et al., 2010). Chutes indicate an abandoned main channel or semi-permanent stream channel that forms due to a change in channel morphology or thalweg location in the channel or valley. The flow to chutes can be eventually cut off as they fill by progressive sedimentation. But, chutes can also remain for long periods and represent typical channel form (Figure 1) (Eekhout and Hoitink, 2015; River Studies, 2021).

Contaminated sediment is not evenly distributed and stored among various in-channel deposits. Different geomorphic features have been shown to contain varying levels of heavy metal concentrations at the same location along a stream (Graf et al., 1991; Ladd et al., 1998; Rhoads and Cahill, 1999). Local variations in metal concentrations among different channel deposits are explained by the variability in hydrologic conditions which results in the sorting of mobile sediment by size and density. For example, in-channel deposits in a low energy environment with longer residence times such as bars and benches typically contain finer sediment and higher metal concentrations. Conversely, deposits in high energy environments with shorter residence times such as channel beds typically have coarser substrate with lower metal concentrations (Whitney 1975; Chao and Theobald 1976; Tessier et al., 1982; Rhoads, 1996; Ladd et al., 1998). The floodplain can become enriched in heavy metals associated with

the finest grain sizes generated during milling as silt- and clay-sized sediments are typically deposited outside of the active channel during overbank flooding (Knox, 1987; Bradley 1989).

In-channel sediment is considered a more temporary source of stored sediment due to its high frequency of mobility compared to overbank floodplain deposits which can remain a source of secondary contamination for thousands of years (Wolfenden and Lewin, 1977; Bradley and Cox, 1986; Moore et al., 1989; Walling et al., 1998; Miller and Orbock Miller, 2007; Davis, 2009). Mining sediment is discharged directly or eroded into the streams where it becomes incorporated into the natural bed or suspended sediment. The sediment can be deposited in either in-channel features or on the floodplain (Knox 1987; Pavlowsky et al., 2017). Floodplain deposits become sinks for fine-grained contaminated sediment which vertically accretes during overbank flooding. This vertical accretion process creates stratification in the floodplain sediment with mining contaminated sediment deposited on top of undisturbed sediment (Knox, 1987). Sediment deposits on floodplains formed as a result of episodes of human activities are referred to as legacy sediment (James, 2013). Coarser sediment is often deposited in beds and bars which are less permanent than sediment stored on floodplains which are higher above the active channel bed and stored laterally across the valley floor, away from erosive flows. After mining operations have ceased for several decades the current contamination trends are controlled more by the remobilization of stored fluvial sediment rather than inputs from the primary mining sites (Bradley, 1989; Moore and Luoma, 1990; Pavlowsky et al., 2010).

Sediment Transport

Mining-contaminated sediment is transported in two distinct forms: passive dispersal and active transformation (Lewin and Macklin, 1987). Passive dispersal occurs when the mining

sediment is transported through the channel without drastically altering the channel morphology. Active transformation occurs when the geomorphological characteristics of a stream are altered by a large influx of mining sediment. An early fluvial study in the Sierra Nevada, California found that accelerated coarse sediment delivery from mining exceeded transport capacity and accumulated in the channel. This caused the bedload to initially aggrade, then degrade, and move downstream over periods of decades (Gilbert, 1917). Another study in England observed a significant change in channel morphology as a direct result of an input of sediment generated from mining activities (Lewin and Macklin, 1987). These changes in channel morphology directly alter the rate of sediment storage and dispersal of fluvial sediment (James, 1991; Gallart et al., 1999). The vast majority of Pb and Zn transport occurs in the solid particulate phase attached to sediment particles, especially in streams where acid mine drainage has not developed (Martin and Meybeck, 1979; Rhoads and Cahill, 1999). Furthermore, different metals often exhibit different transportation rates. This can be related to different geochemical behaviors, as well as differences in sediment grain size and density (Macklin and Klimek, 1992). Mining sediment containing denser ore particles may be transported at a slower rate since they require higher flow velocities to mobilize (Macklin and Dowsett, 1989). Therefore, mining-related metals are transported with sediment and dispersed by the same mechanisms that dictate natural sediment transportation and control channel form.

Sediment storage is largely controlled by the factors that are linked to sediment transportation. The changes in rate and magnitude of fluvial processes that follow mining activities have a large effect on the spatial distribution of heavy metals as well as their probability of being remobilized (Lewin and Macklin, 1987; Macklin and Lewin, 1989). Sediments of varying grain size have different entrainment thresholds with fine sediment

requiring less energy to transport than coarse sediment (Hjulstrom, 1939). Gravel bed rivers typically require a near-bankfull discharge to mobilize median grain size bed sediment (Henderson, 1961; Buffington, 2012).

Fine sediments typically contain the highest metal concentrations due to their greater relative surface area which allows for greater adsorption of trace metals onto the grain surface (Håkanson, 1984; Horowitz, 1991). However, watersheds impaired by mining can show high metal concentrations in both fine and coarse tailings (Moore et al., 1989; Pavlowsky et al., 2010; Pavlowsky et al., 2017). Metal concentrations also tend to decrease downstream exponentially with distance from the source of contamination (Marcus, 1987; Macklin and Dowsett, 1989; Miller, 1997). Although, this trend can become less evident in watersheds that exhibit many point sources of contamination distributed throughout the watershed (Pavlowsky, 1996).

The Tri-State Mining District and Joplin Subdistrict

The Tri-State Mining District (TSMD) is an area rich in mining history. One of the earliest documents of the regional ore deposits come from Henry Schoolcraft's journal during his famed expedition of the Ozarks between 1818 to 1819 where he noticed Pb outcropping at the surface west of present-day Springfield (Schoolcraft, 1996). Hunters and trappers were some of the earliest people to mine these surficial Pb deposits in the 1820s to make bullets beginning (Schoolcraft, 1996). Mining communities were soon established throughout the region with commercial operations beginning in Joplin around 1850 (Figure 2) (Pope, 2005). For the first 20 years, mining focused on crude operations working the shallow galena Pb deposits. These operations were limited in depth due to the lack of heavy machinery (Gibson, 1972). Despite the

higher overall abundance of Zn mineralization in the district, it was not produced until 1874 due to the development of new smelting technology (Gibson, 1972).

During the 1870s railroads were established throughout the TSMD. This allowed heavy machinery to be brought into the Joplin subdistrict which resulted in improved ore processing techniques and the ability to access deeper ore deposits (Gibson, 1972). Mine output in the Joplin subdistrict substantially decreased in 1918 due to the depletion of ore deposits and the discovery of large ore deposits in Oklahoma and Kansas (Stewart, 1986). However, mining in the Joplin subdistrict saw a brief resurgence in the 1940s during WWII. The last mine located in Missouri closed in 1957 (Gibson, 1972). The Joplin subdistrict produced a total of 32,000,000 Mg of ore throughout its entire history of commercial operations (Stewart, 1986). However, the Joplin subdistrict encompasses nearby adject streams, so production was not isolated to the Turkey Creek watershed.

The results of these historical mining operations have caused concentrations of Pb and Zn in soil and channel sediments to far exceed background values which can be detrimental to the local environment (Skidmore, 1964; Neuberger et al. 1990; Wildhaber et al. 2000; Angelo et al. 2007). The large amount of contaminated mining waste that remained stored in tailings piles prompted the United States Environmental Protection Agency (USEPA) to establish Superfund sites throughout the region to remediate mining impacted areas. The Oronogo-Duenweg Mining Belt Superfund Site, located in the Turkey Creek watershed, began remedial investigations in 1990. To date, the USEPA has completed remediation of residential soils with elevated Pb, Zn, and Cd levels and is actively working to remove mine and mill waste exposed at the surface (USEPA, 2017).

The Joplin subdistrict, which encompasses the Turkey Creek watershed, was once the most productive district in the United States (Wright, 1918). The Turkey Creek watershed, which drains the Joplin subdistrict and a small portion of the Oronogo-Duenweg Mining Belt, has been drastically altered as a direct result of historic mining activity (Figure 3). Numerous studies have concluded that Pb and Zn in Turkey Creek are present at concentrations which can have adverse effects on local wildlife (Pope, 2005; Juracek, 2013; Smith, 2016; Gutiérrez et al., 2019).

TSMD Remediation

The USEPA has conducted extensive remediation efforts throughout the TSMD beginning in the early 1990s. The remediation efforts are ongoing with plans to continue into the future. They have remediated both mine and smelter waste as well as contaminated sediment within residential yards by excavating the top layer of contaminated soil. The EPA has removed numerous tailings piles and sold off the waste primarily as fill for road construction and constructed retention ponds and sediment traps throughout the region to prevent the further distribution of contaminated sediment (USEPA, 2017). Despite remedial efforts, large amounts of contaminated sediment remained stored in tailings piles and channel sediment throughout the watershed. These remediated areas are often along the channel of Turkey Creek. The management goal is for Zn and Pb concentrations in streams to decrease below remediated areas (USEPA, 2017). However, if sediment takes a long time to move throughout the channel, contamination will still be present near the source for a long period of time even after clean-up (Lewin and Macklin, 1987; Merefield, 1987). As remediation continues, the sediment stored in tailings piles will become increasingly less significant, and contamination stored within the fluvial deposits will become a more important source of contamination.

Mining History and Regional Studies

Mining operations in the TSMD lasted for approximately 120 years with many mining camps established throughout the Turkey Creek watershed (Gibson, 1972). Mining contamination remains a persistent issue due to these past mining operations (Smith, 2016; USEPA, 2017). A major source of mining contamination is the ongoing erosion of tailings piles which store processed ore wastes which contain large percentages of unrecovered heavy metals including Pb and Zn which waste into the channel (Barks, 1977). These heavy metals make their way into streams where they have damaging effects on the ecosystem and human health (Beyer et al., 2004; Park et al., 2020).

The mining related contamination throughout the TSMD has been the focus of many studies. In general, previous studies on Turkey Creek have not focused solely on the watershed itself. Most studies include sampling several sites in Turkey Creek within a larger scope of study that encompassed sampling throughout the greater TSMD. Numerous studies have focused on the biological effects of heavy metal contamination on the health of the overall ecosystem. Wild birds have been observed to contain Pb tissue concentrations associated with adverse biological function and poisoning (Beyer et al., 2004). Crayfish and mussel populations were significantly lower at sites impaired with heavy metals from mining activities (Allert et al., 2012; Besser et al., 2015). The negative impacts of mining contamination extend beyond local wildlife. Increased heavy metal concentrations from mining have negatively affected the health of nearby humans through increased Pb blood levels and mortality rates (Park et al., 2020).

Other studies have sought to understand the dispersal and contamination of heavy metals throughout the TSMD. Past TSMD studies have focused on channel sediment have analyzed trace metal concentrations of clay and silt-sized streambed sediment (Pope, 2005), transition

zone widths of tailings piles where concentrations shift to maximum background values (USFWS, 2013), concentrations and distribution of streambed sediment compared to background values (Gutiérrez et al., 2015), mobility of heavy metals as determined by bioavailability and Fe-oxides (Gutiérrez et al., 2019), and total mass of contaminated sediment stored in gravel bar deposits (Smith, 2016). All studies agree that Pb and Zn concentrations commonly exceed background values with the largest concentrations observed near old smelters and tailings piles (Gutiérrez et al., 2015).

Previous studies have also focused on mining contamination associated with floodplain sediment. A former study analyzed the heavy metal concentrations in the floodplain with respect to depth and lateral extent throughout the Spring River and its tributaries (Juracek, 2013). Another study looked at the relationship between depth and concentration of floodplain and low terrace deposits in the Spring River and its tributaries (Smith, 2016). It concluded that elevated Pb and Zn concentrations are typically restricted to the upper 0.3 to 0.6 m of the floodplain with an occasional increased depth of contamination near the channel or in areas disturbed by mining. The greatest depth of elevated metal concentrations in the floodplain was observed at 3.0 meters in Turkey Creek (near R-km 4.5).

In order to quantify longitudinal metal trends from previous research conducted in Turkey Creek, the published data from two scientific studies and one contractor report were compiled to determine Pb and Zn concentration values throughout active channel sediment (Table 1) (Peebles, 2014; Smith, 2016; HGL, 2019). The longitudinal trends of these active channel samples indicate that concentrations of both Pb and Zn generally increase with distance downstream reflecting both locations of mining areas and expected sediment fining downstream (Figure 4). Smith furthered the understanding of spatial metal concentrations by using freeze-

coring to determine the maximum vertical depth at which <2 mm sediment exceeded the probable effects concentration (PEC) (Smith, 2016). He found that metal concentrations were often elevated above the PEC all the way down to bedrock.

Research Contribution of This Study

The coarse fraction (2 – 16 mm) as a source of metal contamination in streams affected by mining has been rarely investigated in most studies and omitted from previous assessments in Turkey Creek (Pope, 2005; USFWS, 2013; Gutiérrez et al., 2015; Smith, 2016). The coarse fraction can be an important source of mining sediment in the TSMD since mills produced large quantities of coarse tailings during jigging locally referred to as "chat" wastes (Wright, 1918; Gibson, 1972; Moore et al., 1989; Pavlowsky et al., 2010; Pavlowsky et al., 2017). This study will compare contamination levels and storage amounts between fine and coarse sediments in Turkey Creek. Only analyzing fine sediment does not accurately represent the entire metal burden in channel storage.

Contamination trends can vary among different channel deposits in mining areas (Pavlowsky and Owen, 2016; Smith, 2016). In general, variations in depositional history, topography across the valley floor, and the influence of sediment sorting and dilution during transport can cause variations in both sediment size and metal storage among different deposits (Graf 1996; Ladd et al., 1998; Rhoads and Cahill, 1999). Therefore, this study will compare sediments and geochemistry among bed, bar, bench, and chute deposits in Turkey Creek. No studies in Turkey Creek or other streams in the TSMD have evaluated the concentrations and distribution of metals among different geomorphic features in the channel. Understanding the

geomorphic factors that control sediment distribution and storage can be useful in estimating where contaminated sediment will be stored in the channel.

The downstream dispersal of metal contamination and storage trends will reflect the influence of larger-scale hydraulic and geomorphic controls related to the characteristics of the channel network and the sediment transport capacity of the channel (Marcus, 1987; Knighton, 1989; Knighton, 1991; Lewin and Macklin, 1987; Macklin and Lewin, 1989). Few studies quantify the influence of geomorphic variables or contamination trends in watersheds in general, let alone those affected by mining. Channel network variables include the downstream dilution and mixing of sediment over increasing drainage areas and distance from the source (Lewin and Macklin, 1987; Marcus, 1987; Bradley, 1989; Graf, 1996; Pavlowsky, 1996). Therefore, metal concentrations are expected to decrease downstream from mining impacted areas and increase in areas that drain a high percentage of mined areas.

Sediment transport variables include channel width which relates the area available for deposition and storage. Previous research on streams in the Viburnum Trend has indicated a strong relationship ($R^2 = 0.91$) between storage and channel width (Pavlowsky and Owen, 2016). The widest portions of the stream are expected to store the greatest amounts of sediment due to its greater relative geometry and association with land use disturbances (Jacobson, 1995). In addition, channel slope and mobile sediment depth on the channel bed can indicate the available transport capacity of the reach (Gilbert and Murphy, 1914; Robert, 2003). Areas of low slope are expected to store greater amounts of sediment, since they have a lower transport capacity and represent areas of deposition. Similar to channel width, thicker deposits of mobile sediment on the channel bed can positively correlate with metal storage due to their greater relative geometry and association with bed aggradation due to high sediment inputs and channel modifications

which commonly occur in watersheds affected by historical mining activities (Jacboson, 1995; Pavlowsky et al., 2017).

Past studies in the Turkey Creek watershed have not analyzed the influence of different geomorphic variables with respect to dispersal trends and storage such as channel width (active, bankfull, and floodplain), slope, depth of sediment to bedrock (measured at the thalweg), drainage area, and downstream distance. These variables have been documented to control sediment transport, so they could serve as a predictor for storage trends throughout the watershed (Montgomery and Buffington, 1997; Sambrook Smith and Ferguson, 1995; Buffington, 2012; Jacobson, 1995). The United States Geological Survey (USGS) has recognized the importance of quantifying sediment storage in contaminated streams. Smith has quantified the total volumetric storage of sediment within the gravel bars in Turkey Creek (Smith, 2016). This study seeks to advance the understanding of Pb and Zn storage throughout the Turkey Creek watershed by quantifying storage values with respect to grain size and geomorphic features.

Purpose and Objectives

The purpose of this study is to determine the amount of contaminated sediment stored within different depositional features in both fine and coarse grain sizes in the Turkey Creek main channel and its tributaries. The objectives of this study are to (i) assess volumetric and mass sediment storage among different deposits and size fractions, (ii) evaluate longitudinal metal concentrations in different size fractions and deposits, and (iii) develop predictive equations that quantify downstream trends in metal storage as a function of geomorphic variables such as transport distance, stream power, and valley controls. Contaminated features may become more significant sources of contamination as they are reworked and dispersed

downstream. Therefore, understanding the amount of contaminated sediment stored within these geomorphic deposits is important for developing remediation plans.

Table 1. Lead and zinc concentrations in active channel sediments in Turkey Creek (n = 38, <2 mm). If a series of depth-integrated samples were collected at a site, the concentrations were averaged to generate a single value for that site (Peebles, 2014; Smith, 2016; HGL, 2019).

Element	Concentration (ppm)					
	Mean	Minimum	25%-tile	Median	75%-tile	Maximum
Pb	543	48	240	455	587	2,671
Zn	5,065	325	2,748	4,890	7,372	12,800

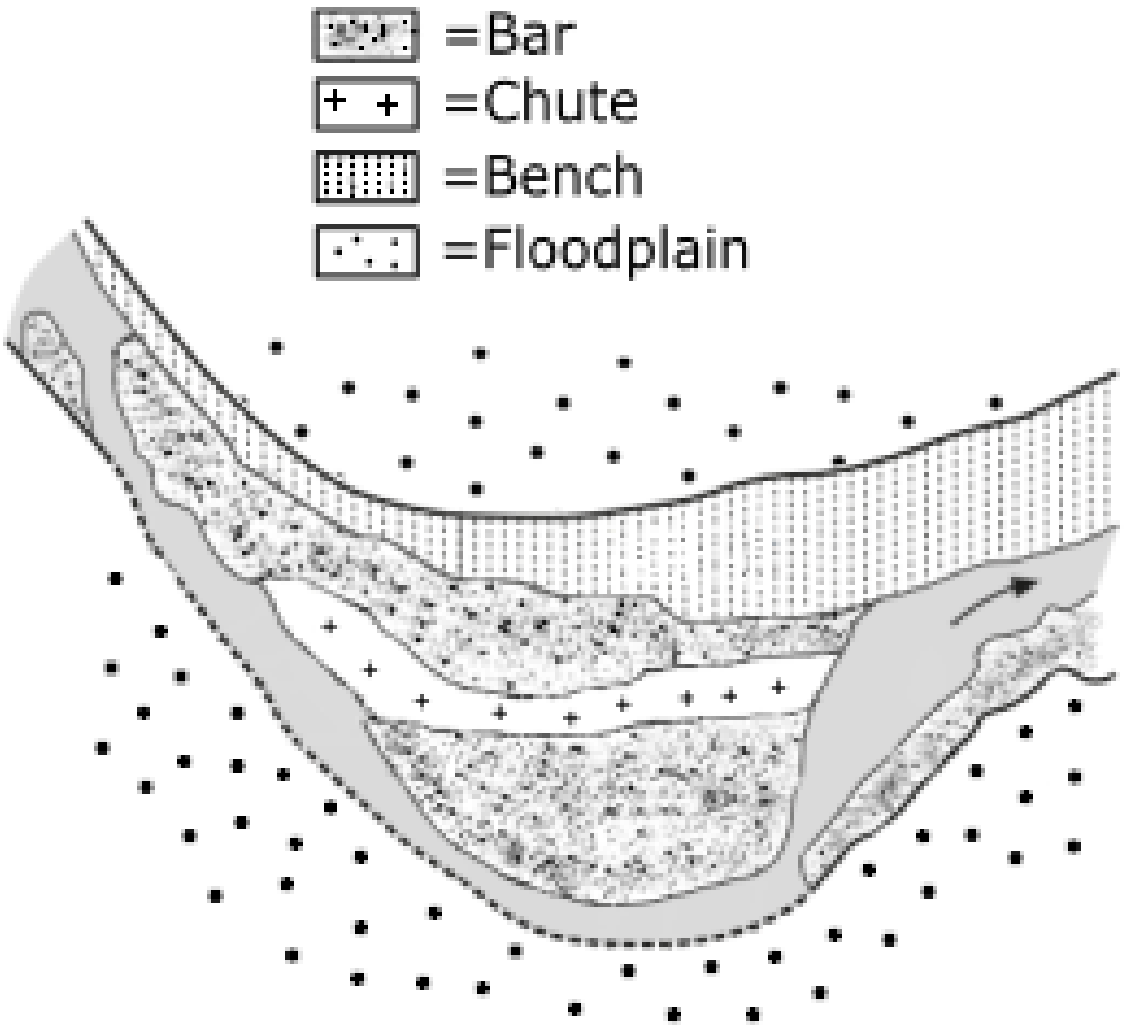

Figure 1. Orthogonal view of a stream planform showing the various deposits analyzed in this study (River Studies, 2021).

Figure 2. Turkey Creek Mining Camp, Missouri (Gibson, 1972).

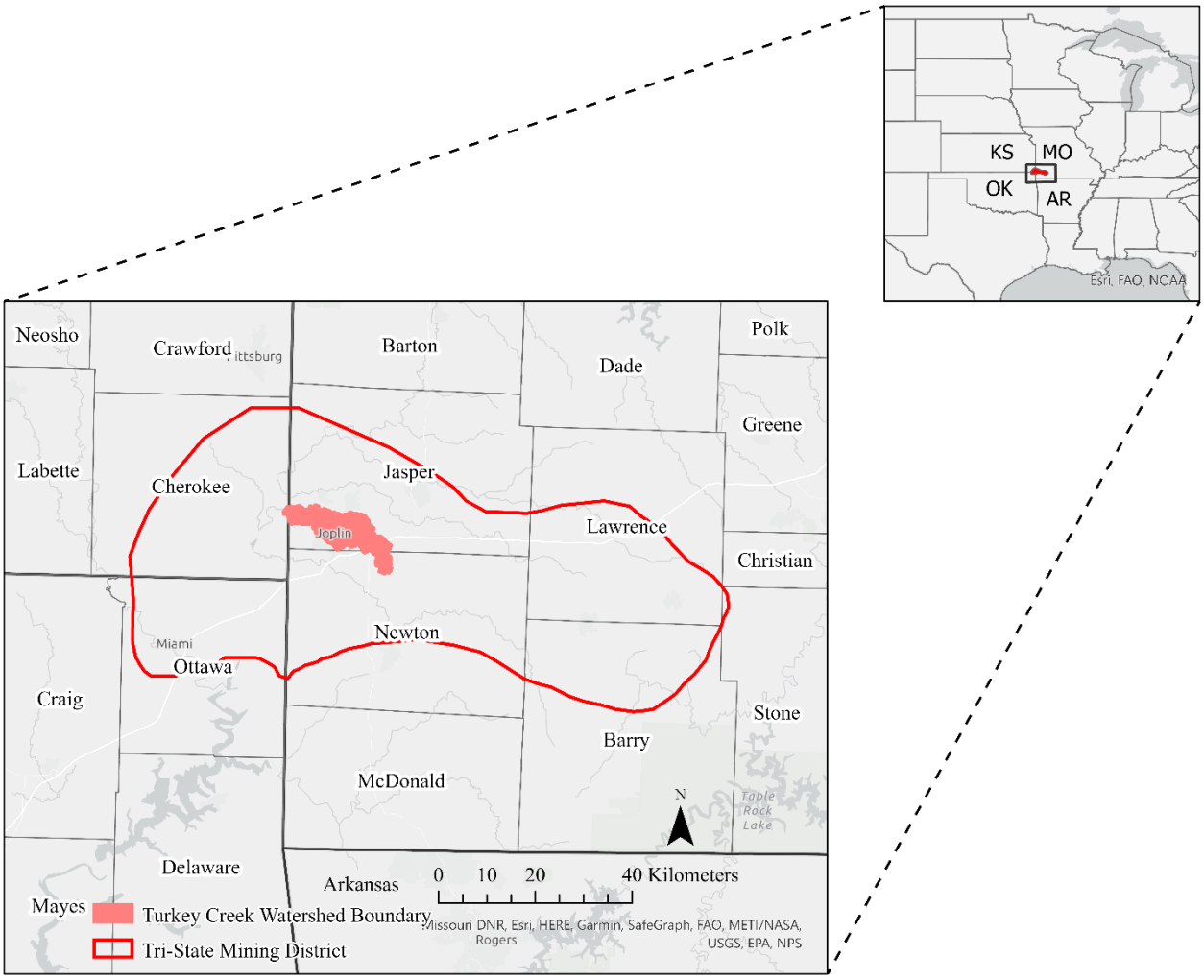

Figure 3. Location of the Tri-State Mining District and Turkey Creek watershed.

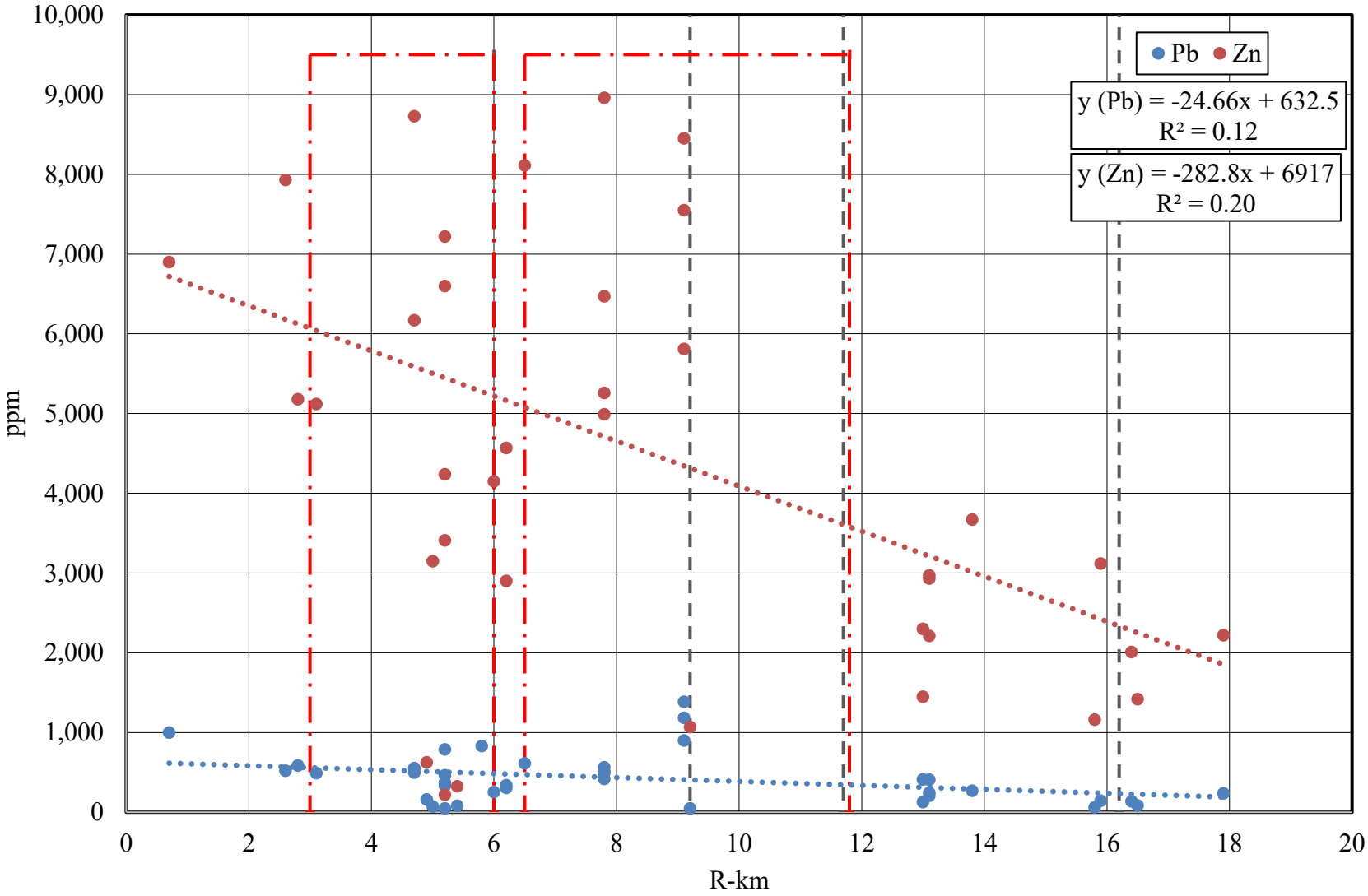

Figure 4. Polynomial longitudinal trends of Pb and Zn in active channel sediment (<2 mm) in Turkey Creek (n=38) (Peebles, 2014; Smith, 2016; HGL, 2019). Tributary confluences are shown in dashed gray lines, and general mine waste areas are shown between red dash-dot lines.

STUDY AREA

Turkey Creek (119 km^2) drains a HUC-12 watershed (hydrologic unit code 110702070901) watershed in Jasper (MO), Newton (MO), and Cherokee (KS) counties (Figure 3) (Seaber et al., 1987). It is located in the heart of the Tri-State Mining District (TSMD) which covers a total area of approximately 6,574 km^2 in the states of Missouri, Kansas, and Oklahoma. The main stem of Turkey Creek flows 33.8 km from the Diamond Grove Conservation Area, through Joplin, MO and discharges into the Spring River in Kansas. Two EPA superfund sites (Oronogo-Duenweg Mining Belt and Cherokee County) are located within the Turkey Creek watershed (USEPA, 2017).

Geology and Soils

The Turkey Creek watershed is entirely contained within the Ozark Highland Level III Ecoregion with karst topography and frequent losing streams (Nigh and Schroeder, 2002; USEPA, 2013). Mississippian-aged limestone bedrock underlies most of the watershed with minor amounts of Pennsylvanian shale (Howe and Koenig, 1961) (Table 2 and Figure 5). The previously mined Pb and Zn sulfide deposits are classified as Mississippi Valley-Type (MVT) Deposits. These epigenetic Pb and Zn deposits are stratabound in the Mississippian aged Keokuk and Warsaw Formations which are composed of cherty limestone (Brockie et al., 1933). These MVT deposits were mineralized by hydrothermal saline brines rising through permeable zones in the rock. This fluid cooled when it reached the Mississippian aged limestones where it precipitated into ore minerals (Appold and Garven, 1999; Plumlee et al., 1994; Stoffell et al.,

2008; Johnson et al., 2016). The carbonate host rock that contains the ore acts as a natural buffer preventing acid mine drainage from developing in Turkey Creek (Gutiérrez et al., 2019).

The upland soils in the Turkey Creek watershed primarily originate from cherty carbonate rock residuum (USEPA, 2013). They are generally composed of silt loams often with significant amounts of cherty rock fragment in the subsoil (NRCS, 2020). Alluvial floodplains and terrace soils cover an area of 12.2 km^2 representing 10.2% of the total watershed. These soil series are described as frequently, occasionally, or rarely flooded. The majority of floodplain soils are mapped as the Cedargap series composed of gravelly silt loam (Table 3) (NRCS, 2020). Recent legacy sediment deposited as the result of agricultural settlement and poor soil conservation practices in the past cover floodplains to depths of 0.5 to 2 m in Turkey Creek (Smith, 2016; Eades et al., 2021).

Climate and Hydrology

Southwestern Missouri experiences hot summers and cold winters. Weather records from the previous 30 years indicate the average annual temperature is 13.7 C. The coldest month is January with an average temperature of 1.1 C, and the warmest month is July with an average temperature of 25.5 C (MRCC, 2021). Southwestern Missouri receives an average annual precipitation of 110.4 cm. The wettest month was May which had an average precipitation of 13.7 cm (Table 4) (MRCC, 2021).

No United States Geological Survey (USGS) gaging stations are located directly within the watershed, so hydrologic trends were assessed using two nearby stations: Shoal Creek above Joplin, MO draining 1,106 km^2 (#07187000) and Spring River near Baxter Springs, KS draining 6,340 km^2 (#07187600) located in the HUC-#11070207 watershed. The gage on Shoal Creek has

a well-established history since 1941, while the gage on the Spring River was installed relatively recently in 2009. Both gaging stations have significantly larger drainage areas than the Turkey Creek watershed (119 km^2). The Shoal Creek and Spring River gages have mean annual flows of 12.5 and 74.8 m^3/s, respectively. The largest flood occurred in 1941 on Shoal Creek where discharge peaked at 1,758.5 m^3/s with a gage height of 5.1 m. The Spring River gage recorded the largest flood in 2015 with a peak discharge of 4,134.3 m^3/s and a gage height of 9.7 m (Table 5) (USGS, 2021).

Mining History

Early Pb milling began in the 1820s and involved crushing the Pb ore by hand and sorting it via sluicing. In 1874 miners began to process Zn due to new developments in smelting technology. Around 1880 miners transitioned from the sluice to a jigging process which used a screen and hydraulic pulses to separate the denser ore from the rock (Gibson, 1972). By the 1910s, shaking tables were added to the end of jigs to further process the finer sediment (Wright, 1918). In 1916 froth flotation separation was introduced to the milling process in a few locations and was prevalent throughout the TSMD by the mid-1920s (Wright, 1918; Gibson, 1972; Hinrichs, 1996). However, mining in the Joplin subdistrict substantially declined in 1918 due to the depletion of economic ore deposits.

Ore Production. The ore deposits in the TSMD were scattered throughout the TSMD with significantly variable ratios of Pb and Zn sulfides (Kitson, 1919; Brockie et al., 1933). Two types of orebodies were mined throughout the TSMD. The first ore deposit discovered was the “upper run”. These deposits were located at the surface and could extend to a depth of up to approximately 50 meters. The second “sheet ground” deposits were more productive and were

located about 75 m below the surface in the Mississippian aged Keokuk and Warsaw limestone formations which had a combined thickness of approximately 80 m (Kitson, 1919; Brockie et al., 1933; McCauley et al., 1983). These ore bodies were typically mined for six months to six years (Kitson, 1919; Gibson, 1972). Due to the scattered distribution of ore deposits and relatively low topographic relief, ore was most often processed on-site. The lack of a centralized mill resulted in many small mills scattered throughout the Joplin subdistrict which created many chat piles at these mill sites (Figure 6) (Kitson, 1919; Gibson, 1972).

Throughout the mining history of the TSMD, there have been numerous ore processing techniques which have produced wide ranges of tailings composed of different mine waste including: coarse chat (from sluices and jigs), sands (from tables), fines and slimes (from flotation), and ultra-fine particles (from mill overflows and effluents) (Wright, 1918; Gibson, 1972; Hinrichs, 1996). Unprocessed ore was typically crushed to <13 cm before being processed by the mill. Once the ore arrived in the mill, it was further ground to pass through 8 – 13 mm screens. Some mills treated ore greater than 13 mm in diameter. However, it is presumed that mills treating ore >13 mm did not include sediment significantly larger than this diameter (Table 6) (Wright, 1918; Gibson, 1972). After crushing, the ore was separated into concentrate, "middling" (a significantly less enriched product than concentrate), and tailings (Wright, 1918). There were three main ways that ore was treated to concentrate Zn and Pb minerals for the smelter:

Jigging. After crushing, the ore was treated on a series of rougher and cleaner jigs to concentrate the product. Jigs are used in ore processing to separate materials with different densities by flowing water over a pulsing screen. This causes the denser material to settle at the bottom of the jig where it can be recovered. A rougher jig was used to remove a large amount of

coarse waste material and concentrate the ore to 10 – 25% Zn. The enriched material collected from the rougher jig was then treated on a cleaner jig to further concentrate the ore to 50 – 60% Zn (Wright, 1918; Hinrichs, 1996). The ore from the rougher and cleaner jig was processed on a dewatering trommel with 1.5 – 2 mm openings. The size fraction that passed through was sent off for further processing at the tabling and flotation sections of the mill. The fraction that was collected on the screen was sent off to the chat pile as waste (Wright, 1918).

Tabling. Once the ore <2 mm in diameter reached the tabling section, it was passed over a slightly inclined table where the higher density ore was separated from the host rock by a horizontal oscillatory motion. This results in a Pb and Zn concentrate approximately 55% Zn (Wright, 1918).

Flotation. Froth flotation was used to process the finest mining sediment (<0.07 mm) (Wright, 1918). Very fine ore particles produced during milling tended to congest milling machinery and were difficult to process, except by flotation (Wright, 1918; Taggart, 1945). The finest sediment was mixed with a chemical solution to create a slime mixture which allowed mill operators to extract Pb and Zn resulting in a highly concentrated final product (Wright, 1918; Gibson, 1972). However, flotation did not become widespread throughout the TSMD until about 1925 which was after the vast majority of mining operations the Joplin subdistrict had ended (Gibson, 1972).

Ore Processing. The milling procedures in the TSMD were not well recorded and often changed on a site-by-site basis. There was no systematic approach by the miners to determine the recovery percentage at different steps in the milling process. However, the mills in Joplin tried to produce as few fines as possible, since large amounts of losses were typically associated with the fine size fractions since finer slimes fouled machinery (Wright, 1918). As ore recovery rates

improved, processed ore stored in chat piles was often re-milled to further recover more Pb and Zn. The absence of standardized milling procedures and variability of ore concentration led to a wide range of tailings sizes produced throughout the region. The highest total amount of Zn generated during milling in the Joplin subdistrict was typically associated with the coarse sediment (>2 mm) which often resented more than 50% of the total Zn produced. However, the highest Zn concentrations were associated with the finest sediment (Table 7).

Tailings Waste

During the entire operation of all mines in the TSMD, jigging produced roughly 80% of all chat tailings (0.4 – 13.3 mm). Tabling operations produced finer tailings which account 12% of mine waste. The finest tailings (<0.07 mm) were generated during flotation and represent 8% of mine waste (Gibson, 1972; USEPA, 1997; Pope, 2005). Flotation tailings were commonly discarded in constructed ponds near the mill (Gibson, 1972). Mine waste generated from jigging and tabling operations contained Pb concentrations from 360 – 1,500 ppm and Zn concentrations ranging from 6,000 – 13,000 ppm with the highest concentrations observed in the finest and coarsest fractions of the tailings since the most efficient metal recovery occurred in the middle-ranges of feed sizes (Taggart, 1945; Wright, 1918; Gibson, 1972). Tailings generated from the flotation process are silt-sized or smaller and have metal concentrations significantly higher than the concentrations observed in mine waste generated from jigging and tabling operations. Flotation tailings have concentrations of 380 – 5,900 ppm Pb and 3,800 – 64,000 ppm Zn (USEPA, 1997). The majority of mill sites and mine tailings piles are drained to Turkey Creek between R-km 2.5 and R-km 12 (Figure 7). In addition, other tailings dumps associated with the

Oronogo-Duenweg Mining Belt along the northeastern boundary of the watershed potentially drained into Turkey Creek near R-km 16 (Figure 7).

Present-day Land Use

In 2016 the Turkey Creek watershed was primarily developed with significant amounts of pasture and deciduous forests (Table 8). Most of the urban developed land was in the central section of the watershed between R-km 9 and R-km 20. Development drastically drops downstream from R-km 9; this section was characterized by both deciduous forests and agricultural land (Figure 8). The upstream portion of Turkey Creek between R-km 25 and R-km 33 was almost exclusively composed of agricultural land (NLCD, 2016).

Mine dumps covered 5.2 km^2 or approximately 4% of the total area of the Turkey Creek watershed. These areas are dispersed throughout the watershed and represent land where mining occurred and processed ore was stored in tailings piles (NRCS, 2020). However, large numbers of tailings piles have been remediated. Since June 2019, the EPA completed remediation on a total tailings area of 12.2 km^2 (10%) with an additional 5.6 km^2 (5%) in active remediation. There are plans to remediate another 4.3 km^2 (4%) of sediment impaired by mine waste when funding becomes available (Figure 7) (USEPA, 2017; USEPA, 2021).

Table 2. Surficial bedrock geology of the Turkey Creek watershed (Howe and Koenig, 1961).

Series	Formation	Geologic Age	Major	Minor	Area (km^2)	Surface Area of Watershed (%)
Meramecian	St. Louis, Salem, Warsaw	Mississippian	Limestone		102.5	86.1
Osagian	Keokuk, Burlington, Elsey, Reeds Spring, Pierson	Mississippian	Limestone	Chert, Dolostone	6.2	5.2
Middle Series (Atokan Stage)	Riverton, Burgner	Pennsylvanian	Shale, siltstone, mudstone	Limestone	9.7	8.2
Holocene	Alluvium	Holocene	Sand, silt, clay	Gravel	0.6	0.5

Table 3. Alluvial floodplain and terrace soil series in the Turkey Creek watershed.

Soil Series	Texture	Flooding Frequency	Area (km^2)	Percent of Area (%)	% Sediment <2 mm (upper 0.5 m)
Cedargap	Gravelly silt loam	Frequently	8.0	65.7	50
Bearthicket	Silt loam	Occasionally	3.1	25.6	95
Verdigris	Silt Loam	Occasionally	0.9	7.0	100
Hepler	Silt Loam	Occasionally	0.2	1.3	100
Secesh	Silt Loam	Rarely	0.0	0.4	89

Table 4. Weather data in southwestern Missouri from 1991 to 2020. (MRCC, 2021)

Month	Average Precipitation (cm)	Average Temperature (°C)	Average Minimum Temperature (°C)	Average Maximum Temperature (°C)
Jan.	5.4	1.1	-5.9	4.6
Feb.	5.8	3.5	-3.7	7.6
Mar.	8.5	8.3	1.1	13.4
Apr.	11.7	13.6	6.5	19.5
May	13.7	18.3	12.1	24.2
June	11.7	23.1	17.2	29.0
July	10.9	25.5	19.4	31.2
Aug.	9.7	24.8	18.2	30.6
Sept.	9.8	20.5	13.7	26.6
Oct.	8.6	14.3	7.1	20.3
Nov.	8.3	8.0	1.3	12.8
Dec.	6.3	2.8	-3.6	6.6
Annual	110.4	13.7	7.0	18.9

Table 5. USGS gaging data at stations near Turkey Creek.

Gage Station Data	Shoal Creek above Joplin, MO, #07187000	Spring River near Baxter Springs, KS, #07187600
Ad (km^2)	1,223	6,340
Available Data	Oct. 1941	Aug. 2009
Mean Annual Flow (m^3/s)	12.5	74.8
Mean Monthly Low Flow (m^3/s)	6.4	29.1
Mean Monthly High Flow (m^3/s)	22.3	218.2
Largest Flood Date	5/18/1943	12/28/2015
Peak Gage Height (m)	5.1	9.7
Peak Discharge (m^3/s)	1,759	4,134

Table 6. The percent weight produced in various size fractions at mills throughout the TSMD (Wright, 1918).

Screen Size (mm)	Percent Weight of Screen Product (%)				
	Webb City Mill	Duenweg Mill	Carterville Mill	Porto Rico Mill	Prosperity Mill
13.3		18.5		6.9	
6.7	29.5	35.9	33.6	32.0	9.9
3.3	28.4	19.5	30.8	26.8	38.8
1.7	15.5	12.6	16.8	18.4	23.8
0.8	16.1	7.3	8.8	9.1	11.4
0.4	5.5	3.2	4.6	2.7	6.2
0.2	1.4	0.7	2.6	1.8	4.1
0.15	0.6	0.5	1.0	0.4	1.9
0.10	0.4	0.5	0.8	0.4	1.5
0.07	0.3	0.3	0.2	0.2	0.2
<0.07	2.4	1.1	0.9	1.3	2.2

Table 7. Zinc composition of mill feeds throughout the TSMD (Wright, 1918).

Screen Size (mm)	Webb City Mill		Duenweg Mill		Carterville Mill		Porto Rico Mill		Prosperity Mill		Average	
	Zn (%)	Total (%)	Zn (%)	Total (%)	Zn (%)	Total (%)	Zn (%)	Total (%)	Zn (%)	Total (%)	Zn (%)	Total (%)
13.3			0.6	21.1			0.3	5.6			0.5	13.3
6.7	0.5	20.0	0.5	31.4	0.3	24.3	0.2	19.3	0.5	12.3	0.4	21.5
3.3	0.7	24.7	0.4	15.5	0.4	31.6	0.2	14.6	0.4	33.8	0.4	24.0
1.7	0.8	15.8	0.4	8.6	0.4	17.3	0.2	9.5	0.3	16.2	0.4	13.5
0.8	0.5	9.3	0.4	5.3	0.3	6.4	0.3	7.4	0.2	5.1	0.3	6.7
0.4	0.4	2.9	0.4	2.2	0.3	3.3	0.6	4.1	0.3	3.7	0.4	3.2
0.2	1.0	1.7	0.7	0.9	0.6	3.3	1.3	6.3	0.3	2.6	0.8	3.0
0.15	1.1	0.9	1.0	1.0	0.6	1.3	2.9	3.5	0.4	1.9	1.2	1.7
0.1	1.3	0.6	0.8	0.8	1.0	2.0	3.4	3.6	1.0	3.3	1.5	2.1
0.07	1.6	0.6	1.4	0.8	1.6	0.8	5.7	3.3	1.2	0.5	2.3	1.2
<0.07	7.9	23.5	6.3	12.6	4.7	9.8	6.6	22.8	4.1	20.7	5.9	17.9

Table 8. Land use in the Turkey Creek watershed in 2016 (NLCD, 2016).

Land Use	Area (km2)	Percent of Area (%)
Open Water	0.3	0.2
Developed, Open Space	14.3	11.9
Developed, Low Intensity	20.6	17.1
Developed, Medium Intensity	8.1	6.7
Developed, High Intensity	5.8	4.8
Barren Land	1.6	1.3
Deciduous Forest	27.5	22.9
Evergreen Forest	0.0	0.0
Mixed Forest	0.7	0.6
Shrub/Scrub	0.4	0.4
Grassland/Herbaceous	0.5	0.4
Pasture/Hay	39.4	32.7
Cultivated Crops	1.0	0.8
Woody Wetlands	0.1	0.0
Emergent Herbaceous Wetlands	0.0	0.0

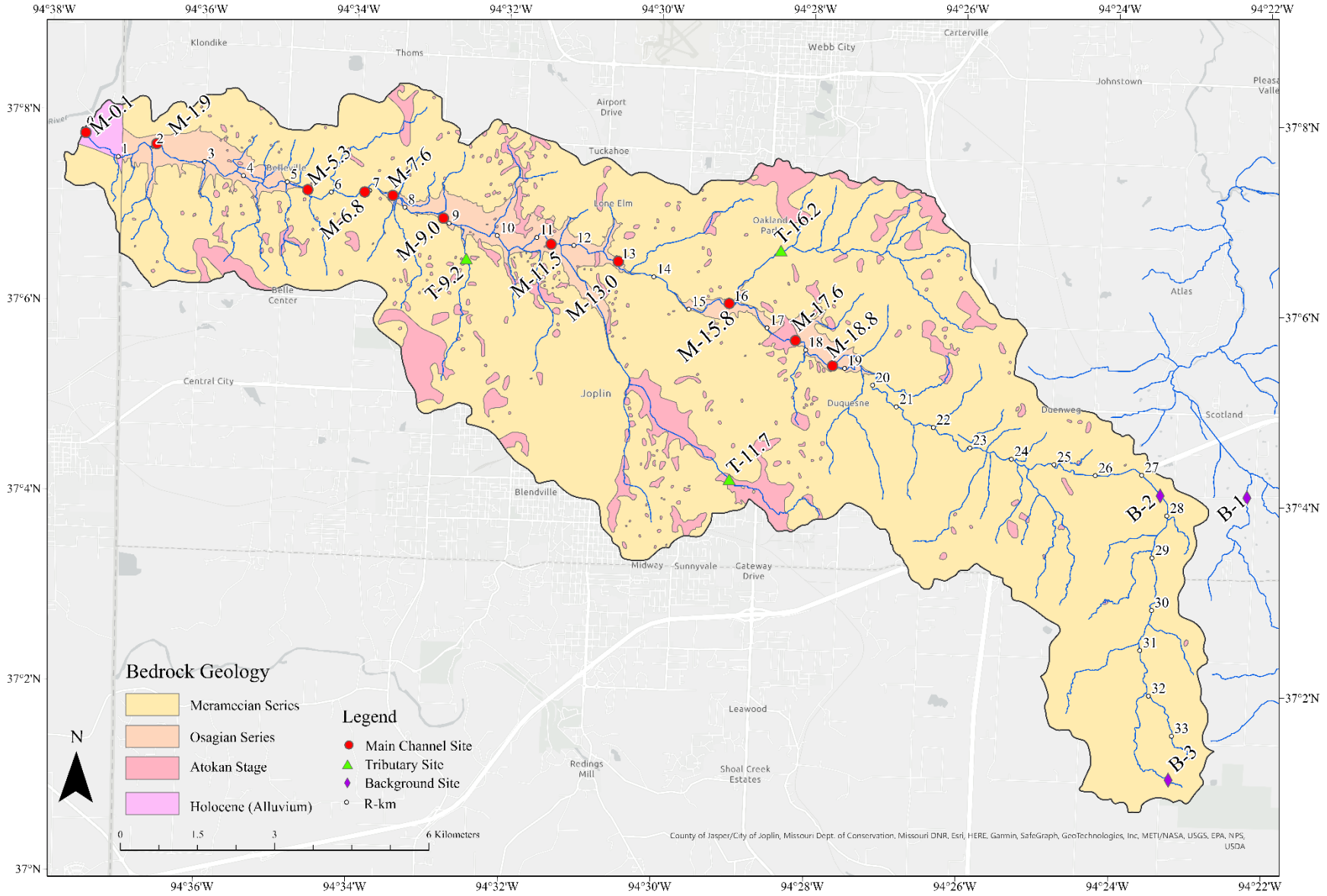

Figure 5. Bedrock geology of the Turkey Creek watershed.

Figure 6. Snowball chat pile located near site T-9.2 at Leadville Hollow. Coarse chat is seen wasting directly into the channel. The tailings pile is overlaying the cherty Cedargap soil series.

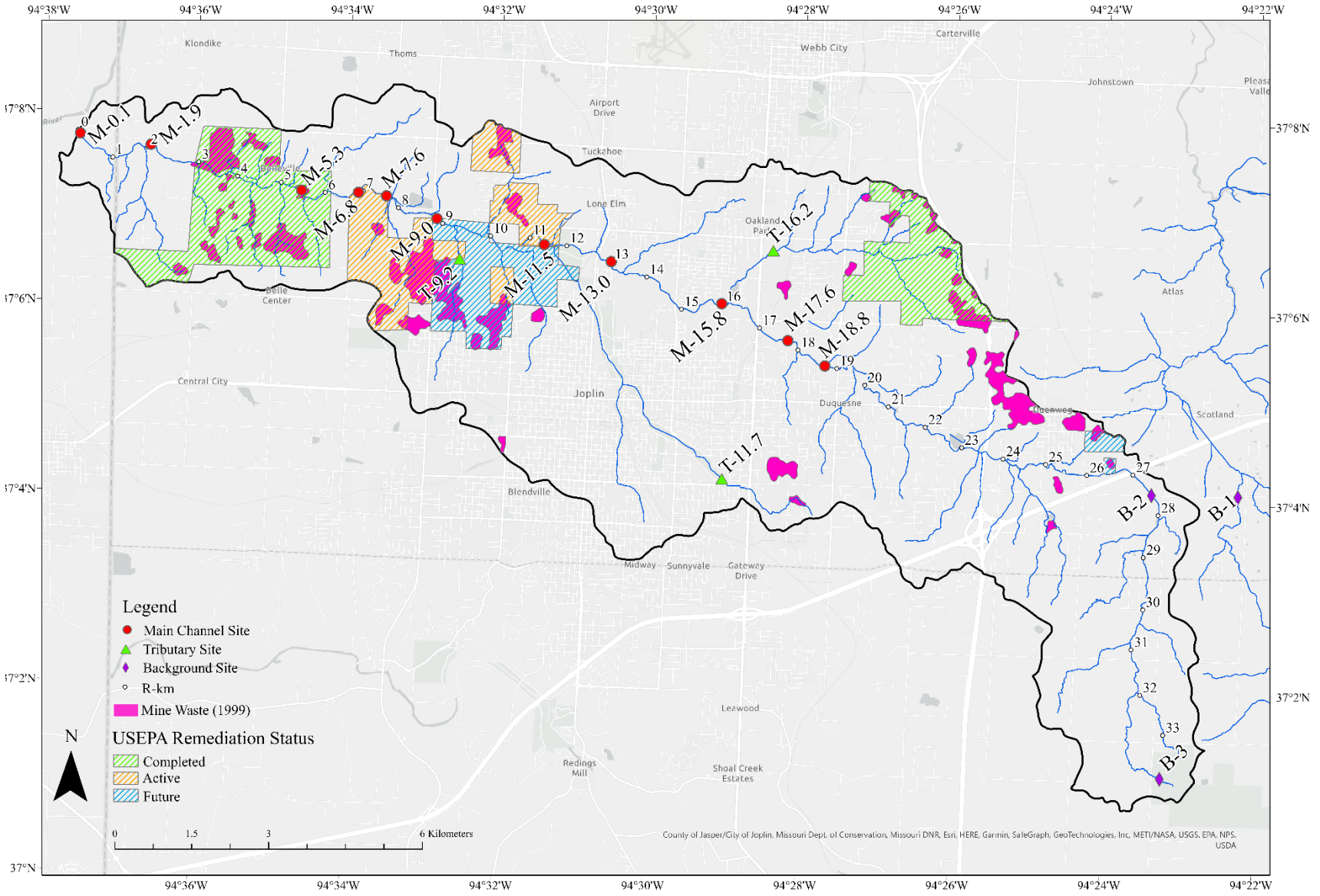

Figure 7. Turkey Creek watershed with sampling sites, mine waste areas, and remediated areas. Sites T1, T2, and T3 enter the Turkey Creek main channel at R-km 16.2, R-km 11.7, and R-km 9.2, respectively.

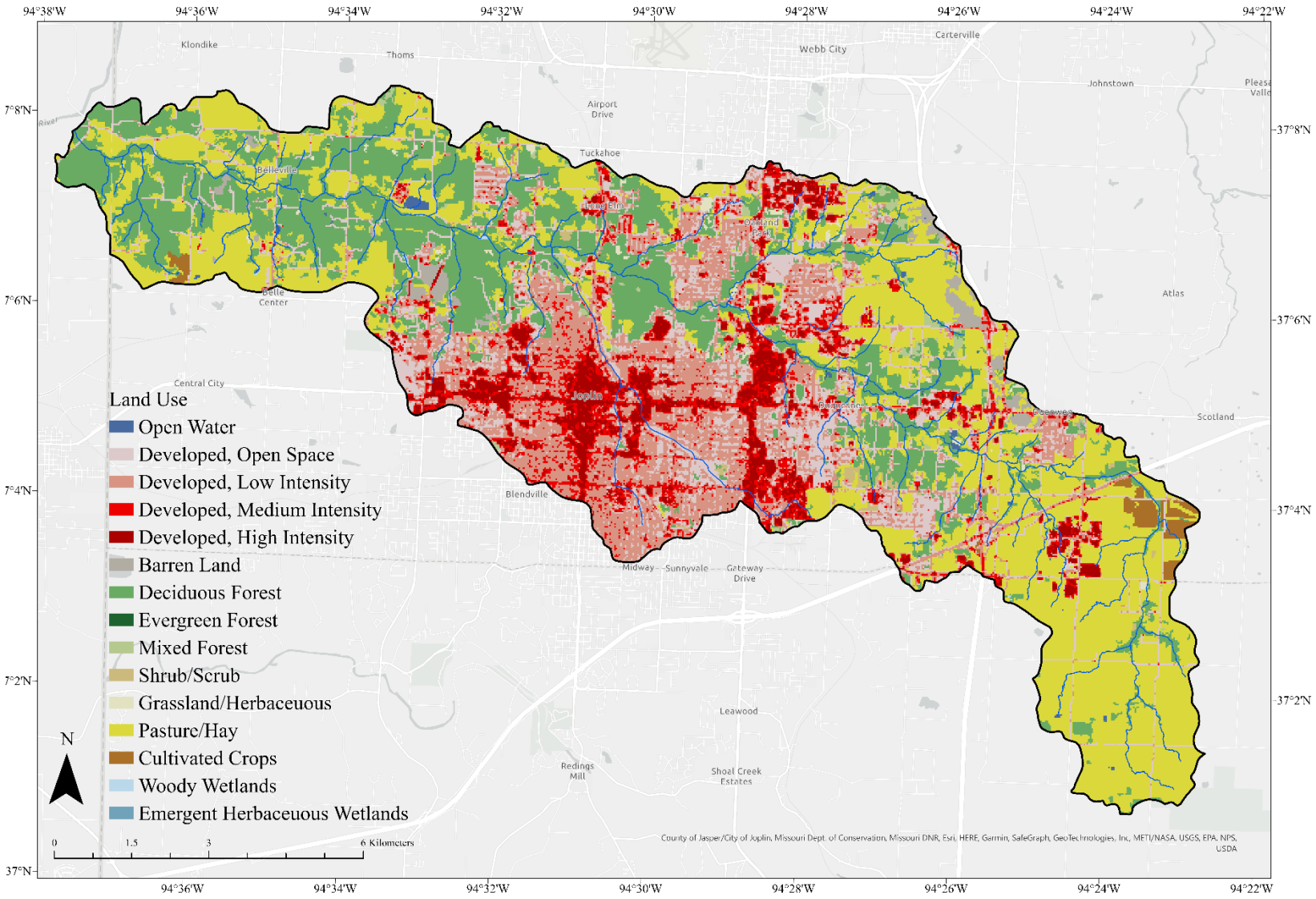

Figure 8. Land use map of the Tukey Creek watershed.

METHODS

Site Selection

Fourteen sites were sampled along the main channel and tributaries of Turkey Creek below mining areas. In addition, three sites were sampled at "background" locations unaffected by mining including one site in Grove Creek located just beyond the eastern border of Turkey Creek (Figure 5). All sites were identified on a river-kilometer (R-km) longitudinal profile to assess downstream storage and geomorphic trends. R-km 0 is located at the confluence of Turkey Creek with the Spring River in Kansas, and R-km 33.8 is at the source of Turkey Creek located in Diamond Grove Prairie Conservation Area. The most significant amount of mine waste areas are located between R-km 3 and R-km 12. Mine waste areas were identified using geospatial data from the Web Soil Survey (last updated in September 2019) and used to determine the percentage of a drainage area composed of mined lands (NRCS, 2020). The influence of both mining areas and urban areas 1.5 km upstream from sites were visually classified as 0 (no influence), 1 (low), 2 (moderate), and 3 (high) (Table 9). Sampling reaches were identified by ease of access and distance from public roads.

Geomorphic Assessment

Sampling sites (excluding background sampling sites) were located between R-km 0.1 to R-km 18.8 (Figure 7). Each sample reach was segmented into seven equally spaced transects excluding site MC-0.1 which had six transects since there was not enough room to place the final transect due to the confluence with the Spring River. Transects were spaced twice the active channel width with the middle transect (TS4) always located on a glide to riffle transition area just above a riffle crest. Active channel widths ranged from 10 m to 50 m among main channel

sites and 2.5 m to 9 m among tributary sites. Sample reach lengths ranged from 120 m to 300 m among main channel sites and 30 m to 108 m at tributary sites. Transects crossed the entire active channel between the highest confining banks including the wetted channel bed, bar and bench surfaces, and chute fills. The coordinates of these transects were recorded on a Trimble Geo 7X (Appendix A).

At each of the 14 main channel and tributary sites, a geomorphic assessment was completed to assess the width and thickness of the different channel deposits present (Figure 9). A stadia rod was used to measure active channel width, bank offsets, bank heights, and water depth. A tile probe was used to measure depth to bedrock or other hard refusal at the thalweg and to check the depth of fine sediment thickness on benches and in chutes (Appendix A). Tile probing is both a cheap and effective method to determine the relative depth to bedrock and thickness of stored sediment, since the tile probe can penetrate sediment associated with historical mining disturbances but not coarse bed material (Jacobson and Primm, 1994; Pavlowsky et al., 2017). The height relative to water surface and width of the following previously described in-channel landforms were also measured with a stadia rod: bed, bar, bench, and chute (Hansen, 1967; Fujita and Muramoto, 1985; Royall et al., 2010; River Studies, 2021) (Figure 1) (Appendix B and Appendix C). Deposit thickness was calculated as the sum of the (i) average height of the primary horizontal surface above the water line, (ii) maximum water depth of the channel at the thalweg, and (iii) probe depth to refusal in the channel bed at the thalweg (Figure 9). Additional probe depths were also recorded at each landform as a check to ensure the refusal depth aligned with the bedrock depth measured at the thalweg. Bedrock was assumed to extend laterally with no change in relief (Figure 9).

Large boulders, logs, and other large debris in the channel were often observed within sampling reaches. The total amount of these obstructions on the channel bed was visually estimated as a volume along a transect and subtracted from the total bed storage volume estimated from the transect. If present, the width of bedrock or cut-earth exposed along the bed was recorded for each transect and zero sediment storage was assumed for these areas. Cut earth indicates areas of scoured residuum exposed in the bed. Exposed bedrock was observed to varying degrees at every sampling reach excluding sites MC-0.1 and T-9.2.

Sediment Sampling

A total of 92 active channel sediment and 22 bank samples were collected for geochemical and textural analysis (Appendix D). Channel samples were used to describe the texture and metal content of stored sediment deposits. Bank samples were utilized to take advantage of the opportunity to gain more information about longer-term storage in floodplain deposits. When possible, multiple samples of each feature present within a reach were collected. Sediment samples were collected in-channel using a shovel or entrenching tool and placed in plastic bags. Sediment samples were gathered from material not in contact with the metal shovel surface. Bed samples were gathered near the center of the wetted channel on glides using a shovel with holes allowing the water to drain from the sediment before it was placed in a plastic bag for storage. When sampling bar deposits, sediment was collected below the top armored layer by digging a sampling pit roughly three times the maximum clast size on the armored layer yielding sampling depths between 10 cm to 30 cm from the surface (Bunte and Abt, 2001). Benches were sampled between 0 cm to 20 cm. Any organic material that could have accumulated on the surface was removed and not collected. It was assumed that size and metal

concentration in surface samples (<30 cm) were representative of the entire deposit. A previous study of Turkey Creek analyzed in-channel depth-integrated core samples and found that Pb and Zn concentrations in sediment were highly elevated throughout the entire unit without correlation to vertical extent indicating that sediment has been impacted by mining waste all the way down to bedrock (Smith, 2016). Another study in southeastern Missouri indicated that surficial metal concentrations in bar deposits were representative of the entire deposit (Pavlowsky et al., 2017). When collecting cut-bank samples, a shovel or trowel was used to remove the surficial sediment to give a sampling surface that was unaffected by weathering.

Twenty-two samples were collected from exposed cut-banks at sites M-18.8, M-13.0, M-7.6, M-6.8, M-5.3, and M-0.1 to estimate metal storage throughout the floodplain (Appendix D). The metal stored in-channel will be evaluated against the total metal stored in the floodplain. Three to seven composite samples were collected from exposed sedimentary units at each cut bank based on visible stratigraphic changes within the bank. Bank heights and depths of stratigraphic units were recorded.

Laboratory Methods

All samples were prepared and analyzed at the Ozark Environmental Water Resources Institute (OEWRI) laboratory at Missouri State University in Temple Hall following standard operating procedures. (https://oewri.missouristate.edu/standard-operating-procedures.htm).

Sample Preparation. All sediment samples were placed in a 60 °C oven for several days to dry. Samples were then disaggregated with a mortar and pestle and hand sieved into the following size fractions: <2 mm, 2 – 16 mm, and >16 mm. Sediment <2 mm contains the finer fraction of tailings produced during milling, including some finer tailings particles that were

processed using jigging and tabling. Samples in the <2 mm size fractions also represent the maximum sediment size analyzed from previous studies in Turkey Creek (Pope, 2005; Peebles, 2014; Gutiérrez et al., 2015; Smith, 2016; HGL, 2019). The 2 – 16 mm is the coarse size fraction and represents the largest amount of chat tailings generated by the jigging process. Milling documents do not indicate that sediment >16 mm was processed (Wright, 1918). The max feed to jigs was typically between 7 to 13 mm (Wright, 1918).

Composite Samples. All bed and bar samples were then composited individually at each main channel, tributary, and background site. Composite samples were created by taking an equal mass of sediment from each individual bed or bar sample collected at a given site for both the fine (< 2 mm) and coarse (2 – 16 mm) size fractions (Figure 10). These composite samples were then sieved to <0.25 mm, 0.25 mm – 2 mm, 2 – 8 mm, 8 – 16 mm, and >16 mm; the masses of these size fractions were recorded. Sediment <0.25 mm includes tailings that was generated during flotation methods. The 0.25 – 2 mm size fraction includes the fine material generated during jigging and tabling, but excludes ore processed with flotation. The 2 – 8 mm size fraction represents the coarser sediment creating during milling. The 8 – 16 mm size fraction signifies the coarsest source of contamination. Samples in this size fraction were not often produced during commercial milling, but earlier crude ore processing could have generated chat in this size. Sediment >16 mm is considered uncontaminated and was sampled only to determine the amount of sediment storage (Wright, 1918).

Powdering of Coarse Particles for Geochemical Analysis. Sediment >2 mm was too coarse for direct geochemical analysis by X-ray fluorescence (XRF). This size fraction was placed in a fine mesh sieve and washed under tap water in a laboratory sink to remove fines. Then, it was dried in a 60 °C oven. This composite size fraction was then powdered in a PQ-N04

Planetary Ball Mill before geochemical analysis (Figure 11). Approximately 50 g of sediment was placed in a tungsten carbide container with 12 – 16 ball bearings. Samples were run in the mill for approximately one to two hours or until the sample had been completely pulverized into a fine power.

Geochemical Analysis

All sediment samples were analyzed by a Niton XL3t series handheld X-ray fluorescence (pXRF) analyzer to quantify elemental concentrations in the <0.25 mm, 0.25 – 2 mm, and 2 – 8 mm for bed and bar composites and <2 mm for all other samples for the following elements: Pb, Zn, Fe, Mn, Ca, and Cd. Geochemical concentrations in the 8 – 16 mm size fraction were derived from preliminary data gathered in Turkey Creek gravel bars (Appendix E). A select set of samples were sent to a commercial laboratory for inductively coupled plasma mass spectrometry (ICP-MS) analysis of aqua regia extracts using hot hydrochloric and nitric acids. The geochemical results of the ICP-MS were compared to pXRF using regression analysis to calibrate the Niton XL3t pXRF results to ICP-MS standard results. There is a 1:1 ratio between pXRF and ICP-MS values for Pb and Zn. Therefore, these elements did not require calibration to ICP-MS derived values. The following elements were corrected from pXRF to ICP-MS using specific equations for each element: Fe, Mn, Ca, and Cd (Table 10). Duplicate pXRF samples were analyzed approximately every 15 samples to ensure quality control. The results of the duplicate samples indicate a mean percent difference of 4.2% for Pb, 2.5% for Zn, 2.3% for Fe, 8.0% for Mn, 1.3% for Ca, and 11.8% for Cd.

Bulk Sediment Density

Bulk sediment density was used to convert the volumetric storge to mass and account for void space within a given deposit. Bulk density values were not determined directly for this study but were assumed from previously reported values. Gravel bed streams typically have a bulk sediment density ranging from 1.7 to 2.6 g/cm^3 with a mean of 2.1 g/cm^3 (Bunte and Abt, 2001; Milhous, 2002). For active channel sediment, this study will use a bulk density of 1.9 Mg/m^3 for fines (<2 mm) and 2.2 Mg/m^3 for coarser sediment (2 – 16 mm) (Manger, 1963; Bunte and Abt, 2001; Pavlowsky et al., 2017). Bulk sediment density for floodplain sediment ranged from 1.2 to 1.6 Mg/m^3 determined from SSURGO data (NRCS, 2020). A value of 1.4 Mg/m^3 was selected for all floodplain deposits.

Sediment Storage Calculations

Sediment storage was calculated using field measurements from in-channel geomorphic features. As described above, each landform is described by the following variables: width, depth or height above water surface, thickness, area, void, and actual area (Table 11). Width, depth, and height above water surface were measured in the field. For the bed, thickness was calculated as the depth of the bedrock relative to water surface minus the average bed depth. For bars, chutes, and benches, thickness was calculated as the height above water surface plus the depth of bedrock relative to water surface. Thickness was multiplied by the measured width of a given feature to calculate the area. If void space was observed, the area was reduced by the estimated percentage of void space (Table 11 and Table 12). If different forms of the same deposit type were found at a transect with different heights of adjacent bar deposits or bars separated by a channel bed or bar, the features were sampled and geochemically analyzed separately. The

geometry of these multiple features was combined using their measured geometries to represent a total feature volume. The total volume of these features was calculated, and they were treated as a weighted percentage of the whole. For example, if a low bar and high bar were observed at a transect, they were sampled and measured individually. If the low bar has a volume of 2 m^3/m and the high bar has a volume of 3 m^3/m, the low bar will represent 40% of total bar storage and the high bar will represent 60% of total bar storage. Splitting similar features in this manner allows for induvial feature concentrations to be applied to total geomorphic unit storage.

The sediment and metal storage values in the active channel sediment were calculated for each in-channel geomorphic unit from field measurements and geochemical analysis. The steps taken to calculate storage are as follows: (i) average cross-sectional area of the deposit within the surveyed reach length was calculated from field measurements by multiplying the width of the deposit by its depth to bedrock; (ii) bulk density of the deposit was multiplied by the volume to yield sediment mass; (iii) sediment mass was multiplied by geochemical elemental concentrations with the background value removed to quantify the mass of mining sourced Pb and Zn within a given unit for each size fraction; (iv) storage of each feature at a transect was added together to represent total in-channel storage; and (v) storage values at each transect of a reach were averaged to represent mean longitudinal storage. Storage values were then divided by the reach length to report unit storage in the mass of sediment or metal stored within a longitudinal meter.

Background metal concentrations were subtracted from total metal analyses of sediment samples for use in storage calculations to assess mining metal storage (also including metals potentially from other anthropogenic sources). Background concentrations for active channel and bank deposits were determined from two sites located in the Turkey Creek watershed and one

site located in Grove Creek in the eastern adjacent watershed (Figure 7). Three in-channel samples at sites B-1 and B-2 indicate a background of (i) 81 ppm Pb and 209 ppm Zn for sediment <2 mm and (ii) 69 ppm Pb and 117 ppm Zn for sediment 2 – 16 mm. Floodplain sampling in three uncontaminated mining sites from five samples indicates background floodplain sediment concentrations of 48 and 253 ppm for Pb and Zn, respectively. These results agree with other studies which estimate the background values of Pb and Zn between 20 – 91 ppm Pb and 100 – 433 ppm Zn (Table 13) (Pope, 2005; Smith et al., 2013; USFWS, 2013; Gutiérrez, et al., 2016). The background values in the TSMD are greater than the national baseline of 20 ppm Pb and 91 ppm Zn (Horowitz and Stephens, 2008). Given that mineralized ore bodies and the mining industry were widely dispersed throughout TSMD, the background streams sampled for this study may have been enriched by mining-related metals to some degree.

Analysis of Geomorphic Variables

The following variables were used to examine relationships among geomorphic variables and channel storage of contaminated sediment: (i) probe depth (measured at the thalweg), (ii) active width, (iii) bankfull width, (iv) floodplain width, (v) slope, (vi) distance downstream, and (vii) drainage area. Probe depth, active width, and bankfull width were determined from field measurements. Floodplain width, slope, distance downstream and drainage area were calculated in ArcGIS. These physiographic variables were then compared to volumetric storage using linear regression modeling. Regression analysis of these variables with sediment storage variables was used to assess which variables are the best indicators of total storage. However, certain variables such as active channel width and average bed depth that were used to calculate volume could result in an inflated R^2 value.

Slope. A 1 m digital elevation model (DEM) was obtained from the Nation Map as part of the 3D Elevation Program and used to calculate slope in the Turkey Creek watershed (USGS, 2020a). The elevations present in this DEM were produced from light detection and ranging data at a resolution of one meter or higher. At each site, a point was placed at site specific transect spacing for three times the sample reach length. At each of these points, the elevation was extracted from the DEM. The slope was then calculated using a simple rise over run equation. The difference in elevation was divided by their distance from each other. Site T-9.2's slope was calculated using the road next to it due to its narrow channel width.

Drainage Area. The drainage area for the entire Turkey Creek watershed was obtained from Watershed Boundary Dataset (USGS, 2020b). These watersheds were determined from topographic and hydrologic features at a 1:24,000 scale (USGS and USDA, 2013). The sub-basin drainage area at each site was calculated in ArcGIS as follows: (i) a 1m DEM was converted to a coverage raster and mosaiced into a single dataset, (ii) the create mosaic tool was used on these coverages to create a single dataset, (iii) a depressionless DEM fill layer was created from the mosaic dataset, (iv) a flow direction layer was created from the fill layer, (v) a flow accumulation layer was created from the flow direction layer, (vi) pour points were created at the first transect for each site and snapped to the highest flow accumulation cell within a 50 m radius, and (vii) the watershed tool was used to calculate the drainage area at the pour point for each reach. For M-0.1, there was no 1m DEM available, so a 3m DEM was used to calculate the Ad at this site following the above procedures.

Floodplain Width. The NRCS soil survey map was used to delineate floodplains throughout the watershed (NRCS, 2020). Mean floodplain width was calculated at each reach with measurements centered on each transect. These measurements were orthogonal to the

channel and stretched across the entire floodplain. The average of these measurements was used as the mean floodplain width in a given reach.

Table 9. Location and characteristics of sampled sites.

Site		Coordinates								Influence	
#	Name	Latitude	Longitude	Length (m)	R-km	Slope	Elevation (m)	Ad (km^2)	Ad Composed of Mined Lands (%)	Mining	Urban
1	M-18.8	37.0902	-94.4605	180	18.8	0.0037	297.7	38.2	2.5	0	3
2	M-17.6	37.0949	-94.4704	120	17.6	0.0027	294.1	41.7	2.3	0	3
3	M-15.8	37.1009	-94.4858	180	15.8	0.0042	288.1	54.7	3.0	1	3
4	M-13.0	37.1080	-94.5085	120	13	0.0040	281.1	60.8	2.7	0	2
5	M-11.5	37.1110	-94.5225	180	11.5	0.0033	276.7	81.0	2.3	0	2
6	M-9.0	37.1142	-94.5453	120	9	0.0035	268.3	93.2	3.6	2	1
7	M-7.6	37.1185	-94.5578	300	7.6	0.0021	265	99.4	3.9	3	1
8	M-6.8	37.1198	-94.5644	240	6.8	0.0026	262.9	100.0	3.9	2	1
9	M-5.3	37.1201	-94.5774	240	5.3	0.0016	259.9	104.8	3.8	2	0
10	M-1.9	37.1270	-94.6095	240	1.9	0.0023	251.8	112.5	4.6	2	0
11	M-0.1	37.1284	-94.6253	200	0.1	0.0016	247.7	118.5	4.4	0	0
T1	T-16.2	37.1104	-94.4726	108	16.2	0.0046	298.8	8.2	7.3	1	3
T2	T-11.7	37.0714	-94.4855	30	11.7	0.0016	308.4	2.8	6.8	1	2
T3	T-9.2	37.1081	-94.5421	30	9.2	0.0133	277.3	3.1	15.0	3	1

Table 10. Calibration curves to convert concentrations from Niton XL3t pXRF to ICP-MS aqua regia to values. $pXRF_{ppm}$ denotes the value determined from geochemical analysis with the handheld Niton XL3t pXRF.

Element	Equation	R^2
Ca	$(-0.000003 * pXRF_{ppm})^2 + (1.3993 * pXRF_{ppm}) - 3221.2$	0.975
Cd	$(1.6804 * pXRF_{ppm}) - 15.905$	0.928
Fe	$0.438 * pXRF_{ppm}^{1.082}$	0.912
Mn	$1.034 * pXRF_{ppm}^{1.004}$	0.821

Table 11. Description of field measurements.

Unit Feature	Description
Active Channel Width (m)	The horizontal distance between the left and right bank relative to water level.
Bankfull Channel Width (m)	The horizontal distance between the left and right bank-tops.
Offset Width (Left and Right) (m)	The horizontal distance between the toe and top of the bank.
Bank Height (Left and Right) (m)	The height of the bank relative to thalweg.
Bankfull Minimum (m)	The height of the lower bank. This represents the water depth required to reach bankfull stage.
Max Water Depth (m)	The depth of the thalweg at water surface.
Max Probe Depth (m)	The refusal depth of a tile probe at the thalweg.
Max Bedrock Depth (m)	The depth of bedrock relative to water surface measured at the thalweg.
Deposit Width (m)	The lateral width of the deposit.
Deposit Depth (m)	The average depth of the bed below water surface. The average was taken from three to five measurements with one measurement including the thalweg.

Table 11 continued.

Unit Feature	Description
Deposit Height Above Water Surface (m)	The average height of the deposit above water surface. The average was taken from three to five measurements.
Thickness (m)	The distance from the top of the feature to the depth of bedrock measured at the thalweg.
Fine Depth (m)	The refusal depth of a tile probe at the top a bench or chute.
Area (m^2)	The cross-sectional area of a deposit calculated from width and thickness.
Bench/Chute Total Area (m^2)	The cross-sectional area of a bench or chute calculated from width and thickness.
Bench/Chute Upper Area (m^2)	The cross-sectional area calculated from the width and fine depth of a bench or chute. Only this is counted towards bench or chute storage.
Bench/Chute Lower Area (m^2)	The cross-sectional area calculated from the width and depth to bedrock minus the fine depth of a bench or chute. This area is counted towards bar storage.
Void (fraction)	The visually estimated area taken up by obstructions at the transect.
Area-act (m^2)	The cross-sectional area with the void space removed.

Table 12. The equations used to calculate storage variables (Figure 9).

Variable	Equation
Bankfull Width	active width + left offset width + right offset width
Max Bedrock Depth	max water depth + max probe depth
Thickness	height above water surface + depth of bedrock
Area	thickness * width
Bar Area	(thickness * width) + chute deposit lower area + bench deposit lower area
Area-act	area – (area * void)
Chute or Bench Deposit Upper Area	width * fine depth
Chute or Bench Deposit Lower Area	(chute or bench deposit total area-act) – (chute or bench deposit upper area)

Table 13. Background values of in-channel and floodplain sediment determined from background sampling (Appendix D).

	In Channel Sediment		
Metal (ppm)	<2 mm	2 - 16 mm	Floodplain Sediment
Pb	81	69	48
Cv%	11.8	4.6	42.2
Zn	209	117	253
Cv%	58.2	35.1	64.2

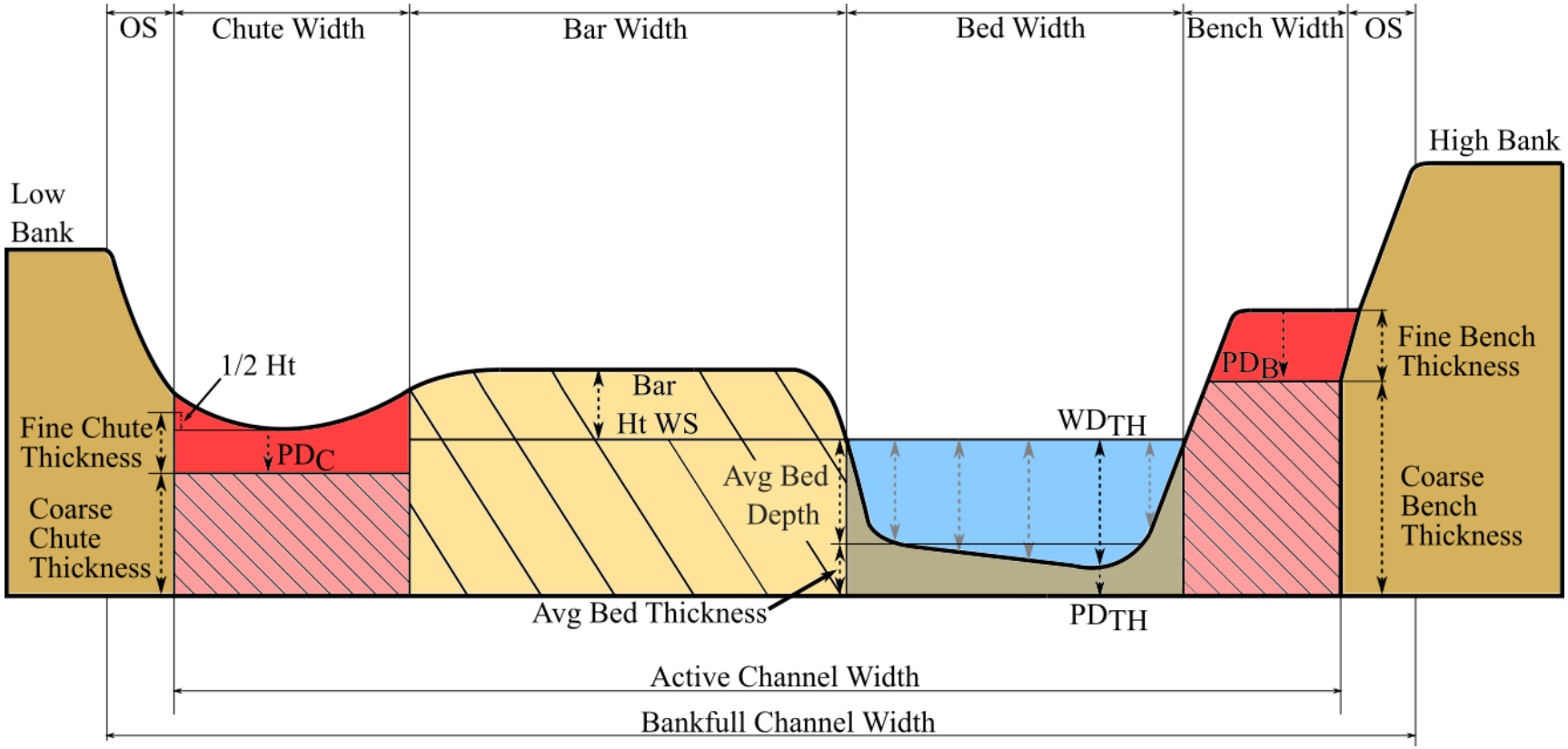

Figure 9. Cross-sectional view of sample reach describing channel features sampled in this study. OS represents bank offsets. WS denotes water depth. PD_C, PD_B, and PD_{TH} represents the probe depths of the chute, bench, and thalweg, respectively. WD_{TH} shows the water depth at the thalweg.

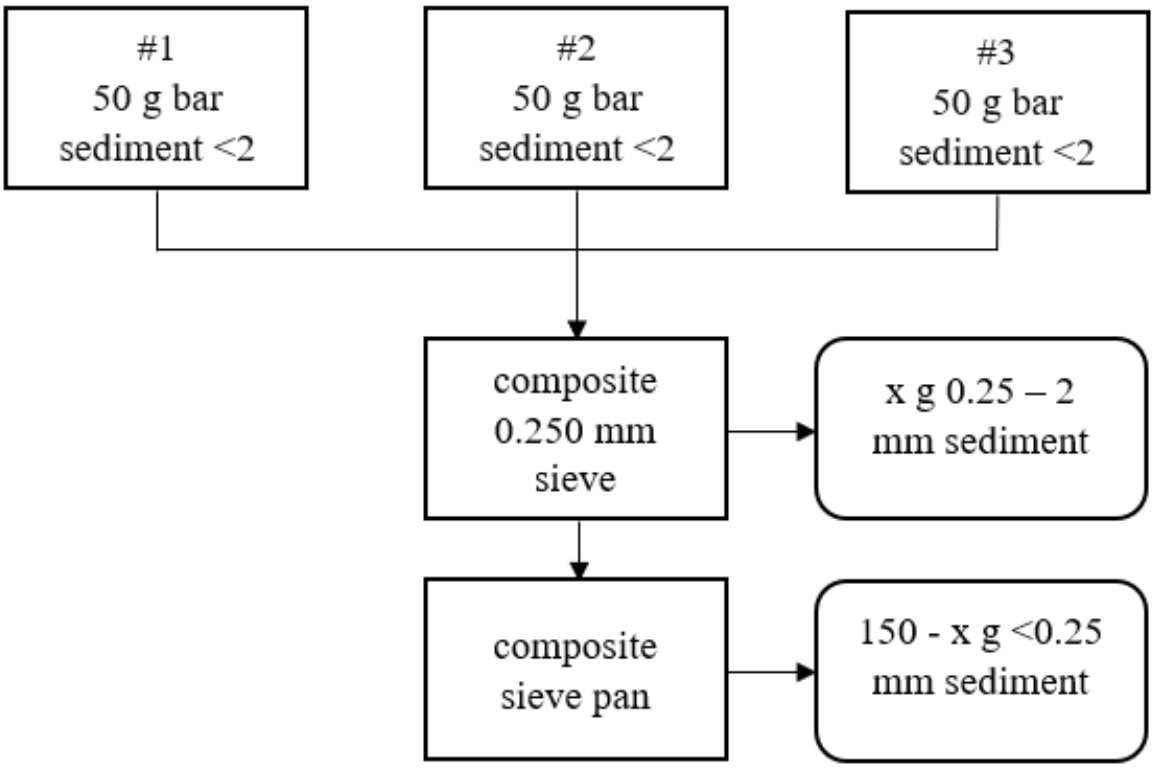

Figure 10. Process used to create composite samples from sediment samples sieved to <2 mm. The same process was used with sediment samples between 2 – 16 mm to create composite samples for the 2 – 8 mm and 8 – 16 mm size fractions.

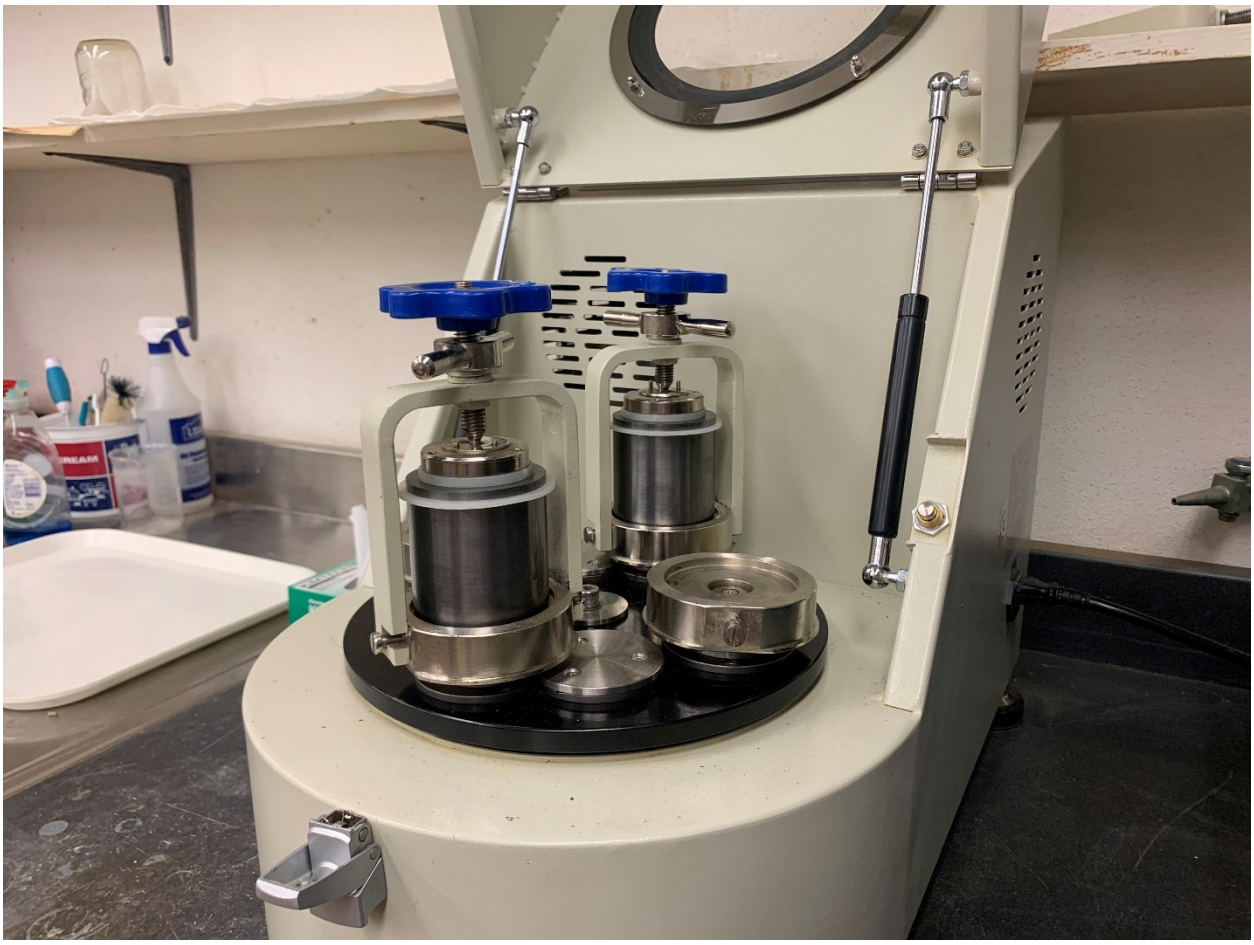

Figure 11. The ball mill used to crush coarse sediment into a fine powder.

RESULTS

Channel Sites and Sediment Sampling

Eleven main channel sites and three tributary sites were sampled in the Turkey Creek watershed. The eleven main channel sites were labeled by a river-kilometer (R-km) along the centerline of the channel with zero at the mouth and distance increasing upstream (Figure 7 and Table 9). A total of 92 active channel sediment samples and 22 bank samples were collected for geochemical and textural analysis (Appendix D). Three channel sediment and five bank deposits samples were collected at background sites assumed to be upstream of mining influence. Of all the active channel sediment samples, 35% were bar deposits, 43% were bed deposits, 20% were bench deposits, and 2% were chute deposits.

Contaminated Sediment Evaluation

The Tri-State Mining District specific probable effects concentration (TSMD-PEC) is commonly used by project managers to determine if sediment is contaminated and will have negative effects on local biota. The TMSD-PEC values for Pb and Zn in fine sediment (<2 mm) are 150 ppm and 2,083 ppm, respectively (Ingersoll et al., 2009). Background values were not removed when considering exceedances above the TSMD-PEC since both natural and anthropogenic concentration values should be considered in this threshold (Table 13). Sediment data indicates that channel deposits are frequently elevated above the TSMD-PEC indicating that the entire sampled channel was contaminated by past mining activity (Table 14). Metal concentrations in the 25th percentile were present at concentrations near or just above the TSMD-PEC threshold. Every site contained metal concentrations in fine sediment that exceeded the TSMD-PEC for either Pb or Zn. Only four sites (M-18.8, M-17.6, M-15.8, and T-16.2) did not

exceed the TSMD-PEC threshold for sites for both Pb and Zn. Due the high metal concentrations in channel deposits, all in-channel sediment is considered contaminated sediment.

Longitudinal Volume and Mass Storage. Volume and mass storage exhibited similar trends since mass storage was calculated from volume storage using bulk density values (Figure 12). Generally, storage values increased in mined areas, and decreased outside of them (Figure 7). Sites between R-km 8 and R-km 18.8 had storage values ranging from 5 Mg/m – 67 Mg/m (3 m^3/m – 31 m^3/m) while sites between R-km 0 and R-km 8 had storage values ranging from 67 – 128 Mg/m (31 m^3/m – 60 m^3/m). The lowest storage values were generally observed at sites between R-km 13 and R-km 18.8 where storage was less than 16 Mg/m (8 m^3/m). Site M-7.6 stored the most sediment at 128 Mg/m (60 m^3/m) (Appendix F and Appendix G). This is significantly higher than the other five sites with the highest storage values (M-11.5, M-0.1, M-5.3, M-6.8, and M-1.9) which ranged from 67 Mg/m (31 m^3/m) to 84 Mg/m (39 m^3/m). Both volume and mass storage increased throughout the channel, peaked at R-km 7.6, and then decreased between R-km 7.6 and R-km 0. The largest storage values are observed in or near mining drained areas (Table 9). The high storage values observed in mined areas could be related to an input of sediment generated during mining activity (Lewin and Macklin, 1987).

Longitudinal Mass Storage by Deposit Type. The percent distribution of sediment stored in various channel deposits varied with downstream distance (Figure 13 and Figure 14). In general, the percentage of bar storage in the channel increased downstream, while the percentage of bed storage decreased. Bed deposits at sites between R-km 13 and R-km 18.8 stored slightly more sediment than bar deposits and represented approximately 46 - 61% of total in channel storage. Bars stored the greatest percentage of sediment at sites between R-km 0 and R-km 14 and often represented greater than 75% of mass storage in this portion of Turkey Creek. Bench

and chute storage increased throughout the channel until around R-km 5 and decreased between R-km 5 and R-km 0. When present, benches and chutes typically represented between 5 - 13% of mass storage. The increase in bar storage could be caused by bar aggradation associated with an input in sediment as a result of sediment generated during mining operation (Jacobson, 1995).

The greatest relative bed storage was observed at site M-18.8 which stored 61% of in-channel sediment, and the largest relative bar storage was observed at site M-1.9 with 85% storage. Bench and chute storage was less than bed and bar storage at every site when these features were present. The greatest bench storage was observed in M-9.0 which represented a total of 22% sediment storage. This high percentage of bench storage is related to a large amount of bedrock exposed in the channel bed which limited the deposition of bed sediment at site M-9.0 which had an average probe depth of only 0.06 m. Bedrock controls can limit the amount of storage creating local variability in storage values (Graf, 1996).

Sediment Size Distribution. Sediment size distributions in channel deposits varied with downstream distance (Figure 15 and Figure 16)**.** Coarse sediment is often overlooked when assessing contamination in streams. The coarse (2 – 16 mm) size fraction stored the greatest amount of sediment throughout the main channel and represented approximately 50 - 60% of active channel storage. The lowest percentage of 2 – 16 mm sediment was observed in mining areas between R-km 5 and R-km 13 which represented approximately 50% of active channel storage. The >16 mm size fraction was the next most significant source of sediment comprising approximately 25 – 30% percent of relative active channel storage. The percent of sediment in this size fraction increased at sites between R-km 18.8 and R-km 14 from approximately 28% to 32% relative channel storage. At sites between R-km 0 and R-km 14, the percent of >16 mm sediment began to decrease from about 32% to 25% of relative active channel storage. Despite

being less mobile than fine sediment, the coarse fraction can remain in the channel for longer periods of time and serve as a secondary source of contamination as metal is released through dissolution and abrasion (Pavlowsky et al., 2017).

The <2 mm fraction accounted for the least amount of sediment contained in channel deposits representing 10-20% of contaminated sediment storage (Figure 16). Generally, the percent of fine sediment increased in mined areas and decreased downstream from them. The percent of <2 mm sediment increased throughout the channel from 15% to 22% from R-km 18.8 to around R-km 7 where it began to decrease to approximately 13%. Also at R-km 7, the percent of 2 – 16 mm sediment began to increase from approximately 50% to 62%. The greatest percentage of <2 mm sediment was generally observed at sites that drained large amounts of mined areas (Table 9). There was an inverse relationship between the relative amount of <2 mm and 2 – 16 mm sediment with downstream distance. The amount of 2 – 16 mm sediment increased near and downstream from mining areas, while the amount of <2 mm sediment decreased. The increased percentage of fine sediment near mined areas suggests that large amounts of fine sediments in the channel originated from milling operations (Gibson, 1972). However, this difference may also be explained by differences in transportations rates between fine and coarse sediment (Macklin and Dowsett, 1989).

Percent <2 mm Mass Storage by Deposit Type. There was little longitudinal variation in the percent of <2 mm sediment stored within different geomorphic deposits (Figure 17). Bar sediment contained slightly more fine sediment which was expected since bar deposits form at a higher elevation and are subjected to lower flow energy compared to the bed (Bridge, 2009). The percent of <2 mm sediment in bed deposits increased from approximately 10% to 15% at sites between R-km 18.8 to R-km 7 then decreased from about 15% to 10% between R-km 7 to R-km

0. The percent of <2 mm sediment remained consistent throughout the channel in bar deposits and represented approximately 15% of bar storage. The percentage of fine sediment in benches increased when progressing downstream. Benches below R-km 9 were greater than 95% fine sediment. The percent of <2 mm stored in bed and bar deposits remained fairly consistent with downstream distance and ranged from 5 - 20%.

Geomorphic Characteristics

Volumetric storage was assessed for longitudinal trends with several geomorphic variables: channel width (active, bankfull, and floodplain), slope, downstream distance, depth to bedrock, and drainage area. Equations were derived from linear regression analysis for these geomorphic characteristics and volumetric storage to determine which geomorphic characteristics could predict channel storage. Tributaries were not included in the analysis of sediment storage and geomorphic relationships due to their different characteristics. Volumetric storage correlated with active ($R^2 = 0.97$) and bankfull width ($R^2 = 0.96$), slope ($R^2 = 0.70$), R-km ($R^2 = 0.74$), probe depth ($R^2 = 0.68$), and drainage area ($R^2 = 0.83$). There was no relationship between sediment storage and floodplain width.

As expected, geomorphic variables were often correlated in Turkey Creek (Figure 18). For example, slope and R-km were inversely correlated ($R^2 = 0.72$) since the highest areas of slope were observed in the upstream portions of the channel. Slope and active channel width were also inversely correlated ($R^2 = 0.61$) indicating that higher channel slopes occur upstream along smaller headwater channels. Active channel width and R-km were positively correlated ($R^2 = 0.57$) indicating that higher channel widths were observed in the downstream portion of Turkey Creek.

Width. Both active channel ($R^2 = 0.97$) and bankfull ($R^2 = 0.96$) width are excellent predictors of the volume of contaminated sediment storage. However, there was no correlation between floodplain width and in-channel sediment storage. Sediment storage was shown to increase linearly with an increase in both active and bankfull channel widths (Figure 19).

Slope. Storage correlated inversely with slope ($R^2 = 0.70$) (Figure 20). Sites with a slope <0.0035 exhibited storage values greater than 30 m^3/m while sites with slopes >0.0035 stored less than 10 m^3/m. This suggests that storage is reduced in segments of the stream with high slopes. Reaches with higher slopes typically store less sediment due to greater stream power and higher transport capacity.

R-km. Storage linearly correlated with R-km ($R^2 = 0.74$) (Figure 21). This trend indicates that more sediment is generally stored in downstream sections of Turkey Creek. This can be partially attributed to an increase in channel width with distance downstream and decrease in slope and sediment transport capacity downstream which leads to an increase in sediment storage.

Depth to Bedrock. Storage linearly correlated with depth to bedrock ($R^2 = 0.68$) with storage values increasing with depth to bedrock (Figure 22). This is intuitive since reaches with a greater probe depth are storing more bed sediment and add to the vertical extent of bar storage too. However, sites M-18.8 (6.6 m^3/m), M-17.6 (7.5 m^3/m), and M-13.0 (4.1 m^3/m) exhibited significantly lower storage values with respect to the trend. This can be explained by relatively narrow active channel widths and generally steeper slopes indicating transport conditions rather than deposition on the bed.

Drainage Area. Storage linearly correlated with watershed area ($R^2 = 0.83$) with an increase in drainage area leading to an increase in storage. However, sites M-9.0 and M-7.6 did

not fit this trend well. Site M-7.6 had the greatest storage value (60.2 m^3/m) compared to all other sites, and site M-9.0 stored relatively little sediment (2.5 m^3/m) compared to other sites with similar drainage areas. This low storage value can be explained by a large amount of observed exposed bedrock (Figure 23).

Larger channel width and an increased depth of bed sediment tend to result in greater areas of storage. However, storage can be reduced in these areas by reach scale variability such as bedrock control and valley confinement (Graf, 1996). These local variations can reduce the precision of relationships between geomorphic variables and sediment storage.

Metal Concentrations

Metal Concentrations by Size Fraction. It is generally assumed that the highest concentrations are associated with the smallest grain size fractions (Håkanson, 1984; Horowitz, 1991). However, the results of the geochemical analysis indicate that this assumption is not always true (Ferguson, 2021) (Table 15). Mean Pb concentrations were highest in the 0.25 – 2 mm size fraction for bed (996 ppm) and <0.25 mm fraction for bar (436 ppm) sediments. Mean Zn concentrations were highest in the <0.25 size fraction for bed (5,820 ppm) and 0.25 – 2 mm size fraction for bar sediments (5,783 ppm). Mean metal concentrations in the 2 – 8 mm size fraction were lower than the finer size fractions. Mean Pb concentrations in the 2 – 8 mm size fraction for bed and bar deposits were 86 ppm and 75 ppm, respectively. Zn concentrations in the 2 – 8 mm size fraction for bed and bar deposits were 2,119 ppm and 2,488, ppm respectively. The lowest concentrations were observed in the 8 – 16 mm size fraction which had mean concentrations of 60 ppm Pb and 1660 ppm Zn. Metal concentrations were generally highest in the fine size fractions and lowest in the coarsest size fractions. High metal concentrations in fine

sediment present a hazard to the environment since they can be readily bioavailable (John and Leventhal, 1995).

Longitudinal Trends in <2 mm Sediment. Lead concentrations in <2 mm bed and bar sediment exhibited similar longitudinal trends (Figure 24). Pb bed and bar concentrations increased from approximately 80 ppm to 350 ppm at sites between R-km 7 and R-km 18.8. Then, between R-km 0 to R-km 7, bar concentrations declined to 275 ppm and bed concentrations declined to 150 ppm. Then, Pb concentrations in bed sediment decreased more sharply than bar sediment between R-km 4 and R-km 0. Concentrations in bench sediment were similar to bed and bar concentrations at sites between R-km 13 and R-km 18.8. Pb concentrations in bench sediment were similar to bed and bar concentrations at sites between R-km 13 and R-km 18.8. Pb concentrations in bench deposits were much higher than bed and bar deposits between R-km 7 and 9 where Pb concentrations were approximately 1,075 ppm. Concentrations in bench sediment drastically decreased to about 600 ppm at R-km 1.9 where the last bench was observed in the channel. Bed and bar deposits exhibited similar Pb concentrations throughout the active channel with the highest concentrations observed near mining areas.

Zn concentrations generally peaked further downstream compared to Pb concentrations. Zinc concentrations within bed and bar deposits followed similar longitudinal trends, however Zn concentrations in bar deposits were slightly higher than bed deposits (Figure 24). Longitudinal Zn concentrations in bed and bar deposits increased from approximately 2,000 ppm from R-km 18.8 to R-km 4.5 where both bed and bar concentrations peaked at approximately 4,750 ppm and 6,250 ppm, respectively. Between R-km 4.5 and R-km 0, Zn concentrations then declined to 4,125 ppm for bars and 3,125 ppm for beds. Bench concentrations were much greater than bed and bar deposits at sites between R-km 6 and R-km 9 where concentrations were 5,600

ppm to 7,200 ppm. Zn concentrations could have peaked further downstream due to differences in metal transportation rates or spatial and temporal variability in mining production (Gibson, 1972; Macklin and Dowsett, 1989; Johnson et al., 2016).

Longitudinal Trends in 2 – 8 mm Sediment. Lead concentrations in both bed and bar deposited exhibited very similar trends and values (Figure 25). Lead concentrations in bed and bar sediment rose from background concentrations to approximately 120 ppm at sites between R-km 18.8 and R-km 9. Concentrations in bed sediment then decreased to 75 - 100 ppm throughout the remainder of the channel. Overall, there was little longitudinal variation in Pb concentrations between bed and bar deposits.

Zinc concentrations in bed and bar both increased with downstream distance but exhibited different concentrations throughout the channel (Figure 25). Zinc concentrations in 2 – 8 mm bed sediment increased throughout the entire channel. Bed concentrations rose from approximately 500 ppm to 5,250 ppm. Zn concentrations in bar sediment increased from 750 ppm to 4,125 throughout the entire channel. The sharpest increase in bar concentration from 1,750 ppm to 4,150 ppm was observed at sites between R-km 0 and R-km 7. Bar concentrations were higher than bed concentrations between R-km 9.5 and R-km 18.8. Between R-km 0 and R-km 9.5, bed concentrations (1,750 ppm – 5,250 ppm) were higher than concentrations observed in bar sediment (1,500 ppm – 4,125 ppm). Zinc concentrations in both bed and bar deposits increased with downstream distance. However, Zn concentrations in bar deposits were higher at sites between R-km 11 and R-km 18.8 of Turkey Creek, while Zn concentrations in bed deposits were higher between R-km 0 and R-km 11. The downstream trend of increasing Zn concentrations in coarse sediments while Pb concentration remained similar could be caused by the greater number of zinc mines downstream (Figure 7) or the increased mobility of lower

density Zn ore minerals (3.9-4.5 g/cm^3) by fluvial transport compared to Pb (7.4-7.6 g/cm^3) (Klein and Hurlbut, 1985; Macklin and Dowsett, 1989).

Metal Storage Relationships

<2 mm and 2 – 16 mm Metal Storage over Width. Due to the significant relationship between active channel width and volumetric sediment storage, the relationships between active width and metal storage in the <2 mm and 2 – 16 mm size fractions were also evaluated. There was a strong correlation between Zn storage in both the <2 mm ($R^2 = 0.89$) and 2 – 16 mm ($R^2 = 0.99$) size fractions and active channel width (Figure 26). The relationship was not as strong for predicting total Pb storage in the <2 mm ($R^2 = 0.63$) size fraction due to the variation in Pb concentrations throughout the channel. However, there was a high correlation between active channel width and Pb storage in the 2 – 16 mm size fraction ($R^2 = 0.90$). These relationships indicate that there is a strong relationship between active channel width and metal storage by size fraction.

Total Metal Storage over R-km and Width. Both Pb and Zn storage increased throughout the channel up to a certain point, but they did not peak at the same downstream distance (Figure 27). Pb storage steadily increased from nearly 0 kg/m to 12 kg/m with distance downstream at sites between R-km 18.8 and R-km 5. Storage began to decrease to about 3 kg/m between R-km 5 and R-km 0. Zn storage increased from 3 kg/m to 220 kg/m at sites between R-km 18.8 and R-km 3.5. After that point, Zn storage began to decrease to 175 kg/m until the confluence with the Spring River. The greatest storage values for both Pb and Zn were observed at site M-7.6. Both Pb and Zn storage increased with downstream distance and then decreased between R-km 7.6 and R-km 0. However, Pb storage peaked approximately 1.5 km further

upstream than Zn storage. Therefore, it seems likely that Zn and/or contaminated sediment is dispersed more readily downstream compared to Pb.

For both Pb and Zn, total metal storage increased with active channel width (Figure 28). Total metal storage highly correlated with active channel width for both Pb (R^2=0.92) and Zn (R^2=0.97) indicating that total metal storage can be calculated throughout Turkey Creek using active channel width. The strong relationship between active channel width and metal storage indicates that active channel width can be used to predict total metal storage in Turkey Creek.

Percent Storage of Metal by Size Fraction over R-km. Generally, the greatest percentage of Pb storage was associated with <2 mm sediment in mined areas (Figure 29). At sites between R-km 12 and R-km 18.8, Pb was stored in near equal proportions in both the fine and coarse size fractions. Between R-km 12 and R-km 2.5, fine sediment stored the greatest percentage of Pb (up to 84%) which indicates that the fines are the most import sink of Pb contamination in mining areas. The relative amount of Pb stored in fine sediment then decreased from 45% to 20% throughout the remainder of the channel.

The percent of Zn by size fraction exhibited similar trends to Pb discussed above. (Figure 29). At sites between R-km 12 and R-km 18.8, the fine fraction stored approximately 40% of in-channel Zn. Between R-km 5 and R-km 12 the fine fraction stored the greatest relative amount of Zn and represented approximately 60% of storage. At the two farthest downstream sites, between R-km 0 and R-km 2, the fine size fraction stored <40% of Zn. The relative amount of Pb and Zn stored in fine sediment increased in mining areas indicating that mining contamination remains near mined areas.

Percent Metal Storage by Deposit Type. The percent of Pb storage among different deposits was highly variable with downstream distance (Figure 30). Lead storage in bed deposits

was highest at sites between R-km 18.8 and R-km 13 where it represented approximately 50% of storage. Bed storage was lowest at sites between R-km 5 and R-km 8 and represented only 10% of storage. At sites between R-km 0 and R-km 12, bar deposits stored the greatest relative amount of Pb. The relative amount of Pb stored in bar deposits increased throughout the channel and represented greater than 70% of Pb storage between R-km 0 and R-km 8. Relative Pb storage in bench and chute deposits was highest at sites between R-km 13 and R-km 6.5 and represented approximately 30% of Pb storage. When present, bench and chute deposits often stored a greater relative amount of Pb than bed deposits since these deposits are contaminated wholly by fine-grained sediment. In the upstream portion of the channel, bed deposits stored more Pb than bar deposits. However, when progressing downstream, bar storage became significantly greater than bed storage.

The proportion of Zn stored among different in-channel deposits varied longitudinally (Figure 30). Zinc storage in bed deposits was greatest at sites between R-km 9 and R-km 18.8 where storage was often >45%. Bed stored decreased to approximately 10 – 20% at sites between R-km 0 and R-km 9. The relative amount of bar storage throughout the channel increased from 40% to 80% for the entire length of Turkey Creek. The highest percentage of Zn storage in bar deposits was observed at site M-5.3 where it represented 94% of total Zn storage. Bench and chute Zn was greatest between R-km 6 and R-km 13 where they represented approximately 20% of Zn storage. Similar to Pb storage trends, Zn storage in bed deposits decreased with downstream distance and Zn storage in bar deposits increased, greatly surpassing bed storage.

Table 14. Distribution of mining metal concentrations in <2mm sediments in main channel deposits. The number of samples are shown in parentheses (n).

Metal	Deposit	Min	Percentile					Max
			5th	25th	50th	75th	95th	
Pb (ppm)	Bed (26)	110	127	191	305	442	594	651
	Bar (31)	106	131	200	300	395	673	719
	Bench & Chute (15)	67	111	229	397	1,394	1,394	1,765
Zn (ppm)	Bed (26)	1,385	1,672	2,228	3,151	4,293	6,909	8,503
	Bar (31)	1,128	1,312	2,061	3,561	5,925	7,852	11,676
	Bench & Chute (15)	1,224	1,334	1,726	5,736	7,181	8,203	8,822

Table 15. Mean concentrations for bed and bar deposits in composite size fractions. Concentrations for the bar in the 8 – 16 mm size fraction were determined from external data (Ferguson, 2021). The ratios between bar deposit concentrations in the 2 – 8 mm and 8 – 16 mm size fractions were used to estimate metal concentrations for bed deposits in the 8 – 16 mm size fraction.

Metal (ppm)	Bed				Bar			
	<0.25 mm	0.25 - 2 mm	2 - 8 mm	8 - 16 mm	<0.25 mm	0.25 - 2 mm	2 - 8 mm	8 - 16 mm
Pb	413.7	996.3	86.3	69.0	435.9	228.7	75.4	60.4
Zn	5,819.6	4946.2	2,118.9	1,412.6	5,366.6	5,783.1	2,487.9	1,659.6

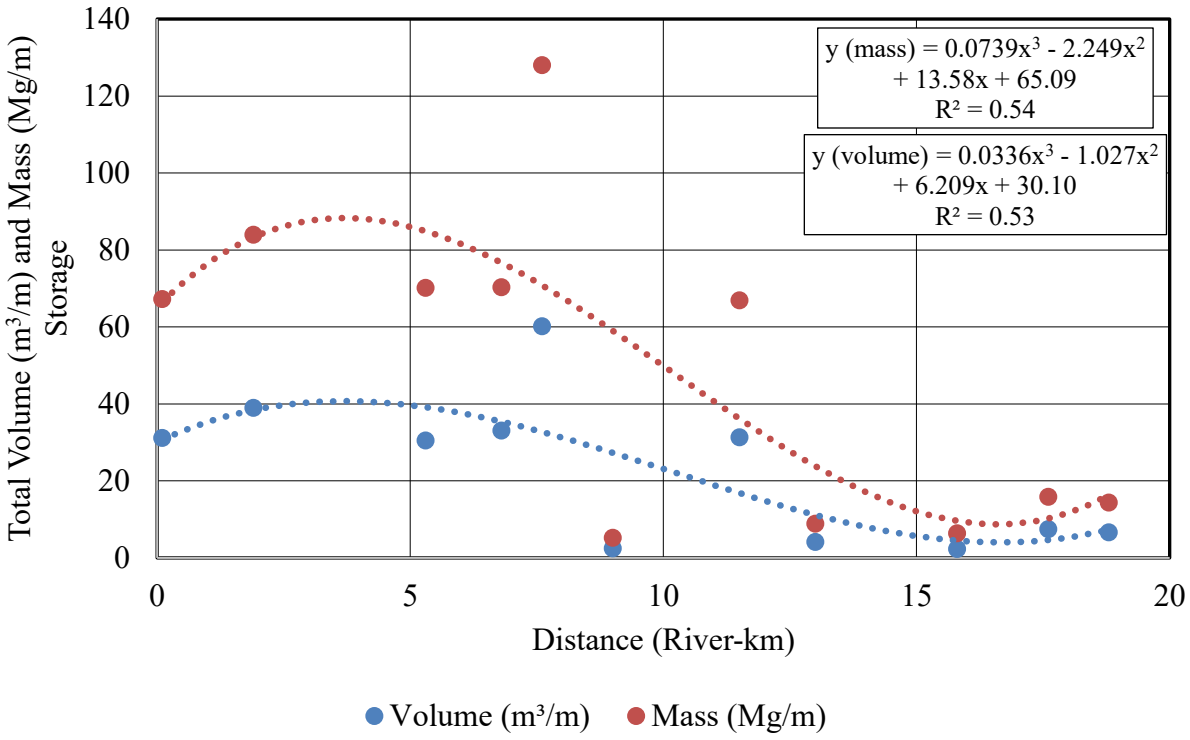

Figure 12. Total volume (m^3/m) and mass (Mg/m) sediment storage.

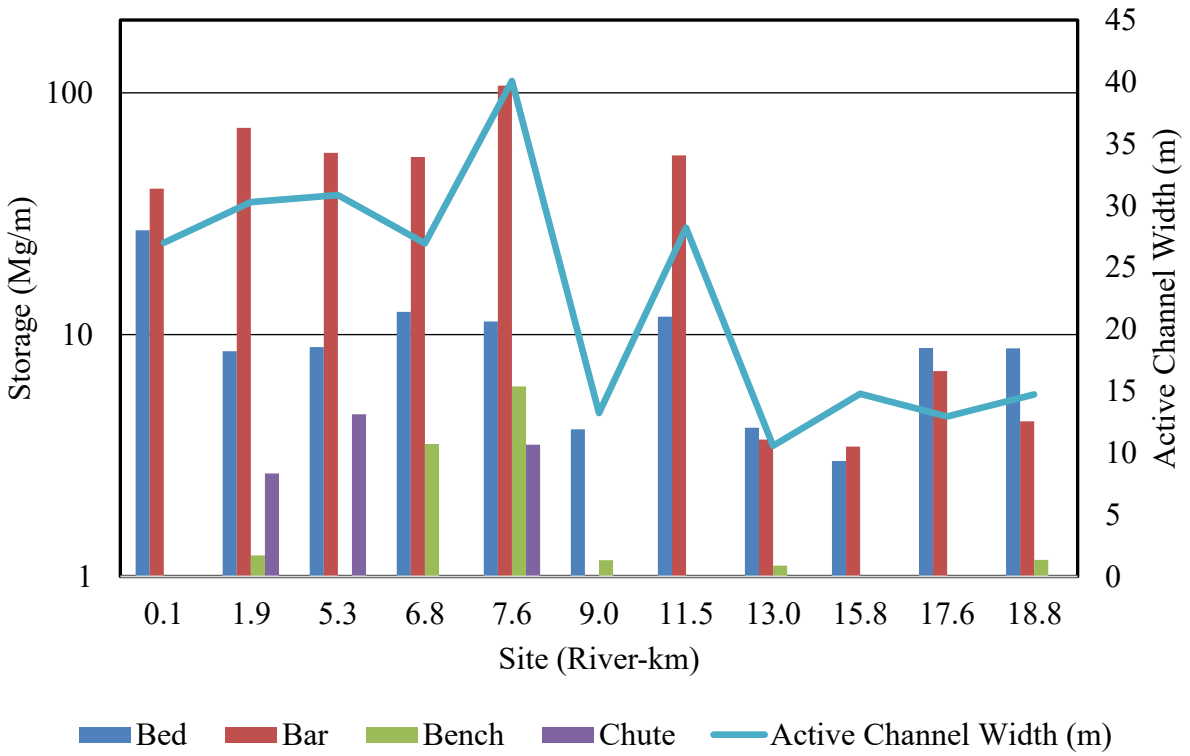

Figure 13. Mass storage by channel deposit type with active channel width on main channel.

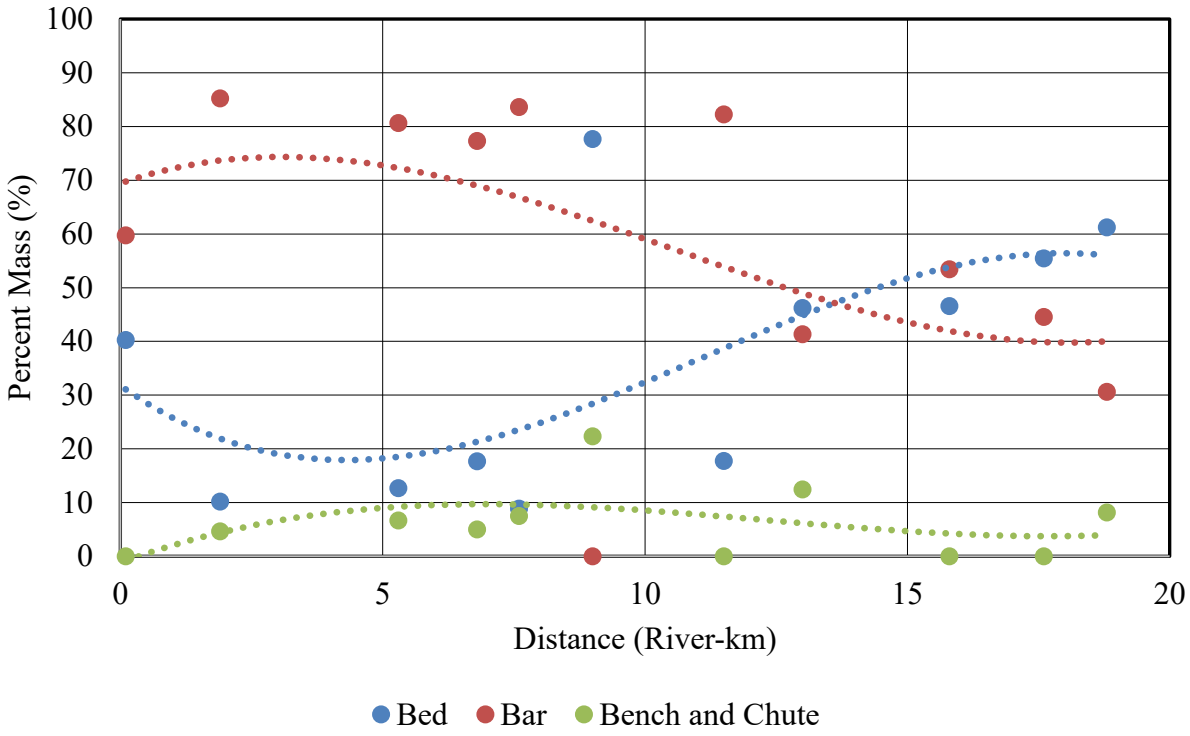

Figure 14. The percentage of total channel storage that each geomorphic deposit contributes with respect to distance downstream on the Turkey Creek main channel.

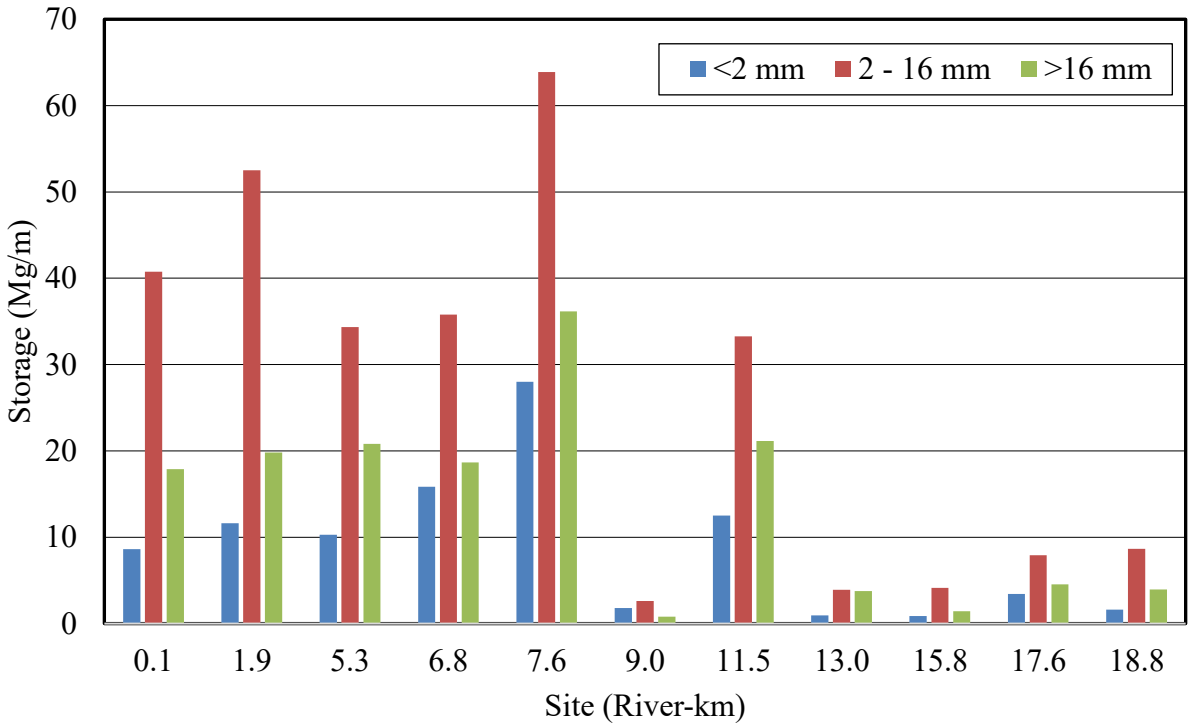

Figure 15. Bar chart size distribution.

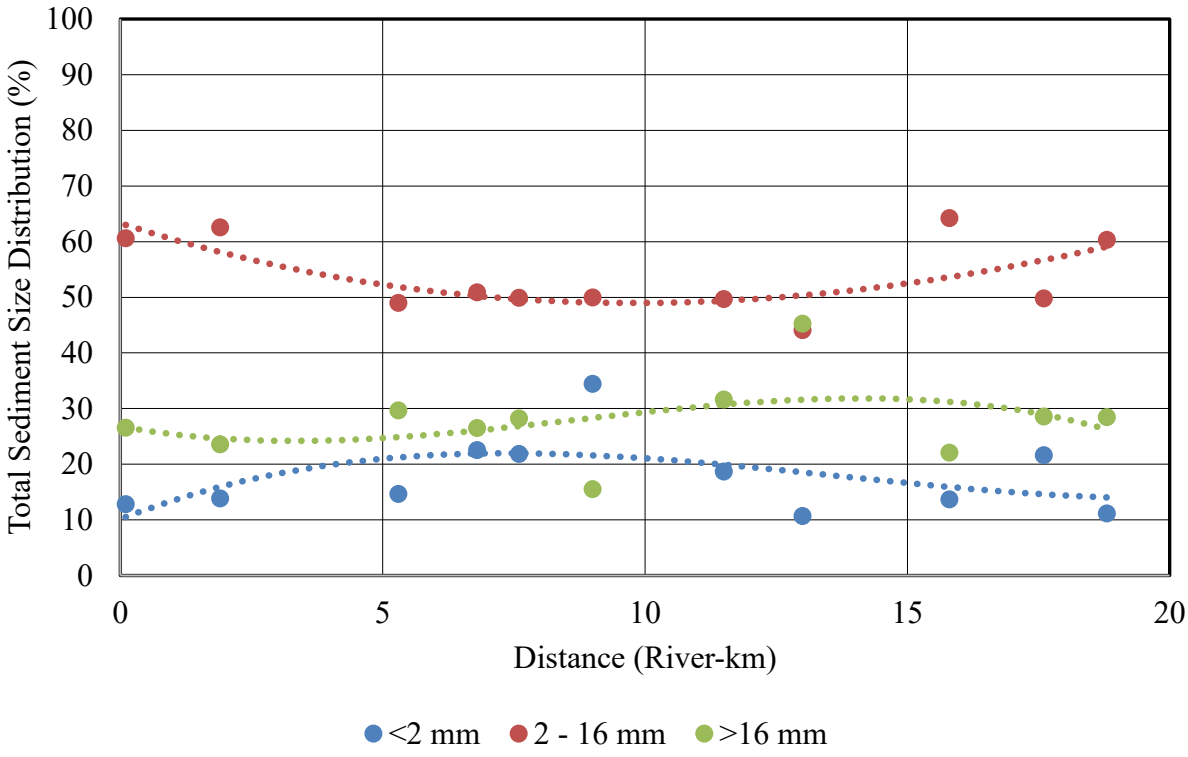

Figure 16. Longitudinal total sediment size distribution by mass in Turkey Creek.

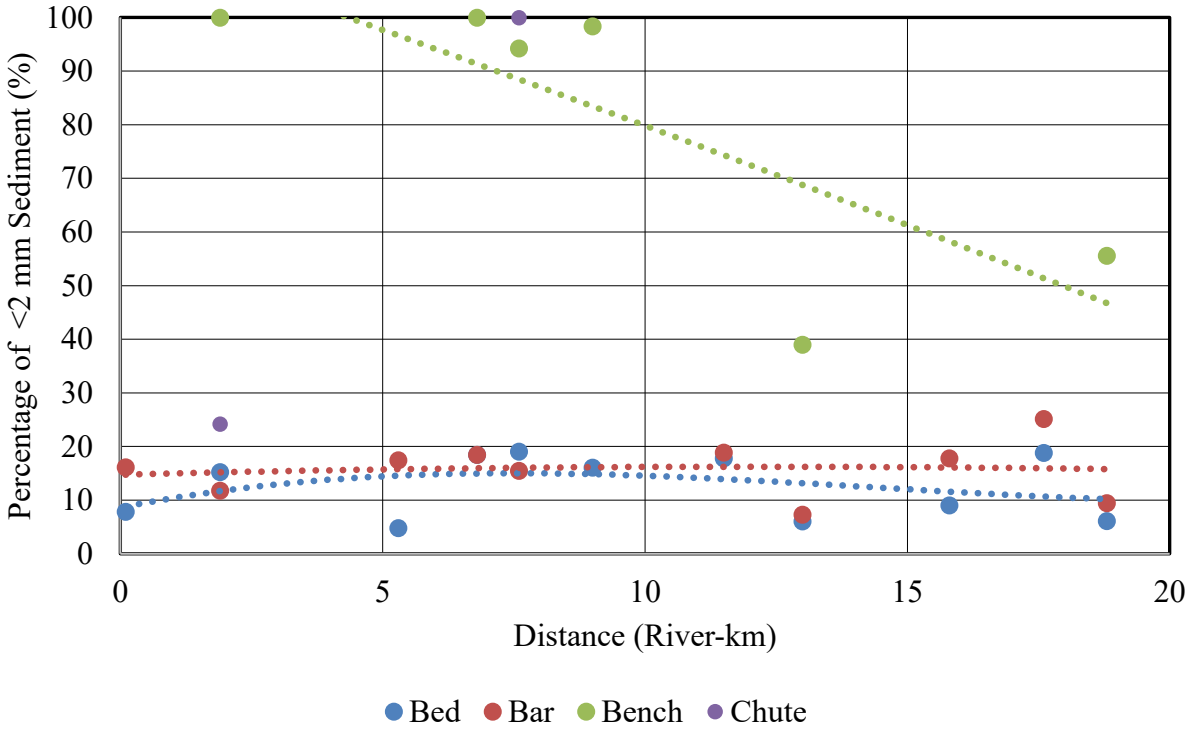

Figure 17. Percentage of <2 mm sediment in each geomorphic deposit.

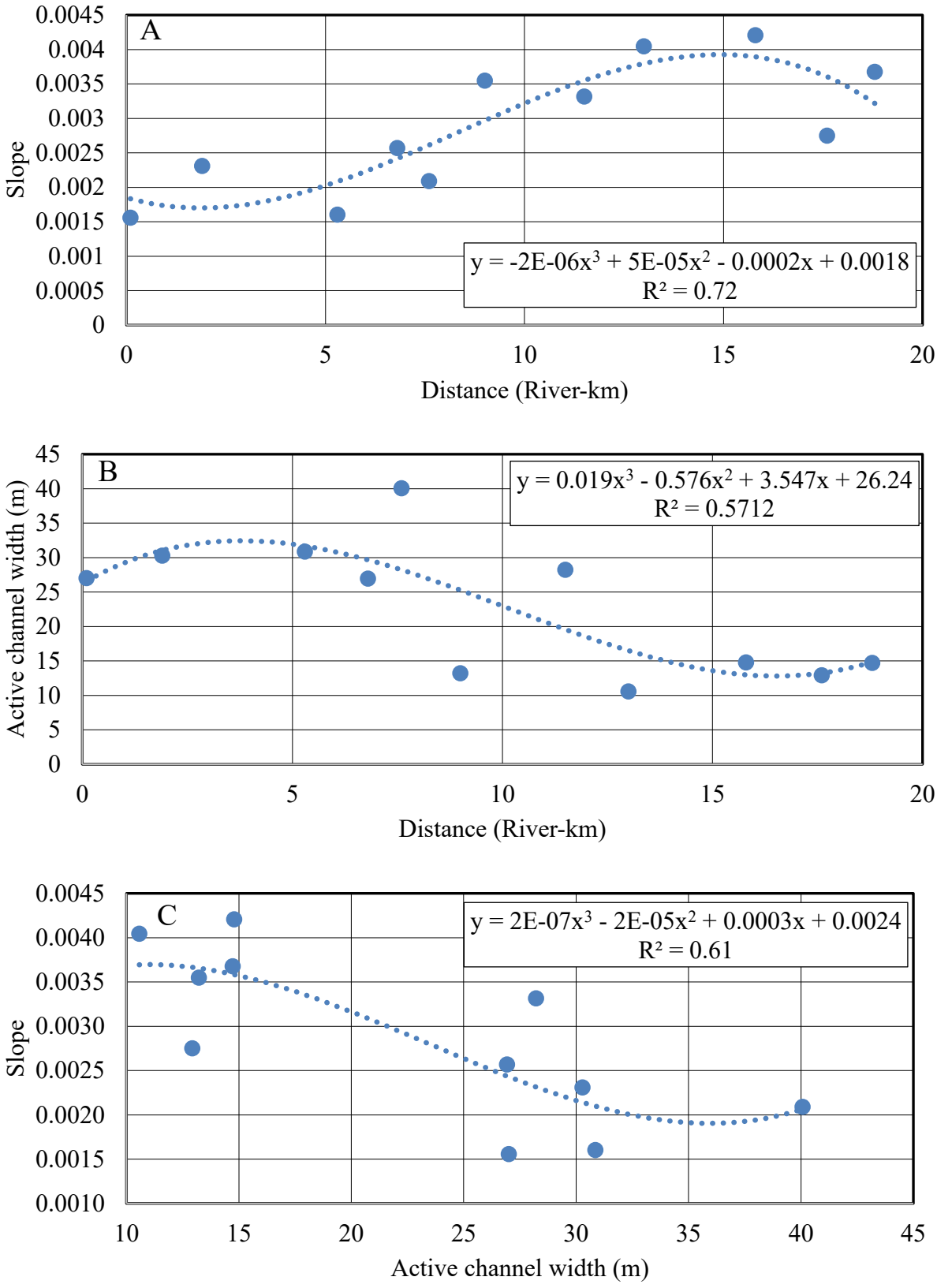

Figure 18. Geomorphic relationships.

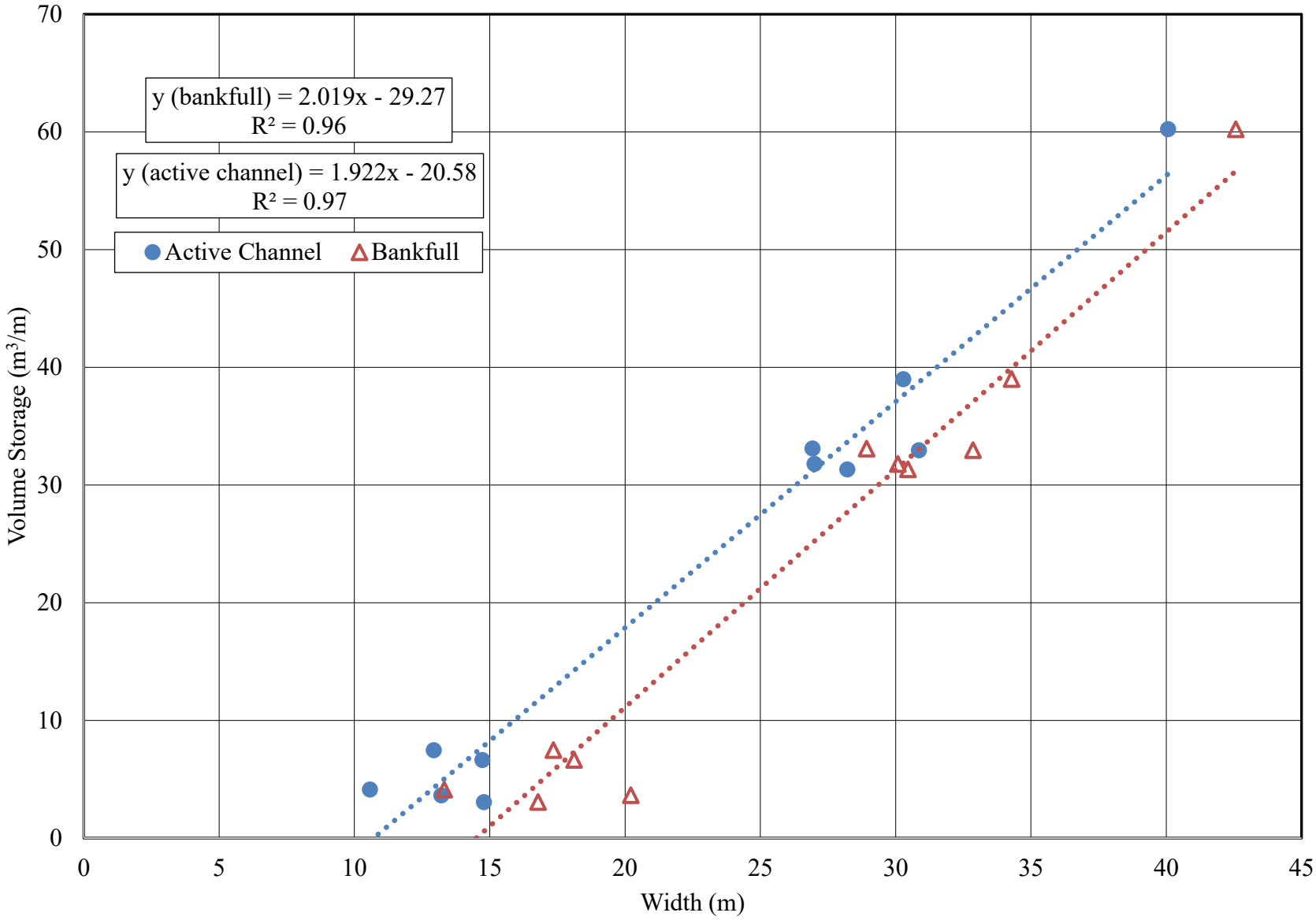

Figure 19. Relationship between volumetric sediment storage and both active channel and bankfull width.

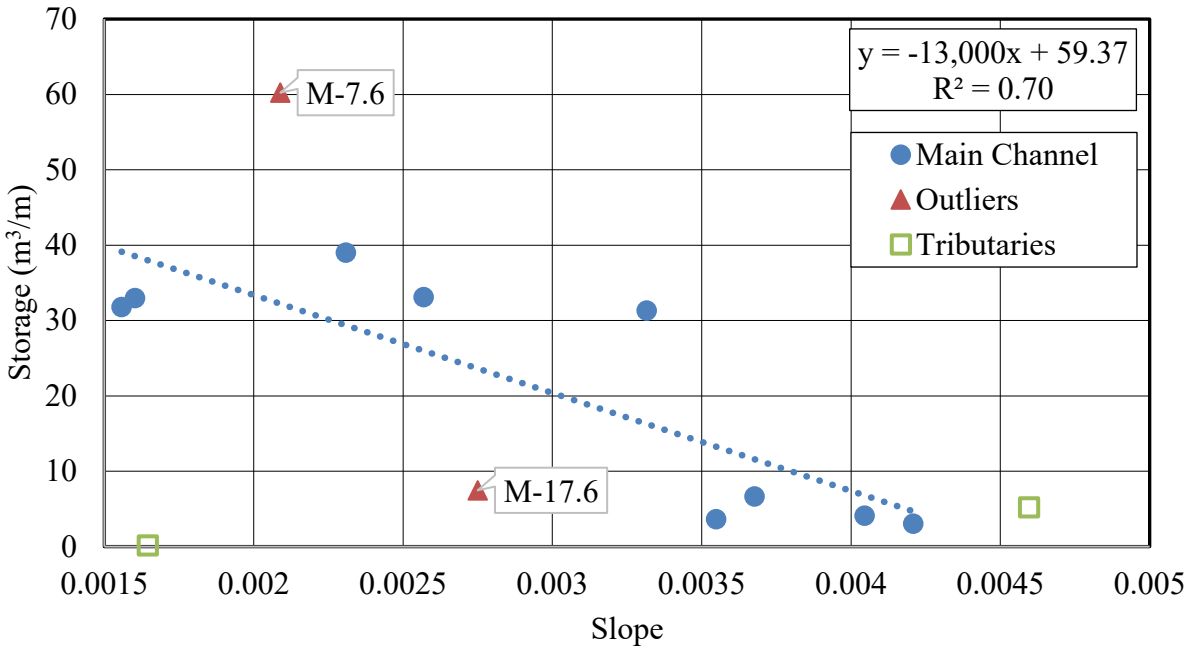

Figure 20. Relationship between volumetric sediment storage and channel slope. Site M-7.6 had a much larger storage value compared to other sites due to its large channel width. Site M-17.6 was removed since it had low storage compared to sites with similar slopes.

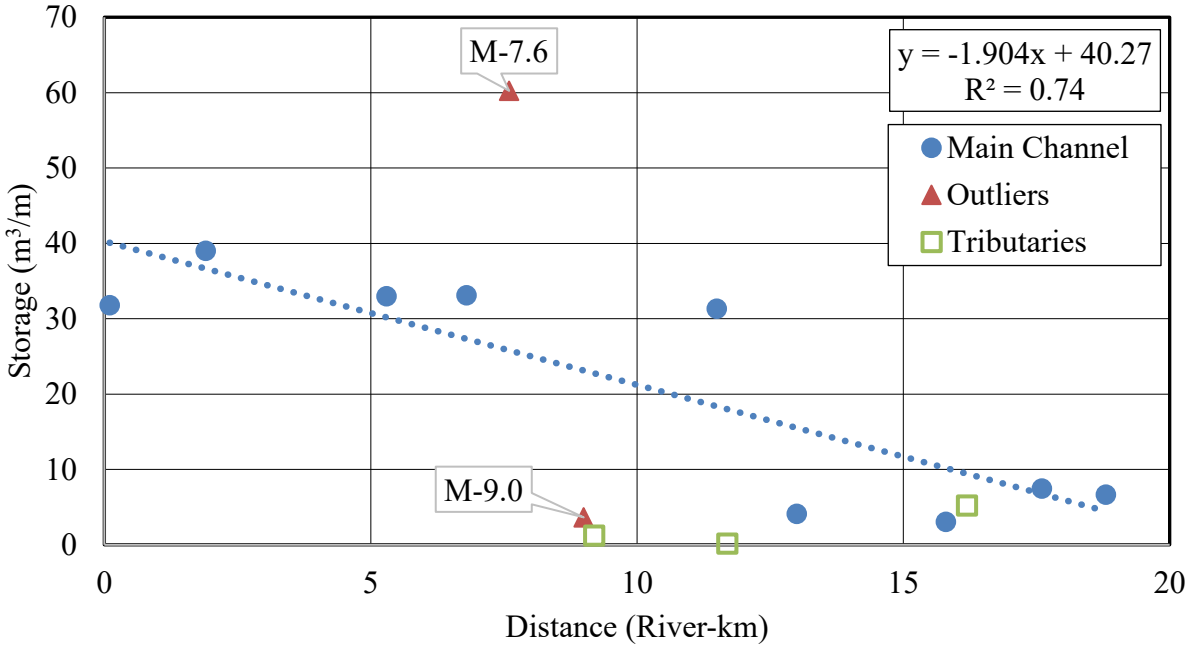

Figure 21. Relationship between volumetric sediment storage and downstream distance. Site M-9.0 was excluded since it had very little storage related to a high percentage of exposed bedrock which reduced bed storage to almost zero and limited the thickness of overlying bar deposits.

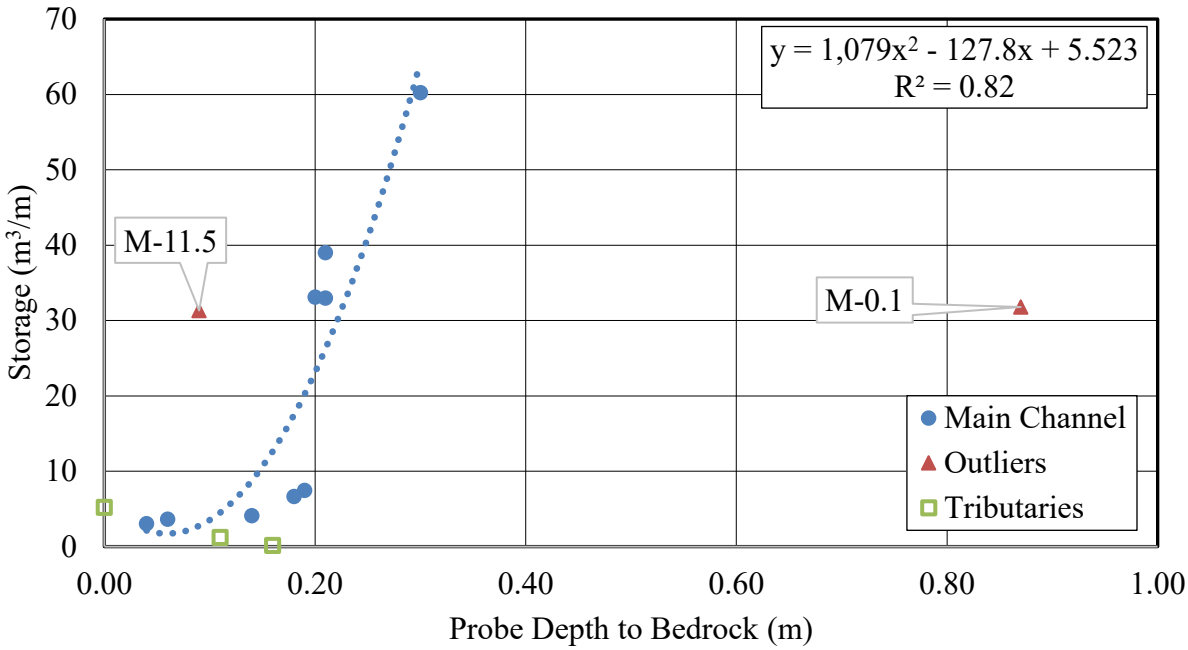

Figure 22. Relationship between volumetric sediment storage and depth to bedrock. M-0.1 was excluded since it had a very large probe depth due to backwater influences. Site M-11.5 had a low probe depth compared to sites with similar store values. However, it had a relatively large channel width which resulted in higher storage.

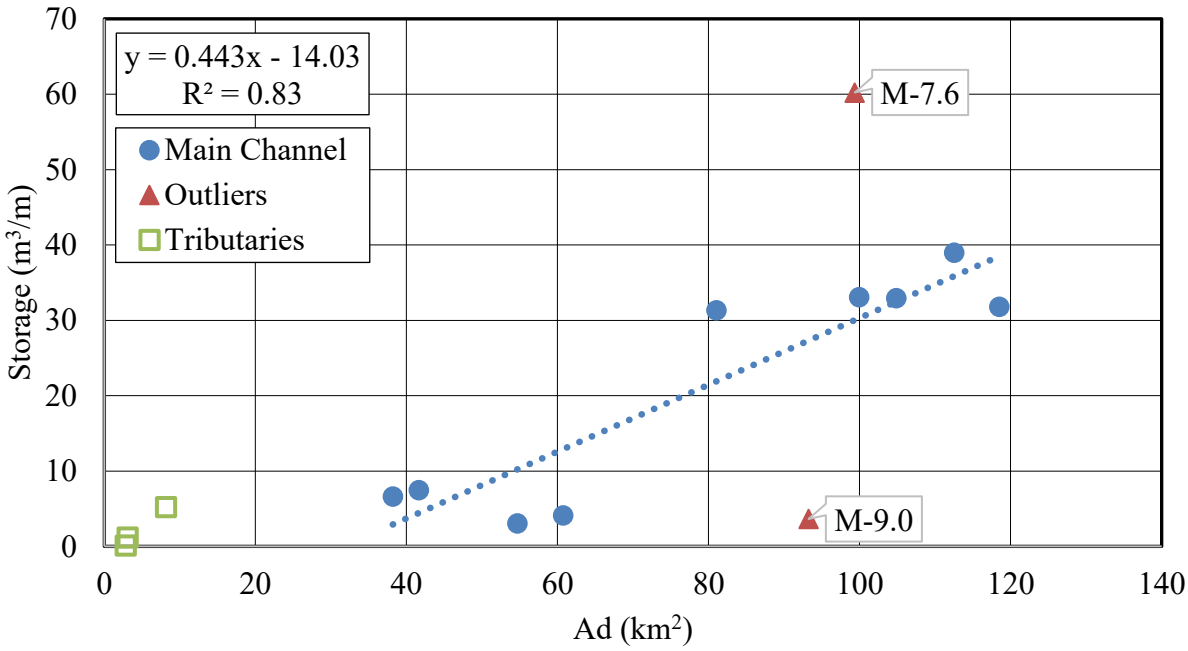

Figure 23. Relationship between volumetric sediment storage and drainage area.

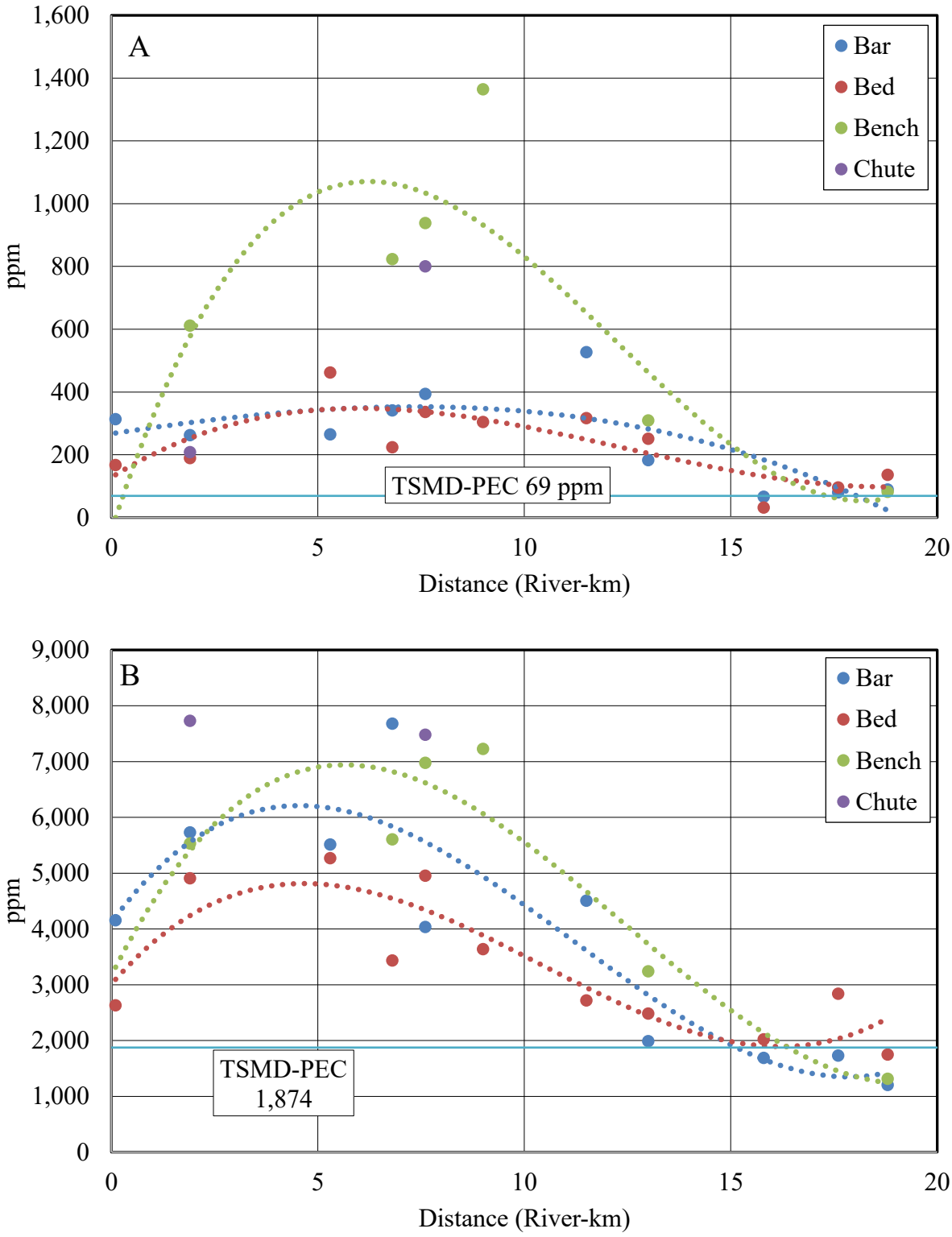

Figure 24. The longitudinal trends of Pb (A) and Zn (B) concentrations in <2 mm sediment. The TSMD-PEC line is shown at its original value minus the respective background metal concentrations since the displayed metal concentrations have had their background concentrations removed.

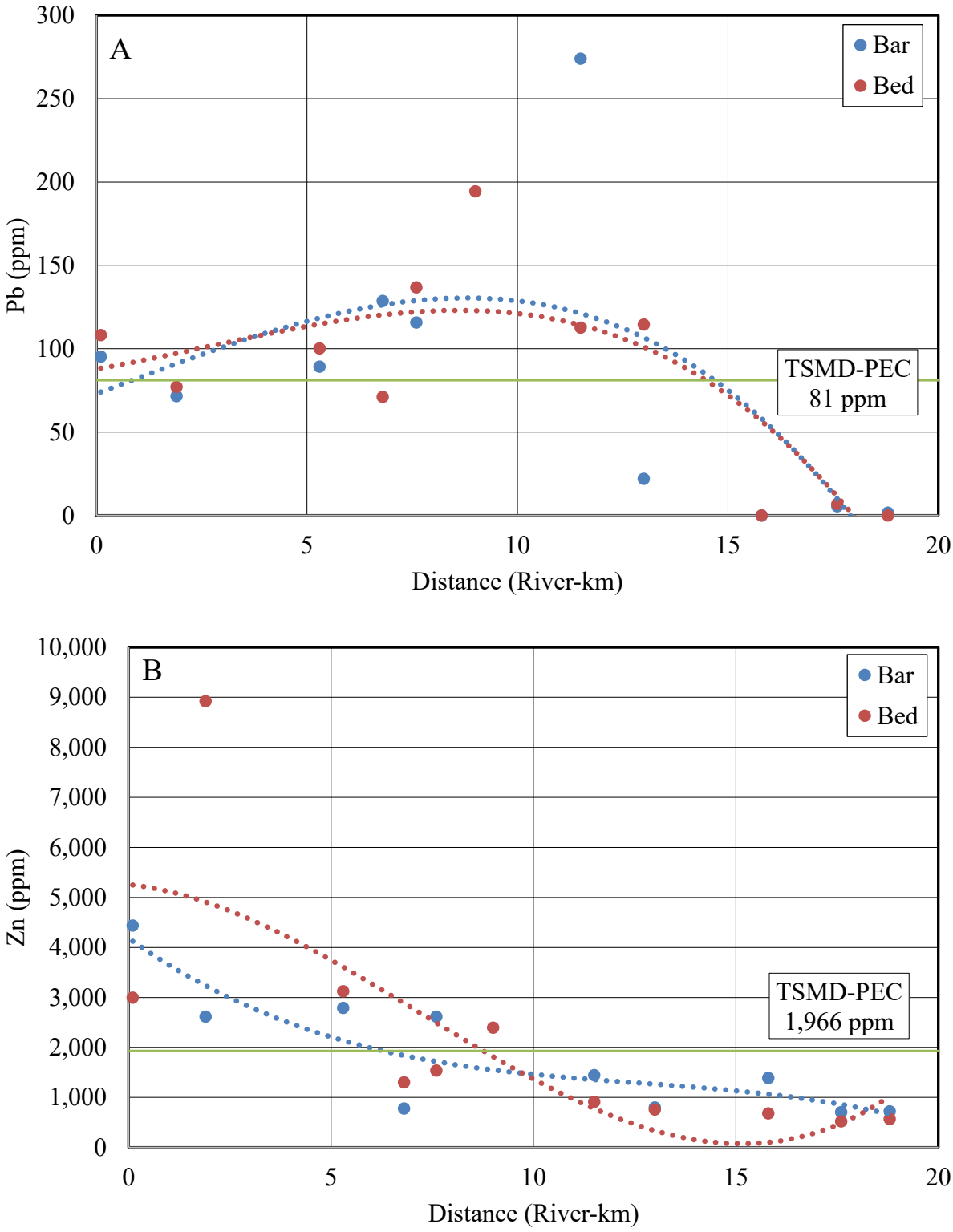

Figure 25. The longitudinal trends of Pb (A) and Zn (B) concentrations in 2 – 8 mm sediment. The TSMD-PEC line is shown at its original value minus the respective background metal concentrations since the displayed metal concentrations have had their background concentrations removed.

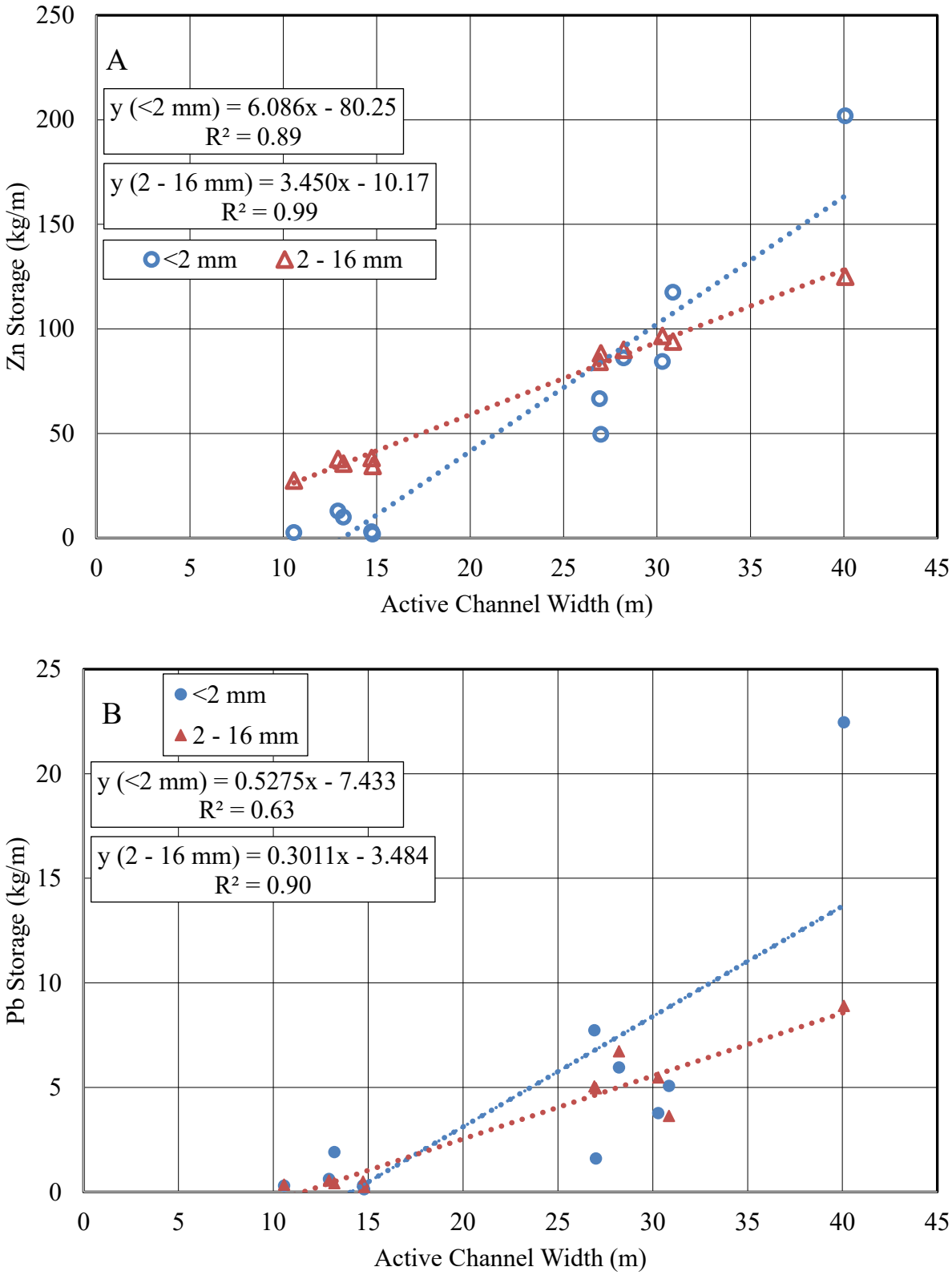

Figure 26. Relationship between active channel width and Zn (A) and Pb (B) storage in the 2 - 16 mm size fraction.

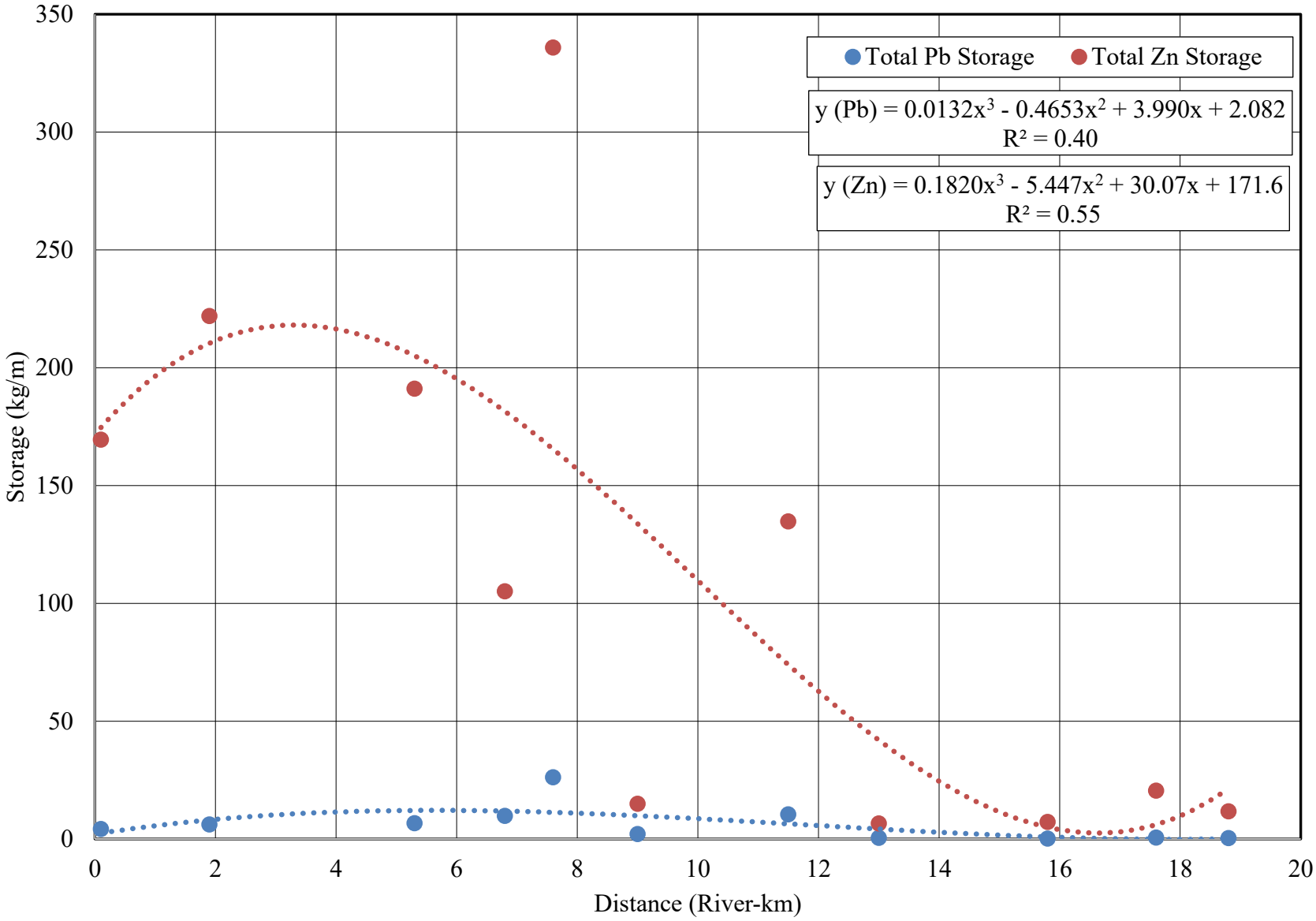

Figure 27. Total Pb and Zn storage in the Turkey Creek main channel.

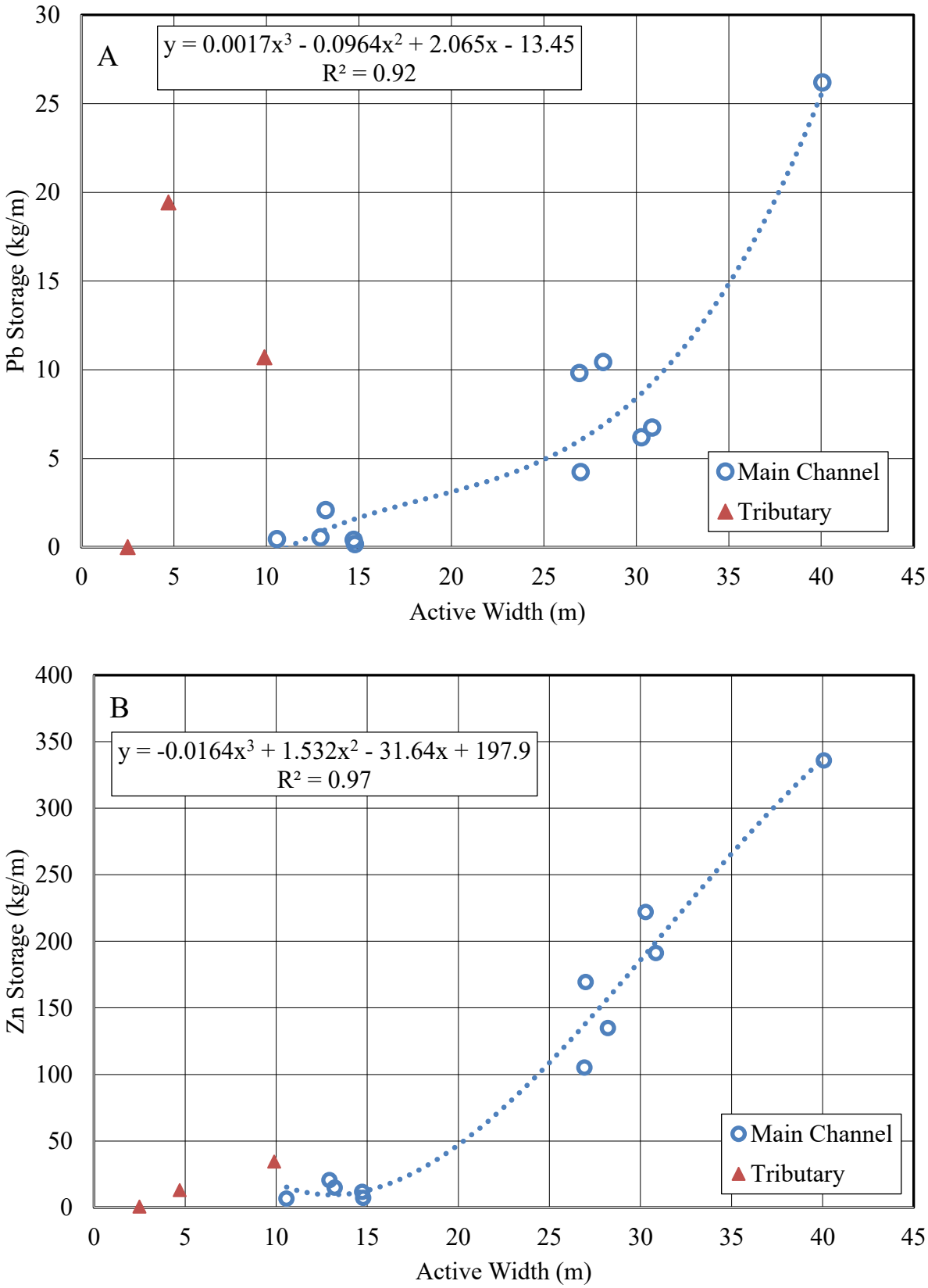

Figure 28. Pb (A) and Zn (B) storage with respect to active channel width.

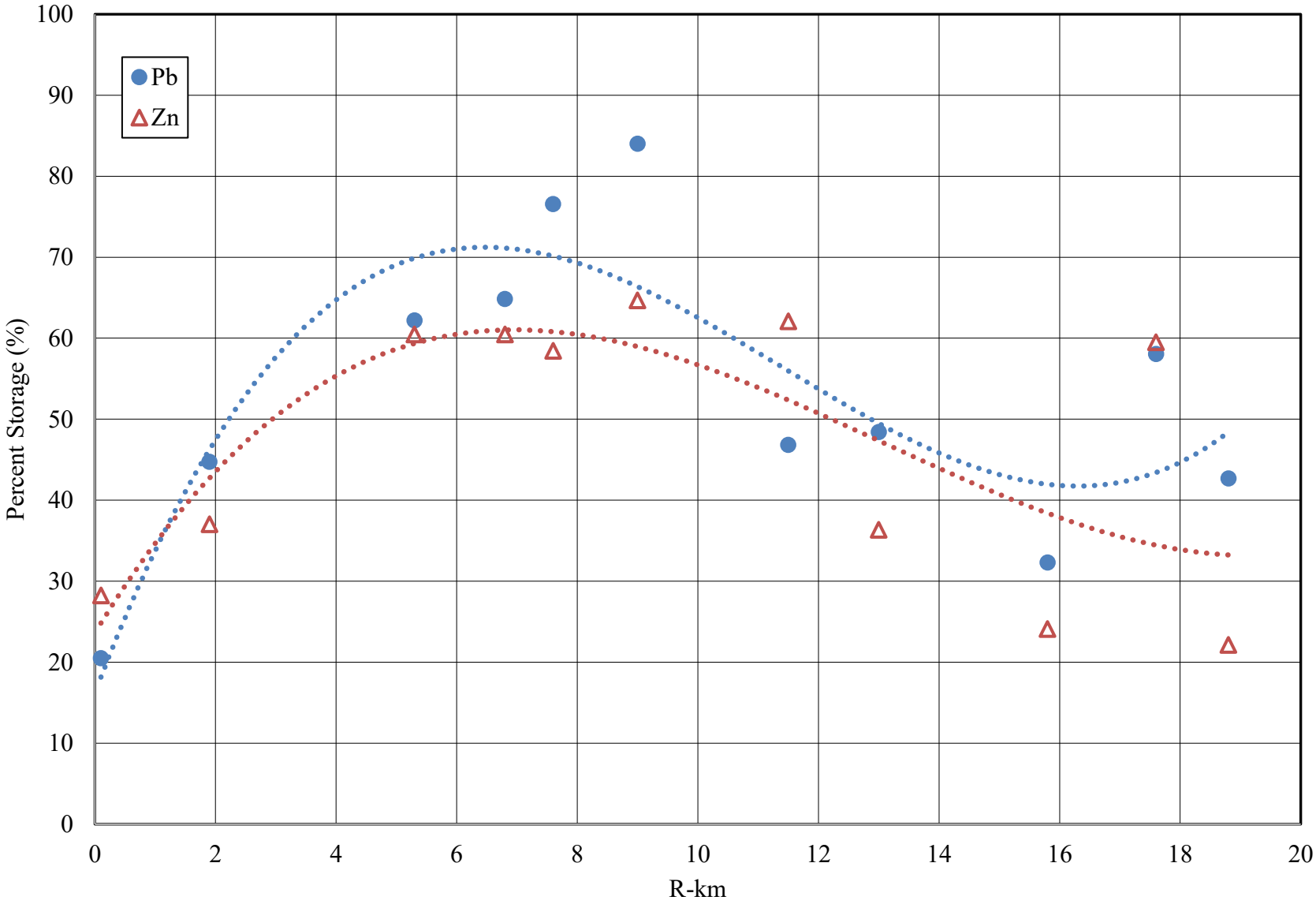

Figure 29. Percent metal storage for the fine size fraction.

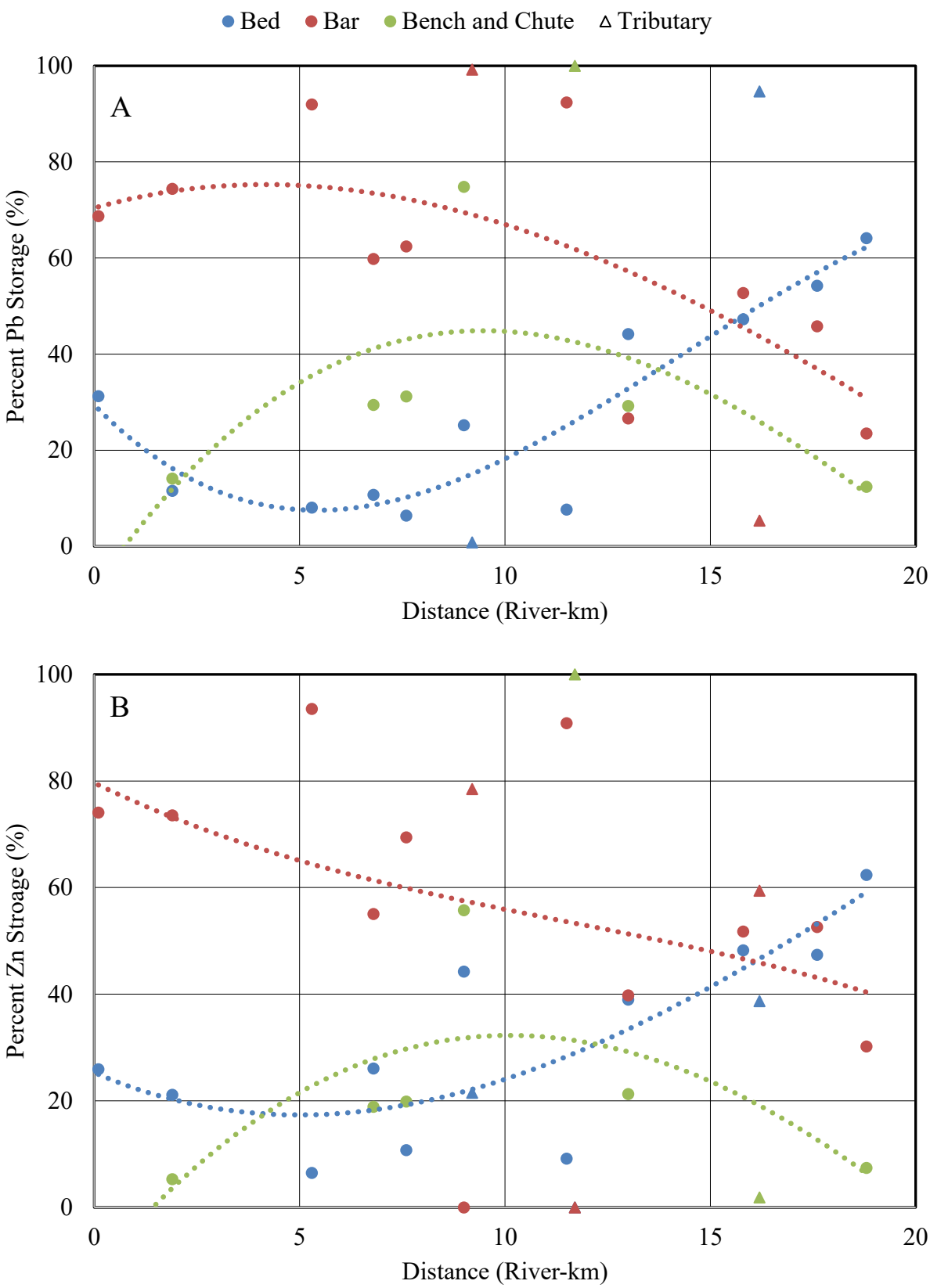

Figure 30. Percentage of Pb (A) and Zn (B) storage by deposit type.

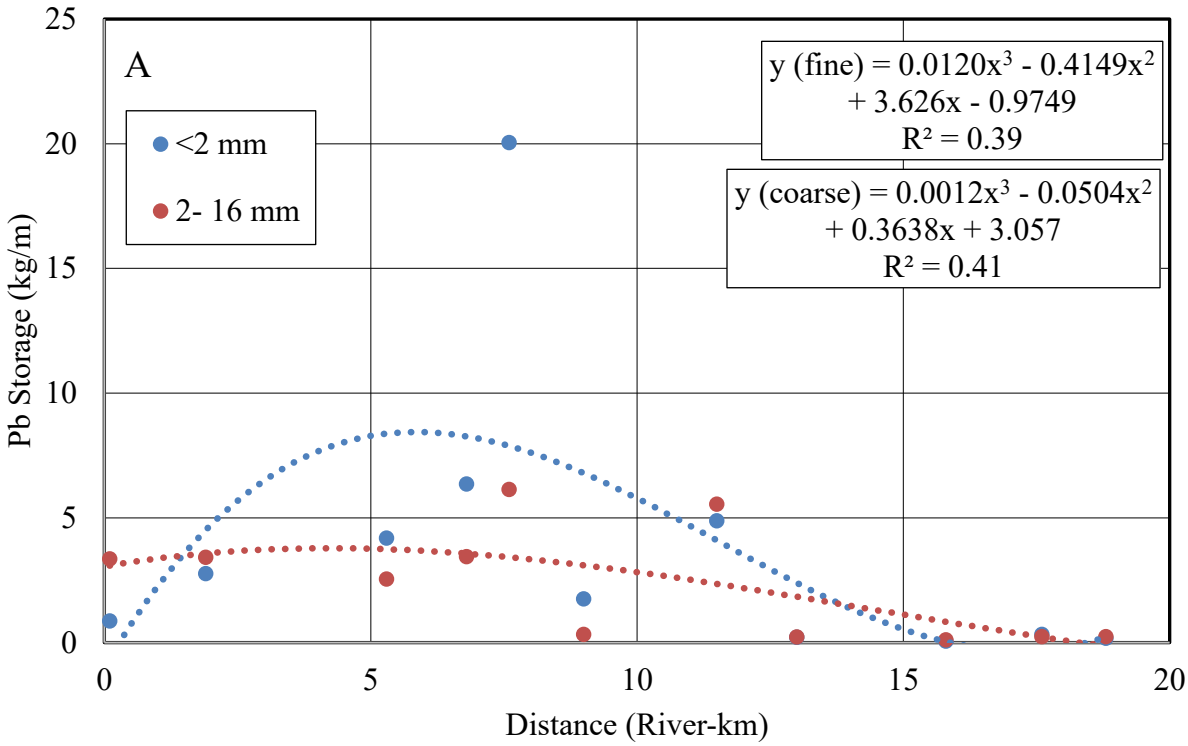

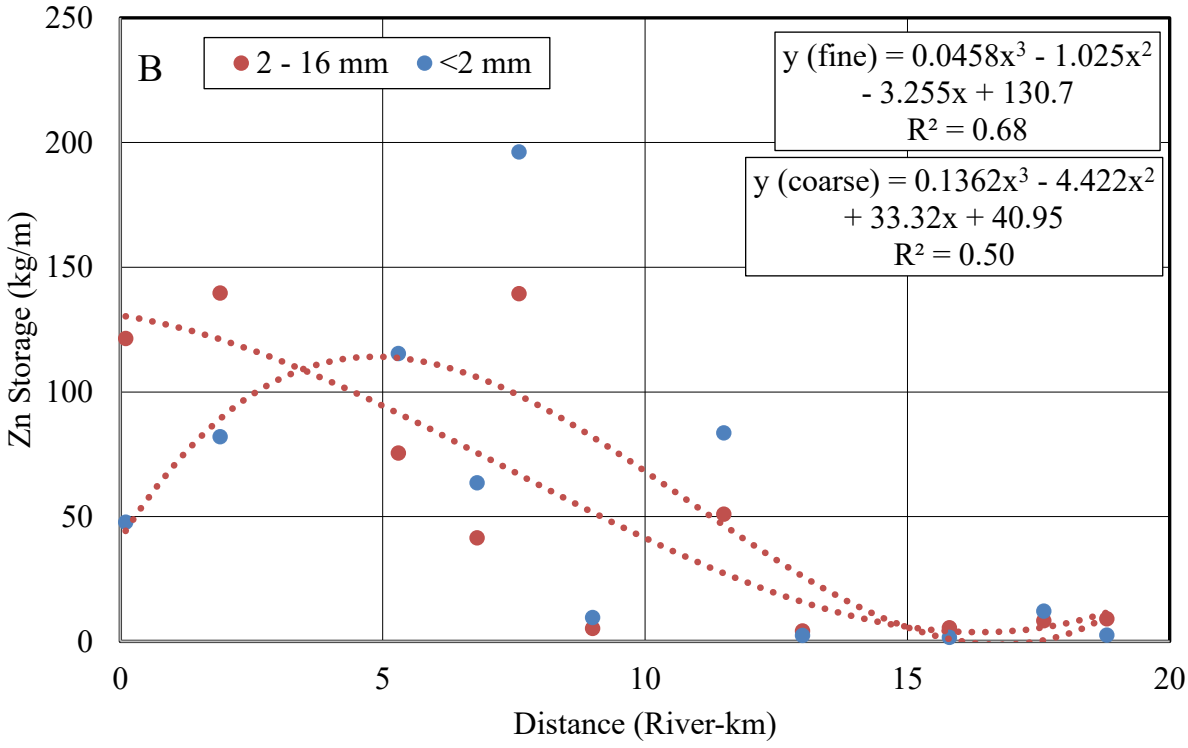

Figure 31. Pb (A) and Zn (B) storage in <2 mm and 2 – 16 mm sediment throughout the Turkey Creek main channel.

DISCUSSION

Distance Regression Models

Distance regression models (DRM) results are summarized for metal concentrations and sediment and metal storages by sediment size fractions and channel deposits for three different main channel segments (Table 16 and Table 17). The divisions of segments were based on proximity to mined area to show how storage and metal concentrations vary with mining intensity. The lower segment was placed just downstream from mined areas. The middle segment was in the most extensively mined areas of the watershed. The upper segment was placed upstream from the most heavily mined segment of the channel (Table 17) (Figure 7). Mined areas located in the Oronogo-Duenweg District at the northeastern corner of the watershed drained into this segment. However, metal concentrations were relatively low below site T-16.2 (65 ppm Pb and 2,018 ppm Zn). Therefore, it does not seem that significant quantities of these tailings and metals were transported to the main channel of Turkey Creek by tributaries (Figure 7). The goal of the discussion chapter is to apply DRM to different segments in the channel and explain the geomorphic factors which affect metal concentrations and contaminated sediment storage.

DRM derived from field data were used to determine storage and concentration values by calculating values at 100 m intervals (Table 16). These values were summed to get storage values and averaged for metal concentrations. Occasionally, these models predicted negative storage in the upper and lower portions of the channel. When that occurred, these values were changed to zero and denoted with an asterisk. Generally, this occurred in the upper reaches where storage values were low. Therefore, zero values had little effect on modeled total storage. Bench and chute storage values were determined by subtracting the sum of bed and bar deposits

from total storage values. The gaps between sampling sites were filled by modelling storage at 100 m increments. Modeling storage and concentration values from these trendlines at 100 m intervals is an appropriate approach to assess longitudinal storage since trends in metal concentrations and storage tend to change gradually (Marcus, 1987; Graf, 1996; Pavlowsky and Owen, 2016).

Longitudinal Modeling of Sediment and Metal Storage. DRM predicts 439,626 m^3 (575,009 yd^3) and 954,231 Mg of sediment is stored between R-km 0 and R-km 18.8 (Table 16 and Table 17, equations 1 and 2) (Figure 12). DRM also estimates fine metal storages of 78,913 kg Pb and 1,121,565 kg Zn, coarse metal storages of 47,763 kg Pb and 1,040,196 kg Zn, and total metal storages of 126,676 kg Pb and 2,161,761 kg Zn indicating that fine sediment stores the most significant amount of Pb and Zn (Table 16 and Table 17, equations 19, 20, 24, 25, 26, and 30) (Figure 31).

Spatial Distribution of Mass and Volume. The largest mass of sediment (74%) is stored in the heavily mined middle segment (Table 16 and Table 17, equation 2). Sediment storage generally increased throughout the channel and then began to decrease around R-km 4 (Figure 12). Similar to total sediment storage, metal storage increased throughout the channel with the highest storage values estimated in the middle segment (Table 16 and Table 17, equations 24 and 30) (Figure 27). This middle segment represents 56 percent of the main channel length assessed and stores 80 percent of total Pb and 77 percent of total Zn. Despite their significantly smaller geometry, tributaries stored a significant amount of contaminated sediment. Sites T-9.2 and T-16.2 stored the second and third greatest amount of Pb in the channel due to high Pb concentrations in fine sediment at site at T-9.2 and coarse sediment at site T-16.2. Total Pb

storage began to decrease near R-km 5 while total Zn storage began to decrease slightly farther downstream at around R-km 3.5.

Sediment and metal storage is not uniform throughout a channel and is controlled by reach scale variability (Graf, 1996; Pavlowsky and Owen, 2016; Martin and Pavlowsky, 2011). The downstream storage trends of sediment can be affected by several factors. First, sediment is not uniformly transported throughout a channel; it is commonly transported discontinuously as sediment waves or slugs (Jacobson 1995; Graf, 1996*).* This results in areas of high and low sediment storage throughout the channel. Second, sediment is deposited when stream power decreases. Areas of deposition include reaches with relatively greater width and lower slope. Third, tributaries deliver sediment to the main channel increasing the total sediment load below them. Fourth, the distribution of mining and milling operations generated large quantities of sediment which make their way into the channel through weathering and erosion increasing the total sediment load. All of these factors combine to control the downstream distribution of mining contaminated sediment.

Active Channel Width and Sediment Storage. Active channel width was the strongest predictor of sediment storage ($R^2 = 0.97$) (Figure 19). The greatest channel widths were observed in the mining impaired middle segment of the channel (Figure 18). Similar channel widths were also observed in the lower segment. Channel width was generally larger in downstream sections of the channel ($R^2 = 0.57$). Ozark streams typically exhibit spatially discrete stable segments and disturbance reaches. These disturbance reaches often trap large quantities of sediment (Jacobson and Primm, 1994; Jacobson, 1995; Martin and Pavlowsky, 2011). These greater channel widths could be caused by channel adjustment due to large sediment inputs related to mining activities which would explain the greater channel widths near mined areas (Pavlowsky and Owen, 2016).

Inflow from tributaries could also be responsible for an increase in channel width at sites downstream from tributaries. For example, sites M-15.8 and M-11.5 were located just downstream from tributary confluences (Figure 7). Both sites had active channel widths greater than sites upstream and downstream from them.

Streams in the Viburnum Trend in the Southeast Missouri Lead Mining District has also shown a strong relationship between active width and volumetric storage (Pavlowsky and Owen, 2016). The regression equations determined from this study and the Viburnum Trend study were compared to determine whether active channel width can serve as a predictor for sediment storage between different study sites. Regression modeling indicated that storage in Turkey Creek was higher than in the Viburnum Trend at all channel widths (Figure 32). The greatest difference between storage values was calculated at an active channel width of 25 m where storage values in Turkey Creek were 1.5 times greater than storage in the Viburnum Trend. At channel widths greater than 25 meters, the relative difference in storage values began to decrease. The least difference between storage values was calculated at an active channel width of 15 m where storage was 1.2 times greater than in Turkey Creek. The width equations and storage estimates presented in this study closely follow the estimates shown in the Viburnum Trend. Therefore, more research is needed to develop a storage modelling framework that applies to a wider range of Ozark streams.

Metal Concentrations

The highest Pb and Zn concentrations were always observed in the middle mining contaminated segment with the exception of coarse Zn concentrations which were highest in the lower segment (Table 16 and Table 17, equations 9 – 18) (Figure 24 and Figure 25). Lead and

Zn, concentrations were typically lower in coarser size fractions than the fine <2 mm fraction. The lowest mean Pb and Zn concentrations were always attributed to the coarsest size fraction (Table 15). Metal concentrations observed in coarse 2 – 8 mm sediments are elevated well above background concentrations and exceed the TSMD-PEC concentrations of 150 ppm for Pb and 2,083 ppm for Zn between R-km 0 and R-km 13 for Pb (excluding site M-1.9) and R-km 0 and R-km 9 for Zn (excluding site M-6.8) (Figure 25) (Ingersoll et al., 2009).

Fine sediment (<2 mm) exhibits concentrations that often far exceed the TSMD-PEC and crossed the threshold for Pb or Zn at every site indicating that the entire sampled length of Turkey Creek was contaminated by past mining and milling operations (Figure 24). These high metal concentrations agree with previous studies which have indicated that fine channel sediments were frequently present above the TSMD-PEC (Peebles, 2014; Gutiérrez et al., 2015; Smith, 2016; HGL, 2019). Smith concluded that Pb and Zn concentrations exceed the TSMD-PEC in nearly every gravel bar sample (Smith, 2016). The measured metal concentrations indicate that fines present in active channel deposits present a direct risk to the ecological health of Turkey Creek.

Lack of Simple Source Decay Trend. Zn concentrations and storage were higher in the downstream portion of the channel when compared to Pb trends (Figure 24; Figure 25; Figure 27). Generally, when progressing downstream from contamination, metal concentrations decrease exponentially due primarily to the mixing of uncontaminated sediment (Glover, 1964; Lewin, 1978; Wolfenden and Lewin, 1978). However, this lack of a simple source decay trend could be caused by several factors related to mining source effects and sediment-metal transport factors. First, the spatial distribution of tailings piles can contribute to the lack of a clear source decay. This watershed had multiple mining and other industrial sources of contamination

scattered across the watershed which added contaminated mining sediment to the natural load increasing metal concentrations in the active channel sediment at different points in the channel network (Figure 7). Second, the total amount, concentration, and size fractions of tailings generated during milling varied spatially and temporally. Throughout the history of the mining district there were numerous ore processing techniques that had varying ore recovery rates and produced different quantities and sizes of tailings (Wright, 1918; Gibson, 1972). The mills in the Joplin subdistrict did not follow a standard milling procedure and produced different sized particulate with varying metal concentrations (Table 6 and Table 7) (Gibson, 1972). Further, as time progressed in the Joplin subdistrict, the amount of ore production changed. The earliest operations only focused on extracting Pb and produced the least amount of ore. Later operations primarily focused on Zn and produced the greatest quantity of tailings (Wright, 1918; Gibson, 1972). It is difficult to quantify the concentrations and amount of tailings produced by different milling sites since mining records were poorly recorded in the Joplin subdistrict (Gibson, 1972).

Transport factors include both sediment and geochemical effects. The third reason for the lack of a simple decay trend may be related to sediment supply. Sediment input from tributaries can influence metal concentrations in the active channel (Marcus, 1987). All of the sampled tributaries exhibited mining impairment to varying degrees (Table 9). Of the three tributaries sampled, fine metal concentrations were all above the TSMD-PEC for either Pb or Zn, so it is likely that they delivered contaminated mining sediment to the active channel and still do today. Tailings were even observed wasting directly into the tributary channel at site T-9.2 (Figure 6). Conversely, tributaries that did not drain mined areas, which were primarily located in the lower and upper segment, would deliver uncontaminated sediment to the channel reducing overall metal concentrations by dilution and mixing in these areas (Figure 7). Fourth, variability in Pb

and Zn geochemistry and mineralogy could be contributing to the lack of a simple source decay trend. Zinc is more geochemically mobile compared to Pb in the TSMD (Johnson et al., 2016; Gutiérrez et al., 2020). Mobile elements dissolve more readily and can adsorb to organic matter and clay particles in the fine size fraction that are easily transported downstream by seasonal floods (Håkanson, 1984; Horowitz, 1991). Zinc could also be transported more easily downstream than Pb since Zn due to differences in mineral densities. Zinc bearing minerals (sphalerite and smithsonite) have specific gravities ranging from 3.9 – 4.5, while the common Pb mineral (galena) has a specific gravity of 7.4 – 7.6 (Klein and Hurlbut, 1985). Therefore, Zn minerals have a lesser entrainment threshold (Macklin and Dowsett, 1989). These factors combine to produce a non-uniform pattern of storage which does not follow a simple decay curve trend.

Concentrations Near Areas of Remediation. Sites M-11.5, M-7.6, M-6.8, and M-5.3 were all located in areas remediated by the EPA. Sites M-11.5, M-7.6, and M-6.8 are under active remediation, and site M-5.3 is completed. The results of geochemical analysis indicate that active channel sediment at these sites is still elevated well above background concentrations. In fact, storage values near remediated sites were often the highest. These results agree with previous research in the region which has also found elevated metal concentrations near remediated areas (Peebles, 2014; Gutiérrez et al., 2015; Smith, 2016; HGL, 2019). Remediation is relatively recent in Turkey Creek and is still ongoing in the watershed (Figure 7). Even after removing the source of contamination, it can still take decades or centuries for concentrations to decrease after clean-up due to the slow dilution of in-transit contaminated sediment and continued release of stored meatal in floodplain deposits (Walling et al., 1998; Davis, 2009).

Sediment and Metal Storage by Deposit

Bar deposits stored the greatest amount of sediment in the channel (Figure 13). In the middle segment, bars stored more than 80 percent of in channel sediment (Table 16 and Table 17; equations 4, 21 - 24, and 27 - 30). Bars also stored the greatest mass of Pb (68% to 78%) and Zn (65% to 75%) in every channel segment (Figure 30). Also, bench and chute deposits stored 23 percent of Pb and 12 percent of Zn in the middle segment despite accounting for only 6 percent of total sediment storage since these deposits are fine-grained with high concentrations of metals. The percent of sediment and Pb storage in bars increased with downstream distance and then slightly decreased around R-km 3 (Figure 14 and Figure 30). The percent of Zn storage in bars increased downstream. Downstream sediment and metal storage trends are typically variable among different deposits due to the spatial distribution of sediment input sources, variance in the concentrations and size of tailings generated, and channel storage capacity (Walling et al., 2003; Pavlowsky et al., 2017).

Comparison to Previous Storage Estimates. Smith reported that 88,000 m^3 of contaminated bar sediment is stored within a 16.3 km stretch of Turkey Creek beginning at the confluence with the Spring River (Smith, 2016). Smith determined the mean depth of contaminated bar sediment and multiplied this value by the aerial extent of gravel bars to determine the volume of contaminated sediment. The present study applies regression modelling to predict bar storage at 100 m segments for the same 16.3 km stretch and estimates that 336,000 m^3 of contaminated sediment is stored within bars for the same segment (Figure 33). The present study could have come to a larger calculation of stored sediment in gravel bars due to the in-channel measurement of bar width and depth. Smith's study used aerial imagery to delineate bar area. The gravel bars observed in the field were often vegetated and located underneath tree

cover creating conditions which could potentially be difficult to delineate from aerial imagery. It is possible that measuring gravel bar areas in the field compared to remote sensing could lead to greater bar areas. The different methods used to calculate sediment volume could also affect the estimate of total bar storage. This study calculated gravel bar volumes at multiple sites and then used regression modelling to determine total channel storage, while Smith determined total bar area in the assessed channel, summed the total bar areas in the reach, and applied the mean depth to bedrock to determine volume of the whole stream. Applying a mean depth of bedrock could also lower the estimate of total storage. Smith's average gravel bar height was 1.4 m. In the present study, sites with high storage values gravel often had bar heights >1.6 m (Appendix B). Smith's evaluation of samples at the PEC instead of background value did not play a major role in reducing storage, since 99 percent of the samples were determined contaminated (Smith, 2016). It is possible that model estimates predict greater bar storage than what is present in the channel since it has a relatively low R^2 value (0.54) (Figure 33). Further, more work needs to be done to refine DRM storage estimates.

Sediment and Metal Storage by Size Fraction.

Fine sediment represents 20% of the total mass of contaminated sediment in the middle segment of the stream whereas coarse 2 – 16 mm sediment represents 52% and sediment >16 mm represents 28%. (Table 16 and Table 17; equations 19, 20, 24 - 26, and 30). Despite accounting for only a fifth of channel storage, the fine fraction stores 67% of Pb and 56% of Zn in this segment. The coarse fraction stored less Pb and Zn in the middle segment compared to the fine fraction. However, in the lower and upper distal segments coarse sediment often stored the most metal. In the lower segment 69% of Pb and 65% of Zn storage was associated with the

coarse fraction. In the upper segment, 59% of Pb and 46% of Zn was associated with the coarse fraction. This association of metals with the coarse size fraction is a result of milling operations which produced large quantities of chat waste (Wright, 1918; Gibson, 1972). Ignoring the coarse fraction in a metal analysis of the stream would exclude 39% of total Pb storage and 48% of total Zn storage.

While this study is the first to quantify total metal storage in the coarse size fraction in the TSMD, previous research on Big River which drains the Old Lead Belt mines in Saint Francis County, Missouri which closed in 1972 indicated that the coarse size fraction accounted for 60 percent of Pb storage in the channel (Pavlowsky et al., 2017). Coarse sediment can remain an important source of contamination since it has a higher transport threshold and can remain in the channel for longer periods of time (Ritcey, 1989). The metal stored in coarse channel sediments can serve as a secondary source of contamination as these metals are released to the environment through abrasion and dissolution (Pavlowksy et al., 2017). For these reasons, coarse sediment should be considered when assessing contamination.

Future Work

Contaminated Sediment in Floodplain Deposits. Floodplains represent a significant source of sediment storage within a watershed. The mass of contaminated floodplain sediment was estimated and compared to the mass of channel sediment in Turkey Creek. The floodplain area was determined as 6,755,000 m^2 from the web soil survey with active channel and completed remediation areas removed (NRCS, 2020). Both frequently and occasionally flooded soil series were delineated as the floodplain. Floodplain sediment in Turkey Creek is wholly fine-grained (<2 mm) (Eades et al., 2021). The mean depth of floodplain contamination is 0.5 m

(Smith, 2016). However, floodplain sediment may be contaminated up to depths of 1 m near the channel (Eades et al., 2021). This estimate of contaminated floodplain sediment should be considered a minimum since it does not account for greater depths of contamination near the channel. Multiplying the floodplain area and mean depth of contamination by bulk density (1.4 Mg/m^3) indicates that at least 4,729,000 Mg of contaminated sediment is stored in the floodplains along Turkey Creek. Comparatively, the mass of active channel fine sediment is 197,300 Mg (Table 17). Therefore, fine sediment storage in the floodplain is >10 times compared to the channel. Another storage study conducted in a mining impacted stream in the Ozarks found that active channel and floodplain sediment was stored in a similar ratio (Pavlowsky et al., 2017).

Applying an estimated bank erosion rate of 0.25 m/yr determined from a geospatial analysis of past and present bank lines between 1990 and 2015 to the same depth of contamination (0.5 m) indicates that 7,000 Mg of contaminated sediment between R-km 0 and R-km 18.8 may be entering the channel each year from bank erosion. This would represent approximately 4% of active channel fine sediment storage (197,300 Mg). Although the floodplain stores considerably more fine sediment, this does not make the in-channel contaminated sediment insignificant. Sediment stored within the channel is considered more mobile and can be dispersed throughout the watershed much more readily (Wolfenden and Lewin, 1977; Montgomery and Buffington, 1997). Establishing thicknesses and metal concentrations among different soil horizons throughout the watershed and addressing the remobilization of stored metals in the suspended load as floodplain sediment is weathered into the channel would be beneficial in understanding floodplain storage.

Bank erosion may be a significant source of sediment and metals to the suspended sediment load. However, compared to the suspended sediment load, bank erosion inputs can be significant. For example, suspended sediment yields for five undisturbed watersheds in southwest Missouri (i.e., Springfield Plateau) ranged from 27 to 53 Mg/km^2 with a median of 35 Mg/km^2 (Pursley, 2021). At a 119 km^2 drainage area for Turkey Creek that would estimate a suspended load of about 4,165 Mg/yr while bank erosion estimates 7,000 Mg/yr. Therefore, bank erosion may be a significant source of fine sediment and metals to Turkey Creek, but more research is needed to verify this possibility.

TMSD Geomorphic Relationships. This study focused on eleven main channel sites in Turkey Creek which represents only a small portion of the greater TSMD. Turkey Creek is one of many streams that has been impaired by historic mining (Johnson et al., 2016; Juracek and Drake, 2016; Smith, 2016). A more in-depth study including multiple streams draining mined areas throughout the TSMD could apply a similar approach of modelling sediment storage with the geomorphic variables addressed in this study. Adding multiple streams could provide further support for the geomorphic trends established in this study (Figures 19 - 23). A broader studying focusing on multiple streams throughout the TSMD would help inform project managers as to the spatial distribution of contaminated sediment throughout channels in the region. Channel width may be a better predictor of sediment and metal storage than river-kilometer based on downstream measurements of active width using aerial photography (Pavlowsky and Owen, 2016). However, this aspect was beyond the scope of the present study but may offer opportunities for future studies.

Sediment Monitoring. Since metal concentrations and sediment transport are variable with time, setting up a long-term sediment monitoring program may be beneficial to

understanding the future distribution of sediment throughout the channel (Rhoads and Cahill, 1999). Assessing channel sediment concentrations over time would help to establish the effects of remediation in reducing overall metal contamination throughout the channel. If implemented, future monitoring sites are suggested to be located at sites M-1.9, M-5.3, M-7.6, T-9.2, and M-11.5 (Figure 7). Site M-1.9 is located downstream from a competed area of remediation. Site 5.3 is in an area of completed remediation. Sites M-7.6, T-9.2, and M-11.5 are all located in areas of active remediation. Site M-7.6 is arguably the most important site for future monitoring since it stored by far the greatest quantity of contaminated sediment. Placing monitoring sites in areas with different remediation statuses would allow for an understanding of the effect of remediation on longitudinal metal concentrations. These monitoring sites should focus on bar deposits since they store the greatest amount of contaminated sediment. The locations of past, present, and future gravel bars could be delineated using LiDAR or aerial imagery to establish the rate at which sediment is moving throughout the channel (Flener et al., 2013; Nelson and Dubé, 2016). This would give a time frame as to when metal concentrations in the channel are expected to decrease since new sediment entering the channel should be uncontaminated due to the remediation of tailings piles and floodplain soils.

Table 16. Distance regression equations used to predict storage and concentration trends. Asterisks denote the equations predicted negative values at certain distance values.

Equation #		Equation (x = R-km)	n	R^2
1	Total Volume (m^3/m)	$0.0336x^3 - 1.027x^2 + 6.209x + 30.10$	11	0.53
2	Total Mass (Mg)	$0.0739x^3 - 2.249x^2 + 13.58 + 65.09$	11	0.54
3	Total Bed Storage (Mg/m)	$-0.0058x^3 + 0.2526x^2 - 3.484x + 22.411$	11	0.57
4	Total Bar Storage (Mg/m)	$0.0691x^3 - 2.1728x^2 + 14.554x + 42.773$	11	0.53
5	Total Bench and Chute Storage (Mg/m)*	$0.0739x^3 - 2.2494x^2 + 13.583x + 65.089$	7	0.54
6	Total <2 mm Storage (Mg/m)	$0.0169x^3 - 0.5536x^2 + 4.1901x + 6.8923$	11	0.45
7	Total 2 - 16 mm Storage (Mg/m)	$0.0349x^3 - 0.9997x^2 + 4.735x + 42.13$	11	0.59
8	Total >16 mm Storage (Mg/m)	$0.0185x^3 - 0.5885x^2 + 3.8824x + 16.255$	11	0.5
9	Pb Bed Concentrations <2 mm Sediment (ppm)	$0.2422x^3 - 8.995x^2 + 81.865x + 128.12$	11	0.67
10	Pb Bar Concentrations <2 mm Sediment (ppm)	$-0.0512x^3 - 0.8177x^2 + 20.467x + 266.74$	11	0.58
11	Pb Bench Concentrations <2 mm Sediment (ppm)*	$1.1844x^3 - 43.401x^2 + 402.76x - 40.518$	6	0.74
12	Zn Bed Concentrations <2 mm Sediment (ppm)	$3.7893x^3 - 118.54x^2 + 857.03x + 3010$	11	0.75
13	Zn Bar Concentrations <2 mm Sediment (ppm)	$4.1287x^3 - 138.7x^2 + 1005.2x + 4118.7$	11	0.81
14	Zn Bench Concentrations <2 mm Sediment (ppm)	$4.5566x^3 - 169.98x^2 + 1483x + 3164.3$	6	0.88

Table 16 continued.

Equation #		Equation (x = R-km)	n	R^2
15	Pb Bed Concentrations 2-8 mm Sediment (ppm)*	$-0.0517x^3 + 0.4174x^2 + 4.3284x + 87.832$	11	0.66
16	Pb Bar Concentrations 2 - 8 mm Sediment (ppm)*	$-0.0461x^3 + 0.0679x^2 + 9.4997x + 73.021$	11	0.42
17	Zn Bed Concentrations 2 - 8 mm Sediment (ppm)	$2.6058x^3 - 56.409x^2 - 85.561x + 5257.2$	11	0.56
18	Zn Bar Concentrations 2 - 8 mm Sediment (ppm)	$-1.0762x^3 + 40.657x^2 - 570.97x + 4181.4$	11	0.77
19	Total Pb Mass <2 mm Sediment (kg/m)*	$0.012x^3 - 0.4149x^2 + 3.6263x - 0.9749$	11	0.39
20	Total Pb Mass 2 - 16 mm Sediment (kg/m)*	$0.0012x^3 - 0.0504x^2 + 0.3638x + 3.057$	11	0.41
21	Total Pb Mass Bed Sediment (kg/m)	$0.0004x^3 - 0.0115x^2 + 0.046x + 1.0378$	11	0.47
22	Total Pb Mass Bar Sediment (kg/m)	$0.0077x^3 - 0.2793x^2 + 2.4311x + 1.8722$	11	0.38
23	Total Pb Mass Bench & Chute Sediment (kg/m)*	$0.0128x^3 - 0.4233x^2 + 3.6902x - 4.7052$	6	0.54
24	Total Pb Mass (kg/m)	$0.0132x^3 - 0.4653x^2 + 3.990x + 2.082$	11	0.4
25	Total Zn Mass <2 mm Sediment (kg/m)	$0.1362x^3 - 4.422x^2 + 33.32x + 40.95$	11	0.5
26	Total Zn Mass 2 - 16 mm Sediment (kg/m)	$0.0458x^3 - 1.029x^2 - 3.255x + 130.7$	11	0.68
27	Total Zn Mass Bed Sediment (kg/m)	$0.0111x^3 - 0.1631x^2 - 2.8349x + 46.337$	11	0.75
28	Total Zn Mass Bar Sediment (kg/m)*	$0.13x^3 - 3.92x^2 + 21.436x + 129.68$	11	0.53

Table 16 continued.

Equation #		Equation (x = R-km)	n	R^2
29	Total Zn Mass Bench & Chute Sediment (kg/m)*	$0.0927x^3 - 3.0281x^2 + 25.647x - 26.665$	6	0.45
30	Total Zn Mass (kg/m)	$0.1820x^3 - 5.447x^2 + 30.07x + 171.6$	11	0.55

Table 17. Sediment storage and metal concentrations in distinct segments in Turkey Creek.

		Segment (R-km)			
		Lower (0 – 2)	Middle (2 - 12.5)	Upper (12.5 - 18.8)	Total
Sediment Storage	m^3	73,450	326,477	39,700	439,626
	yd^3	96,068	427,016	51,925	575,009
	Mg	159,078	706,966	88,187	954,231
	Mg (%)	16.7	74.1	9.2	100.0
Sediment Distribution by Mass (%)	<2 mm	14.3	20.4	14.5	18.8
	2 - 16 mm	60.2	51.7	51.9	53.2
	>16 mm	25.6	27.8	33.5	28.0
	Bed	25.4	14.0	53.5	19.5
	Bar	71.9	80.3	47.9	75.9
	Bn & Ch	2.6	5.8	-1.5	4.6
Pb Mass (%)	<2 mm	31.1	67.0	40.8	60.8
	2 - 16 mm	68.9	33.0	59.2	39.2
	Bed	19.6	9.0	30.4	11.7
	Bar	72.1	67.6	77.7	68.8
	Bn & Ch	8.4	23.4	-8.1	19.5
	Total (Mg)	14,851	104,267	10,749	129.9
Zn Mass (%)	<2 mm	35.2	55.9	53.7	51.9
	2 - 16 mm	64.8	44.1	46.3	48.1
	Bed	22.2	13.9	36.5	16.5
	Bar	75.0	74.5	65.4	74.2
	Bn & Ch	2.7	11.6	0.0	9.4
	Total (Mg)	408,760	1,658,806	94,196	2,161.8

Table 17 continued.

		Segment (R-km)			
		Lower (0 – 2)	Middle (2 - 12.5)	Upper (12.5 - 18.8)	Total
Metal Concentration Pb <2 mm (ppm)	Bed	198.2	306.7	141.5	239.6
	StDev	40.3	37.1	37.4	85.6
	Cv%	20.3	12.1	26.5	35.7
	Bar	286.0	334.8	177.7	277.0
	StDev	11.6	16.1	80.1	86.3
	Cv%	4.0	4.8	45.1	31.2
	Bn & Ch	307.4	887.1	209.4	596.8
	StDev	195.8	161.0	146.3	363.6
	Cv%	63.7	18.2	69.9	60.9
Metal Concentration Pb 2 - 8 mm (ppm)	Bed	92.6	115.0	62.8	96.7
	StDev	3.1	7.2	30.6	29.2
	Cv%	3.3	6.3	48.7	30.2
	Bar	82.5	119.4	65.2	98.8
	StDev	5.9	10.6	33.0	31.8
	Cv%	7.1	8.9	50.6	32.2
Metal Concentration Zn <2 mm (ppm)	Bed	3713.0	4096.6	2107.6	3391.0
	StDev	394.9	695.6	194.4	1066.9
	Cv%	10.6	17.0	9.2	31.5
	Bar	4947.0	5257.1	1937.0	4116.0
	StDev	465.4	966.3	519.6	1739.0
	Cv%	9.4	18.4	26.8	42.3
	Bn & Ch	4424.6	6059.7	2330.2	4634.9
	StDev	721.5	835.5	849.9	1897.0
	Cv%	16.3	13.8	36.5	40.9

Table 17 continued.

		Segment (R-km)			Total
		Upper (0 – 2)	Middle (2 - 12.5)	Lower (12.5 - 18.8)	
Metal Concentration Zn 2 - 8 mm (ppm)	Bed	5100.0	2646.3	313.1	2141.2
	StDev	118.3	1370.0	252.7	1816.9
	Cv%	2.3	51.8	80.7	84.9
	Bar	3663.7	1918.3	1040.8	1819.7
	StDev	306.5	529.0	179.6	874.1
	Cv%	8.4	27.6	17.3	48.0

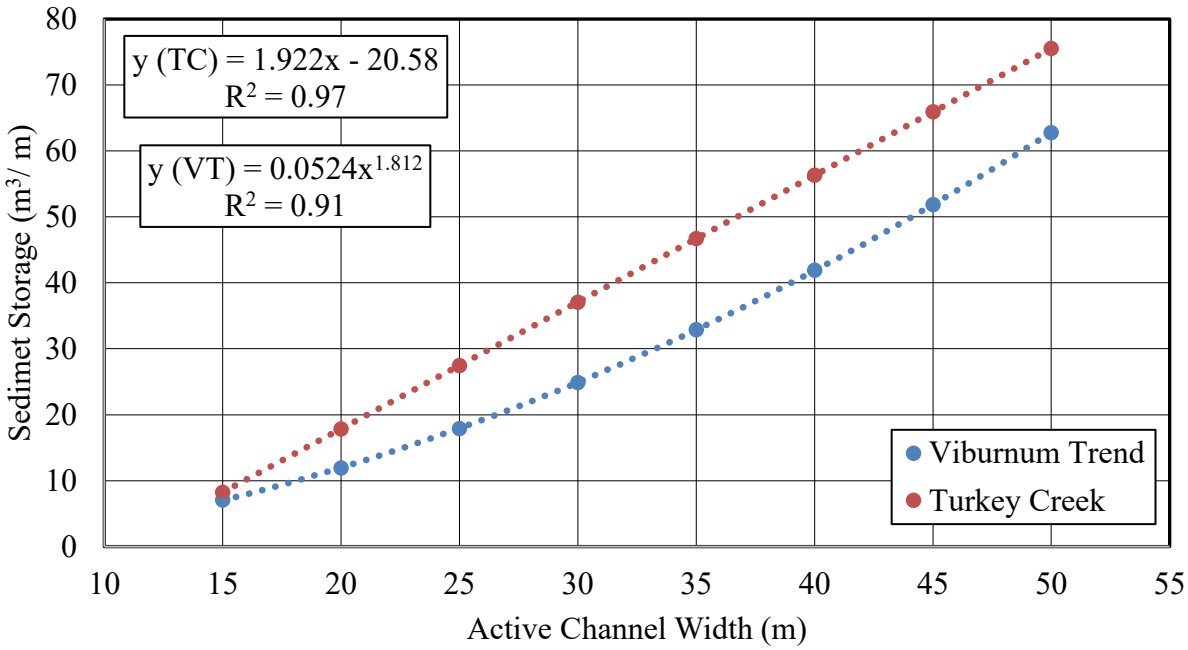

Figure 32. Relationship between volumetric sediment storage in Turkey Creek (TC) (n=11) and six streams the Viburnum Trend (VT) (n = 62).

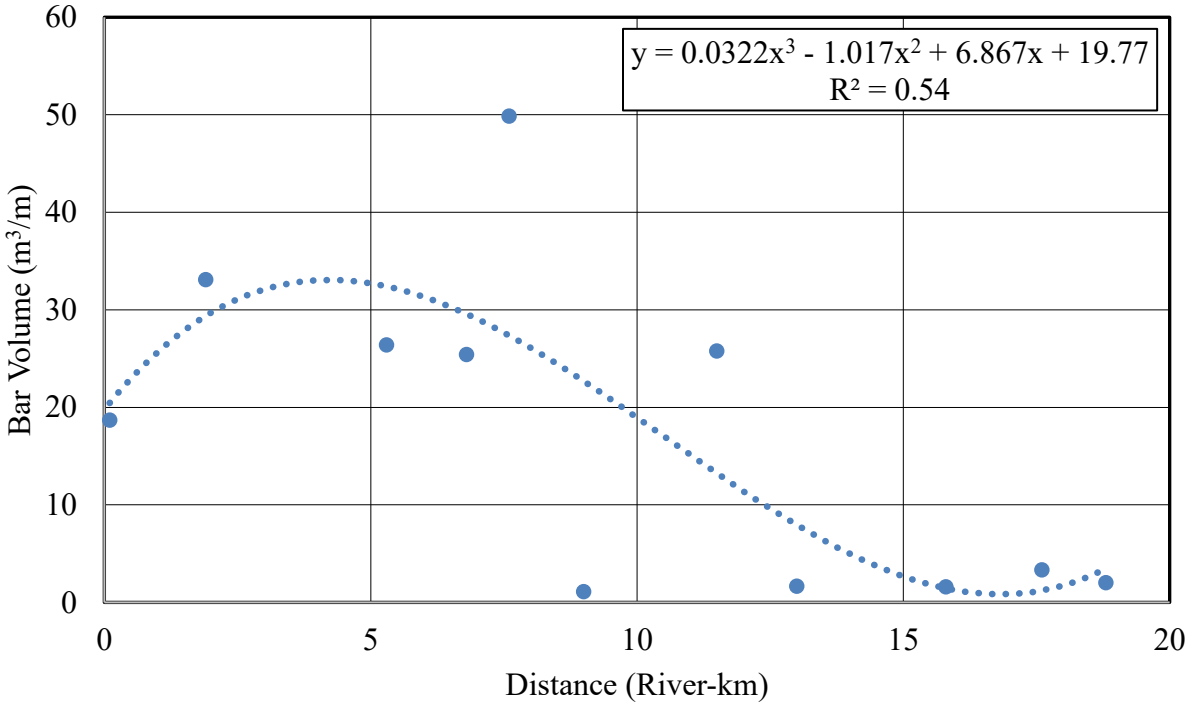

Figure 33. Downstream trend for contaminated sediment storage in channel bar deposits.

CONCLUSION

Despite most mining activities ending in the 1920s, Pb and Zn contaminated sediment is dispersed throughout Turkey Creek and its tributaries located below mining sites. This study provides information on the spatial trends of metal concentrations in the main channel and tributaries, quantifies the storages of Pb and Zn in both fine and coarse sediment, and among different fluvial deposits. In addition, in-channel storage of sediment and metals is explained by geomorphic characteristics using regression modelling. There have been no previous studies in the region that have considered coarse-grained sediment or applied a geomorphic approach when assessing mining-related contamination. This study has filled a research gap by quantifying the amount of Pb and Zn stored within fine and coarse grain size fractions and determining the relationships between different geomorphic characteristics and sediment storage. Further, the results of this study can be useful for informing project managers throughout the region on the location of metalliferous channel deposits for remediation.

Storage values were calculated from field surveys of channel deposits, sediment size analysis, and geochemical analysis. Mining activities generated large amounts of "chat" in coarse size fractions which accounts for 39 percent of Pb and 48 percent of Zn storage in the active channel including bed, bar, bench, and chute deposits. Therefore, coarse sediment management should be considered when assessing contamination throughout the watershed. Once contaminated sediment enters the channel, it can remain as a secondary source of contamination for extended periods of time through remobilization by geochemical weathering, dissolution, and abrasion. To date, this is the only study in the TSMD to determine Pb and Zn storage trends in

multiple sediment size fractions and different channel deposits. The primary conclusions of this study are:

1. Mass sediment storage increased downstream from R-km 16.5 until R-km 4 where it began to decline. The largest storage values were observed in gravel bars which stored 76 percent of contaminated sediment mass overall.
2. Active channel width, downstream distance (R-km), and drainage area strongly correlated with volumetric storage showing that channel geometry can be used to estimate total metal storage within the Turkey Creek main channel using linear regression modeling.
3. The highest Pb and Zn concentrations were observed in fine sediment with metal concentrations often far exceeding the Tri-State Mining District specific probable effects concentration. Metal concentrations did not follow a standard distance decay trend. Lead concentrations in channel sediment began to decrease farther upstream compared to Zn for both fine and coarse size fractions. Mining history, clustered mining sites, and variable geomorphic controls on sediment storage contributed to the non-uniform dispersal of contaminated sediments.
4. Approximately 440,000 m^3 (575,000 yd^3) of sediment, 127,000 kg of Pb, and 2,200,000 kg of Zn are stored within the Turkey Creek main channel below R-km 18.8. Coarse sediment stored 47,800 kg of Pb and 1,040,000 kg of Zn. Seventy-four percent of was sediment storage, 80 percent of Zn storage, and 77 percent of Zn storage, was located in the middle segment which was characterized by draining mined areas.

Understanding longitudinal storage and metal trends, metal storage by size fraction and deposit, and the relationship between storage and geomorphic characteristics all aid in remediating contained sediment in Turkey Creek. Knowing the spatial distribution of metal in the channel can guide remediation efforts to focus on reaches in Turkey Creek with the greatest remaining contamination. The coarse sediment size fractions are often overlooked in studies assessing heavy metal contamination. However, this study concludes a significant percentage of Pb and Zn in the active channel is associated with coarse sediment. Evaluating storage in size fractions could help predict future trends of contaminant dispersal since residency time is directly related to grain size. The relationship between active channel width and sediment storage

could potentially be used to estimate total volume of sediment for similar streams, but more research would be required to validate the claim.

REFERENCES

Ahmed, J., Constantine, J.A., Dunne, T., 2019. The role of sediment supply in the adjustment of channel sinuosity across the Amazon Basin. Geology 47 (9), 807-810.

Allert, A.L., DiStefano, R.J., Schmitt, C.J., Fairchild, J.F., Brumbaugh, W.G., 2012. Effects of mining-derived metals on riffle-dwelling crayfish in southwestern Missouri and southeastern Kansas of the Tri-State Mining District, USA. Environmental Contamination and Toxicology 63 (4), 563-573.

Angelo, R.T., Cringan, M.S., Chamberlain, D.L., Stahl, A.J., Haslouer, S.G., Goodrich, C.A., 2007. Residual effects of lead and zinc mining on freshwater mussels in the Spring River Basin (Kansas, Missouri, and Oklahoma, USA). Science of the Total Environment 384 (1/3), 467-496.

Appold, M.S., Garven, G., 1999. The hydrology of ore formation in the Southeast Missouri District; numerical models of topography-driven fluid flow during the Ouachita Orogeny. Economic Geology 94 (6), 913-935.

Barks, J.H., 1977. Effects of abandoned lead and zinc mines and tailings piles on water quality in the Joplin area, Missouri. Water-Resources Investigations Report 77-75. U.S. Geological Survey, Reston, Virginia.

Besser, J.M., Ingersoll, C.G., Brumbaugh, W.G., Kemble, N.E., May, T.W., Wang, N., Roberts, A.D., 2015. Toxicity of sediments from lead–zinc mining areas to juvenile freshwater mussels (Lampsilis siliquoidea) compared to standard test organisms. Environmental Toxicology and Chemistry 34 (3), 626-639.

Beyer, W.N., Dalgarn, J., Dudding, S., French, J.B., Mateo, R., Miesner, J., Spann, J., 2004. Zinc and lead poisoning in wild birds in the Tri-State Mining District (Oklahoma, Kansas, and Missouri). Environmental Contamination and Toxicology 48 (1), 108-117.

Bradley, S.B., Cox, J.J., 1986. Heavy metals in the Hamps and Manifold valleys, North Staffordshire, UK: distribution in floodplain soils. Science of the Total Environment 50, 103-128.

Bradley, S.B., 1989. Incorporation of metalliferous sediments from historic mining into river floodplains. GeoJournal 19 (1), 5-14.

Bridge, J.S., 2009. Rivers and floodplains: forms, processes, and sedimentary record. John Wiley & Sons, Hoboken, New Jersey.

Brockie, D.C., Hare, E.H., Dingess, P.R., 1933. The geology and ore deposits of the Tri-State district of Missouri, Kansas, and Oklahoma. Ore Deposits of the United States, 1967, 400-430.

Buffington, J.M., 2012. Changes in channel morphology over human time scales. Gravel-Bed Rivers: Processes, Tools, Environments 32, 433-463.

Bunte, K., Abt, S.R., 2001. Sampling Surface and Subsurface Particle-size Distributions in Wadable Gravel-and Bobble-bed Streams for Analyses in Sediment Transport, Hydraulics, and Streambed Monitoring. General Technical Report RMRS-GTR-74. U.S. Department of Agriculture, Forest Service, Rocky Mountain Research Station, Fort Collins, Colorado (428 pp.).

Byrne, P., Reid, I., Wood, P.J., 2010. Sediment geochemistry of streams draining abandoned lead/zinc mines in central Wales: the Afon Twymyn. Journal of Soils and Sediments, 10 (4), 683-697.

Chao, T.T., Theobald, P.K., 1976. The significance of secondary iron and manganese oxides in geochemical exploration. Economic Geology 71 (8), 1560-1569.

Davis, L., 2009. Sediment entrainment potential in modified alluvial streams: implications for re-mobilization of stored in-channel sediment. Physical Geography 30 (3), 249-268.

Dean, D.J., Schmidt, J.C., 2013. The geomorphic effectiveness of a large flood on the Rio Grande in the Big Bend region: Insights on geomorphic controls and post-flood geomorphic response. Geomorphology 201, 183-198.

Dickson, K.L., Maki, A.W., Brungs, W.A., 2013. Fate and effects of sediment-bound chemicals in aquatic systems: proceedings of the Sixth Pellston Workshop, Florissant, Colorado, August 12-17, 1984.

Dietrich, W.E., Whiting, P., 1989. Boundary shear stress and sediment transport in river meanders of sand and gravel. River Meandering 12, 1-50.

Eades, H., Arceneaux T., Pavlowsky R.T., 2021. Mining-metal profiles and sediment characteristics in legacy floodplain deposits in Turkey Creek, Tri-State Zn-Pb District, southwest Missouri. Binghamton Geomorphology Symposium, Middle Tennessee State University, Murfreesboro, Tennessee, October 15-17, 2021.

Eekhout, J.P.C., Hoitink, A.J.F., 2015. Chute cutoff as a morphological response to stream reconstruction: The possible role of backwater. Water Resources Research 51 (5), 3339-3352.

Ferguson, M., 2021. Preliminary Research on Sediment Concentrations in Bar Sediment in Turkey Creek. (Unpublished Master's Thesis). Department of Geography, Geology, and Planning, Missouri State University, Springfield, MO.

Fernandes, G.W., Goulart, F.F., Ranieri, B.D., Coelho, M.S., Dales, K., Boesche, N., Soares-Filho, B., 2016. Deep into the mud: ecological and socio-economic impacts of the dam breach in Mariana, Brazil. Natureza & Conservação 14 (2), 35-45.

Flener, C., Vaaja, M., Jaakkola, A., Krooks, A., Kaartinen, H., Kukko, A., Alho, P., 2013. Seamless mapping of river channels at high resolution using mobile LiDAR and UAV photography. Remote Sensing 5 (12), 6382-6407.

Fujita, Y., Muramoto Y., 1985. Studies on the process of development of alternate bars. Bulletin of the Disaster Prevention Research Institute 35 (3), 55–86.

Gallart, F., Benito, G., Martín-Vide, J. P., Benito, A., Prió, J.M., Regüés, D., 1999. Fluvial geomorphology and hydrology in the dispersal and fate of pyrite mud particles released by the Aznalcóllar mine tailings spill. Science of the Total Environment 242 (1/3), 13-26.

Gibson, A.M., 1972. Wilderness bonanza—The Tri-State District of Missouri, Kansas, and Oklahoma. University of Oklahoma Press, Norman Oklahoma.

Gilbert, G.K., Murphy, E.C., 1914. The transportation of debris by running water. Professional Paper 86. U.S. Government Printing Office, Washington D.C.

Gilbert, G.K., 1917. Hydraulic-mining debris in the Sierra Nevada. U.S. Professional Paper 105. Government Printing Office, Washington D.C.

Glover, R.E., 1964. Dispersion of dissolved or suspended materials in flowing streams. U.S. Geological Survey Professional Paper 433-B. Government Printing Office, Washington D.C.

Graf, W.L., Clark, S.L., Kammerer, M.T., Lehman, T., Randall, K., Schroeder, R., 1991. Geomorphology of heavy metals in the sediments of Queen Creek, Arizona, USA. Catena 18 (6), 567-582.

Graf, W.L., 1996. Transport and deposition of plutonium-contaminated sediments by fluvial processes, Los Alamos Canyon, New Mexico. Geological Society of America Bulletin 108 (10), 1342-1355.

Gutiérrez, M., Wu, S.S., Peebles, J.L., 2015. Geochemical mapping of Pb-and Zn-contaminated streambed sediments in southwest Missouri, USA. Journal of Soils and Sediments 15 (1), 189-197.

Gutiérrez, M., Wu, S.S., Rodriguez, J.R., Jones, A.D., Lockwood, B.E., 2016. Assessing the state of contamination in a historic mining town using sediment chemistry. Environmental Contamination and Toxicology 70 (4), 747-756.

Gutiérrez, M., Collette, Z.J., McClanahan, A.M., Mickus, K., 2019. Mobility of metals in sediments contaminated with historical mining wastes: Example from the Tri-State Mining District, USA. Soil Systems 3 (1), 22.

Gutiérrez, M., Qiu, X., Collette, Z.J., Lurvey, Z.T., 2020. Metal content of stream sediments as a tool to assess remediation in an area recovering from historic mining contamination. Minerals 10 (3), 247.

Håkanson, L., 1984. Sediment sampling in different aquatic environments: statistical aspects. Water Resources Research 20 (1), 41-46.

Hammer, T.R., 1972. Stream channel enlargement due to urbanization. Water Resources Research 8 (6), 1530-1540.

Hansen, E., 1967. The formation of meanders as a stability problem. Basic Resource Progress Report. University of Denmark, Lyngby, Denmark, (pp. 9-13).

Henderson, F.M., 1961. Stability of alluvial channels. Journal of the Hydraulics Division 87 (6), 109-138.

Hinrichs, D.R., 1996. Surface waste of the Tri-state mining District. Tailings and Mine Waste '96. CRC Press, Boca Raton, Florida (pp. 577-580).

Hjulstrom, F., 1939. Transportation of detritus by moving water: Part 1. Transportation. Recent Marine Sediments 4, 5-31.

Horowitz, A.J., 1991. A Primer on Sediment-Trace Element Chemistry. 2nd ed. Lewis Publishers, Inc., Chelsea, Michigan.

Horowitz, A.J., Stephens, V.C., 2008. The effects of land use on fluvial sediment chemistry for the conterminous US—Results from the first cycle of the NAWQA Program: Trace and major elements, phosphorus, carbon, and sulfur. Science of the Total Environment 400 (1/3), 290-314.

Howe, W.B., Koenig, J.W., 1961. The stratigraphic succession in Missouri. vol 4. Missouri Geological Survey, Rolla, Missouri.

Hürkamp, K., Raab, T., Völkel, J., 2009. Two and three-dimensional quantification of lead contamination in alluvial soils of a historic mining area using field portable X-ray fluorescence (FPXRF) analysis. Geomorphology 110 (1/2), 28-36.

HydroGeoLogic (HGL), 2019. Untitled Report. Reston, Virginia.

Ingersoll, C.G., Ivey, C.D., Brumbaugh, W.G., Besser, J.M., Kemble, N.E., 2009. Toxicity assessment of sediments from the Grand Lake O' the Cherokees with the amphipod Hyalella azteca. Administrative Report CERC-8335-FY09-20-01. U.S. Geological Survey, Columbia, Missouri.

Jacobson, R.B., Coleman, D.J., 1986. Stratigraphy and recent evolution of Maryland Piedmont flood plains. American Journal of Science 286 (8), 617-637.

Jacobson, R.B., Primm, A.T., 1994. Historical land-use changes and potential effects of stream disturbance in Ozark Plateaus, Missouri. United States Geologic Survey, Open-file Report, 94-333. U.S. Geological Survey, Rolla, Missouri.

Jacobson, R.B., 1995. Spatial controls on patterns of land-use induced stream disturbance at the drainage-basin scale—an example from gravel-bed streams of the Ozark Plateaus, Missouri. Washington DC American Geophysical Union Geophysical Monograph Series 89, 219-239.

Jacobson, R.B., Gran, K.B., 1999. Gravel sediment routing from widespread, low-intensity landscape disturbance, Current River Basin, Missouri. Earth Surface Processes and Landforms: The Journal of the British Geomorphological Research Group 24 (10), 897-917.

James, L.A., 1991. Incision and morphologic evolution of an alluvial channel recovering from hydraulic mining sediment. Geological Society of America Bulletin 103 (6), 723-736.

James, L.A., 2013. Legacy sediment: definitions and processes of episodically produced anthropogenic sediment. Anthropocene 2, 16-26.

James, L.A., Lecce, S.A., 2013. Impacts of land-use and land-cover change on river systems. Editors in chief. In: Shroder, J., Wohl, E. (Eds.), Treatise on Geomorphology. Fluvial Geomorphology vol. 9. Academic Press, San Diego, CA, pp. 768–793.

John, D.A., Leventhal, J.S., 1995. Bioavailability of metals. Preliminary compilation of descriptive geoenvironmental mineral deposit models. Open-file Report 95-831. U.S. Geological Survey, Denver, Colorado (pp. 10-18).

Johnson, A.W., Gutiérrez, M., Gouzie, D., McAliley, L.R., 2016. State of remediation and metal toxicity in the Tri-State Mining District, USA. Chemosphere 144, 1132-1141.

Juracek, K.E., 2013. Occurrence and Variability of Mining-related Lead and Zinc in the Spring River Flood Plain and Tributary Flood Plains, Cherokee County, Kansas, 2009-11. Scientific Investigations Report 2013-5028. U.S. Geological Survey, Reston, Virginia.

Juracek, K.E., Drake, K.D., 2016. Mining-related sediment and soil contamination in a large superfund site: characterization, habitat implications, and remediation. Environmental Management 58 (4), 721-740.

Kim, M.J., Ahn, K.H., Jung, Y., Lee, S., Lim, B.R., 2003. Arsenic, cadmium, chromium, copper, lead, and zinc contamination in mine tailings and nearby streams of three abandoned mines from Korea. Bulletin of Environmental Contamination and Toxicology 70 (5), 942-947.

Kitson, H.W., 1919. The mining districts of Joplin and southeast Missouri. Engineering and Mining Journal 104, 1067.

Klein, C., C.S. Hurlbut, J., 1985. Manual of Mineralogy. 12th ed. John Wiley & Sons, Hoboken, New Jersey.

Knighton, A.D., 1987. Tin mining and sediment supply to the Ringarooma River, Tasmania, 1875–1979. Australian Geographical Studies 25 (1), 83-97.

Knighton, A.D., 1989. River adjustment to changes in sediment load: the effects of tin mining on the Ringarooma River, Tasmania, 1875–1984. Earth Surface Processes and Landforms 14 (4), 333-359.

Knighton, A.D., 1991. Channel bed adjustment along mine-affected rivers of northeast Tasmania. Geomorphology 4 (3/4), 205-219.

Knox, J.C., 1987. Historical valley floor sedimentation in the Upper Mississippi Valley. Annals of the Association of American Geographers 77 (2), 224-244.

Ladd, S.C., Marcus, W.A., Cherry, S., 1998. Differences in trace metal concentrations among fluvial morphologic units and implications for sampling. Environmental Geology 36 (3), 259-270.

Lee, C.G., Chon, H.T., Jung, M.C., 2001. Heavy metal contamination in the vicinity of the Daduk Au–Ag–Pb–Zn mine in Korea. Applied Geochemistry 16 (11/12), 1377-1386.

Leopold, L.B., Wolman, M.G., Miller, J.P., 1964. Fluvial Processes in Geomorphology. Freeman and Company, San Francisco, California.

Lewin, J., 1978. Floodplain geomorphology. Progress in Physical Geography 2, 408–437.

Lewin, J., Macklin, M.G., 1987. Metal mining and floodplain sedimentation in Britain. International Geomorphology 1986, 1009-1027.

Luoma, S.N., 1983. Bioavailability of trace metals to aquatic organisms—a review. Science of the Total Environment 28 (1/3), 1-22.

Macklin, M.G., Dowsett, R.B., 1989. The chemical and physical speciation of trace metals in fine grained overbank flood sediments in the Tyne basin, north-east England. Catena 16 (2), 135-151.

Macklin, M.G., Lewin, J., 1989. Sediment transfer and transformation of an alluvial valley floor: the River South Tyne, Northumbria, UK. Earth Surface Processes and Landforms 14 (3), 233-246.

Macklin, M.G., Klimek, K., 1992. Dispersal, storage and transformation of metal contaminated alluvium in the upper Vistula basin, southwest Poland. Applied Geography 12 (1), 7-30.

Manger, G.E., 1963. Porosity and bulk density of sedimentary rocks. Geological Survey Bulletin 1144-E, 1–55.

Marcus, W.A., 1987. Copper Dispersion in Ephemeral Stream Sediment. Earth Surface Processes and Landforms 12 (3), 217-228.

Martin, J.M., Meybeck, M., 1979. Elemental mass balance of material carried by world major rivers. Marine Chemistry 7 (3), 173-206.

Martin, D.J., Pavlowsky, R.T., 2011. Spatial patterns of channel instability along an Ozark river, southwest Missouri. Physical Geography 32 (5), 445-468.

McCauley, J.R. Brady, L.L., Wilson, F.W., 1983. A study of stability problems and hazard evaluation of the Kansas portion of the tri-state mining area. Kansas Geological Survey 83 (2), 193.

Merefield, J.R., 1987. Heavy metals in Teign Valley sediments: ten years after. Proceedings of the Ussher Society 6 (4), 529-535.

Midwest Regional Climate Center (MRCC), 2021. State and Climate Division Data - Monthly by Year. https://mrcc.illinois.edu/CLIMATE/nClimDiv/STCD_monthly1.jsp.

Milhous, R.T., 2002. Measurement of the bed material of gravel-bed rivers. Hydraulic Measurements and Experimental Methods Specialty Conference, Estes Park, Colorado, July 28 – August 1, 2002.

Miller, J.R., 1997. The role of fluvial geomorphic processes in the dispersal of heavy metals from mine sites. Journal of Geochemical Exploration 58 (2/3), 101-118.

Miller, J.R., Orbock Miller, S.M., 2007. Contaminated Rivers: A Geomorphological-Geochemical Approach to Site Assessment and Remediation. Springer, Dordrecht, The Netherlands (418 pp.).

Montgomery, D.R., Buffington, J.M., 1997. Channel-reach morphology in mountain drainage basins. Geological Society of America Bulletin 109 (5), 596-611.

Moore, J.N., Brook, E.J., Johns, C., 1989. Grain size partitioning of metals in contaminated, coarse-grained river floodplain sediment: Clark Fork River, Montana, USA. Environmental Geology and Water Sciences 14 (2), 107-115.

Moore, J.N., Luoma, S.N., 1990. Hazardous wastes from large-scale metal extraction. A case study. Environmental Science & Technology 24 (9), 1278-1285.

National Land Cover Database (NLCD), 2016. United States Geological Survey. https://www.mrlc.gov/data?f%5B0%5D=year%3A2016.

Natural Resources Conservation Service (NRCS), 2020. Web Soil Survey. United States Department of Agriculture. http://websoilsurvey.sc.egov.usda.gov/.

Nelson, A., Dubé, K., 2016. Channel response to an extreme flood and sediment pulse in a mixed bedrock and gravel-bed river. Earth Surface Processes and Landforms 41 (2), 178-195.

Neuberger, J.S., Mulhall, M., Pomatto, M.C., Sheverbush, J., Hassanein, R.S., 1990. Health problems in Galena, Kansas: a heavy metal mining Superfund site. Science of the Total Environment 94 (3), 261-272.

Nigh, T.A., Schroeder. W.A., 2002. Atlas of Missouri Ecoregions. Missouri Department of Conservation, Jefferson City.

Nriagu, J.O., 1996. A history of global metal pollution. Science 272 (5259), 223-223.

Owen, M.R., Pavlowsky, R.T., Womble, P.J., 2011. Historical disturbance and contemporary floodplain development along an Ozark river, southwest Missouri. Physical Geography 32 (5), 423-444.

Panfil, M.S., Jacobson, R.B., 2001. Relations Among Geology, Physiography, Land Use, and Stream Habitat Conditions in the Buffalo and Current River systems, Missouri and Arkansas. Biological Science Report 2001-0005. U.S. Geological Survey, Columbia, Missouri.

Park, H., Noh, K., Min, J.J., Rupar, C., 2020. Effects of Toxic Metal Contamination in the Tri-State Mining District on the Ecological Community and Human Health: A Systematic Review. International Journal of Environmental Research and Public Health 17 (18), 6783.

Pavlowsky, R.T., 1996. Fluvial transport and long term mobility of mining-related zinc. Tailings and Mine Waste '96. CRC Press, Boca Raton, Florida (pp. 395-404).

Pavlowsky, R.T., Owen, M.R., Martin, D.J., 2010. Distribution, geochemistry, and storage of mining sediment in channel and floodplain deposits of the Big River system in St. Francois, Washington, and Jefferson Counties, Missouri. The Ozarks Environmental and Water Resources Institute (OEWRI), Springfield, Missouri.

Pavlowsky, R.T., Owen, M.R., 2016. Stream Sediment and Floodplain Soil Contamination in the Viburnum Trend in Crawford, Dent, Iron, Reynolds, and Washington Counties in Southeast Missouri. The Ozarks Environmental and Water Resources Institute (OEWRI), Springfield, Missouri.

Pavlowsky, R.T., Lecce, S.A., Owen, M.R., Martin, D.J., 2017. Legacy sediment, lead, and zinc storage in channel and floodplain deposits of the Big River, Old Lead Belt Mining District, Missouri, USA. Geomorphology 299, 54-75.

Peebles, J.L., 2014. Spatial Analysis of Mining Related Contamination of Turkey Creek Watershed in the Tri-State Mining District, Joplin, MO. (Master's Thesis). Department of Geography, Geology, and Planning, Missouri State University, Springfield, MO.

Plumlee, G.S., Leach, D.L., Hofstra, A.H., Landis, G.P., Rowan, E.L., Viets, J.G., 1994. Chemical reaction path modeling of ore deposition in Mississippi Valley-type Pb-Zn deposits of the Ozark region, US Midcontinent. Economic Geology 89 (6), 1361-1383.

Pope, L.M., 2005 Assessment of Contaminated Streambed Sediment in the Kansas Part of the Historic Tri-State Lead and Zinc Mining District, Cherokee County. Scientific Investigations Report 2005-5251. U.S. Geological Survey, Reston, Virginia.

Pursley, T.J., 2021. Spatial variability of nonpoint source yields in Ozark Highlands watersheds under historical and recent land use conditions. (Master's Thesis). Department of Geography, Geology, and Planning, Missouri State University, Springfield, MO.

Rhoads, B.L., 1996. Mean structure of transport-effective flows at an asymmetrical confluence when the main stream is dominant. Coherent Flow Structures in Open Channels. John Wiley & Sons, Hoboken, New Jersey, (pp. 491-517).

Rhoads, B.L., Cahill, R.A., 1999. Geomorphological assessment of sediment contamination in an urban stream system. Applied Geochemistry 14 (4), 459-483.

Ritcey, G.M., 1989. Tailings Management: Problems and Solutions in the Mining Industry. Elsevier, Amsterdam.

River Studies, 2021. Compound bank-attached bar. https://riverstyles.com/?portfolio=compound-bank-attached-bar.

Robert, A., 2003. River Processes: An Introduction to Fluvial Dynamics. Routledge, Oxfordshire, England, U.K.

Rosgen, D.L., Silvey, H.L., 1996. Applied river morphology. vol 1481. Wildland Hydrology, Pagosa Springs, Colorado.

Royall, D., Davis, L., Kimbrow, D.R., 2010. In-channel benches in small watersheds: examples from the southern Piedmont. Southeastern Geographer 50 (4), 445-467.

Sambrook Smith, G.H., Ferguson, R.I., 1995. The gravel-sand transition along river channels. Journal of Sedimentary Research 65 (2A), 423-430.

Schoolcraft, H., 1996. Rude Pursuits and Rugged Peaks: Schoolcraft's Ozark Journal, 1818-1819. University of Arkansas Press, Fayetteville, Arkansas.

Seaber, P.R., Kapinos, F.P., Knapp, G.L., 1987. Hydrologic Unit Maps. Open-file Report 2294. U.S. Geological Survey Water, Denver, Colorado.

Simon, A., Dickerson, W., Heins, A., 2004. Suspended-sediment transport rates at the 1.5-year recurrence interval for ecoregions of the United States: transport conditions at the bankfull and effective discharge?. Geomorphology 58 (1/4), 243-262.

Skidmore, J.F.,1964. Toxicity of zinc compounds to aquatic animals, with special reference to fish. The Quarterly Review of Biology 39 (3), 227-248.

Smith, D.B., Cannon, W.F., Woodruff, L.G., Solano Federico, Kilburn, J.E., Fey, D.L., 2013. Geochemical and mineralogical data for soils of the conterminous Technical Report 801-3378323. U.S. Geological Survey, Reston, Virginia.

Smith, D.C., 2016. Occurrence, distribution, and volume of metals-contaminated sediment of selected streams draining the Tri-State Mining District, Missouri, Oklahoma, and Kansas, 2011–12. Scientific Investigations Report 2016-5144. U.S. Geological Survey, Reston, Virginia.

Stewart, D.R., 1986. A Brief Description of the Historical, Ore Production, Mine Pumping, and Prospecting Aspects of the Tri-State Zinc-Lead District of Missouri, Kansas, and Oklahoma. Association of Missouri Geologists, Rolla, Missouri.

Stoffell, B., Appold, M.S., Wilkinson, J.J., McClean, N.A., Jeffries, T.E., 2008. Geochemistry and evolution of Mississippi Valley-type mineralizing brines from the Tri-State and northern Arkansas districts determined by LA-ICP-MS microanalysis of fluid inclusions. Economic Geology 103 (7), 1411-1435.

Swennen, R., Van Keer, I., De Vos, W., 1994. Heavy metal contamination in overbank sediments of the Geul river (East Belgium): Its relation to former Pb-Zn mining activities. Environmental Geology 24 (1), 12-21.

Taggart, A.F., 1945. Handbook of Mineral Dressing: Ores and Industrial Minerals. John Wiley and Sons, New York.

Tessier, A., Campbell, P.G., Bisson, M., 1982. Particulate trace metal speciation in stream sediments and relationships with grain size: implications for geochemical exploration. Journal of Geochemical Exploration 16 (2), 77-104.

Trimble, S.W., 1983. A sediment budget for Coon Creek basin in the Driftless Area, Wisconsin, 1853-1977. American Journal of Science 283 (5), 454-474.

United States Environmental Protection Agency (USEPA), 1997. EPA Superfund Record of Decision—Cherokee County, Kansas. Open-file Report 97-073. U.S. Environmental Protection Agency, Lenexa, Kansas.

United States Environmental Protection Agency (USEPA), 2013. Level III and IV Ecoregions of the Continental United States. https://www.epa.gov/eco-research/level-iii-and-iv-ecoregions-continental-united-states.

United States Environmental Protection Agency (USEPA), 2017. Fourth Five-Year Review Report For Oronogo-Duenweg Mining Belt Superfund Site Jasper County, Missouri. U.S. Environmental Protection Agency, Lenexa, Kansas.

United States Environmental Protection Agency (USEPA), 2021. Oronogo-Duenweg Mining Belt Joplin, MO Cleanup Activities. https://cumulis.epa.gov/supercpad/SiteProfiles/index.cfm?fuseaction=second.cleanup&id=0701290.

United States Fish and Wildlife Service (USFWS), 2013. Tri-State Transition Zone Assessment Study. U.S. Fish and Wildlife Service, Tulsa, Oklahoma.

United States Geological Survey (USGS), United States Department of Agriculture (USDA), 2013. Federal Standards and Procedures for the National Watershed Boundary Dataset (WBD). Techniques and Methods. 4th ed. U.S. Geological Survey, Reston, Virginia.

United States Geological Survey (USGS), 2020a. 3D Elevation Program. https://apps.nationalmap.gov/downloader/#/.

United States Geological Survey (USGS), 2020b. National Hydrography Dataset. https://apps.nationalmap.gov/downloader/#/.

United States Geological Survey (USGS), 2021. USGS Water Data for the Nation. https://waterdata.usgs.gov/nwis.

Venkateswarlu, K., Nirola, R., Kuppusamy, S., Thavamani, P., Naidu, R., Megharaj, M., 2016. Abandoned metalliferous mines: ecological impacts and potential approaches for reclamation. Reviews in Environmental Science and Bio/Technology 15 (2), 327-354.

Walling, D.E., Owens, P.N., Leeks, G.J., 1998. The role of channel and floodplain storage in the suspended sediment budget of the River Ouse, Yorkshire, UK. Geomorphology 22, (3/4), 225-242.

Walling, D.E., Owens, P.N., Carter, J., Leeks, G.J.L., Lewis, S., Meharg, A.A., Wright, J., 2003. Storage of sediment-associated nutrients and contaminants in river channel and floodplain systems. Applied Geochemistry 18 (2), 195–220.

Whitney, P.R., 1975. Relationship of manganese-iron oxides and associated heavy metals to grain size in stream sediments. Journal of Geochemical Exploration 4 (2), 251-263.

Wildhaber, M.L., Allert, A.L., Schmitt, C.J., Tabor, V.M., Mulhern, D., Powell, K.L., Sowa, S.P., 2000. Natural and anthropogenic influences on the distribution of the threatened Neosho madtom in a Midwestern warmwater stream. Transactions of the American Fisheries Society 129 (1), 243-261.

Wolfenden, P.J., Lewin, J., 1977. Distribution of pollutants in floodplain sediments. Catena 4 (3), 309-317.

Wolfenden, P.J., Lewin, J., 1978. Distribution of metal pollutants in active stream sediments. Catena 5 (1), 67-78.

Wood-Smith, R.D., Buffington, J.M., 1996. Multivariate geomorphic analysis of forest streams: implications for assessment of land use impacts on channel condition. Earth Surface Processes and Landforms 21 (4), 377-393.

Wright, C.A., 1918. Mining and Milling of Lead and Zinc Ores in the Missouri-Kansas-Oklahoma Zinc District, Bulletin 154. Bureau of Mines, Department of Interior, Washington DC: United States Government Printing Office.

APPENDICES

Appendix A. The Measured Geometry at Each Transect for Every Sample Site.

Site	Transect	Coordinates (DD)		Width (m)				Max Depth (m)			Bank Height (m)		
		Latitude	Longitude	Active	Left offset	Right offset	Bankfull	Water	Probe	Bedrock	Left	Right	Bankfull (min)
1	1	37.0902	-94.4605	13.5	2.0	0.3	15.8	0.82	0.05	0.87	3.72	1.82	1.82
1	2	37.0903	-94.4608	13.0	2.0	2.0	17.0	0.82	0.05	0.87	2.82	3.82	2.82
1	3	37.0902	-94.4612	12.0	3.0	3.0	18.0	0.66	0	0.66	4.66	2.96	2.96
1	4	37.0903	-94.4615	17.0	0.5	1.0	18.5	0.36	0.2	0.56	2.46	2.16	2.16
1	5	37.0903	-94.4618	19.4	0.5	1.0	20.9	0.35	0.1	0.45	1.95	2.15	1.95
1	6	37.0904	-94.4621	14.0	2.0	0.5	16.5	0.45	0.45	0.9	3.35	1.45	1.45
1	7	37.0904	-94.4623	14.2	3.0	3.0	20.2	0.15	0.43	0.58	3.05	3.05	3.05
2	1	37.0949	-94.4704	10.5	1.0	4.0	15.5	0.36	0.23	0.59	2.16	2.06	2.06
2	2	37.0950	-94.4706	11.5	2.0	2.0	15.5	1.15	0.00	1.15	2.95	3.85	2.95
2	3	37.0950	-94.4708	16.0	2.0	2.0	20.0	0.80	0.10	0.90	2.60	3.50	2.60
2	4	37.0949	-94.4710	21.0	3.0	3.0	27.0	0.15	0.10	0.25	2.25	2.55	2.25
2	5	37.0949	-94.4713	9.0	4.0	2.0	15.0	0.35	0.00	0.35	2.45	2.15	2.15
2	6	37.0950	-94.4715	11.5	0.0	3.0	14.5	0.60	0.30	0.90	3.00	3.00	3.00
2	7	37.0950	-94.4717	11.0	1.5	1.5	14.0	0.40	0.60	1.00	2.40	2.40	2.40
3	1	37.1009	-94.4858	16.5	0.0	2.0	18.5	0.30	0.25	0.55	2.60	2.70	2.60
3	2	37.1009	-94.4862	18.0	0.0	0.5	18.5	0.35	0.00	0.35	2.35	1.85	1.85

Appendix A Continued.

Site	Transect	Coordinates (DD)		Width (m)				Max Depth (m)			Bank Height (m)		
		Latitude	Longitude	Active	Left offset	Right offset	Bankfull	Water	Probe	Bedrock	Left	Right	Bankfull (min)
3	3	37.1011	-94.4863	13.0	0.0	1.5	14.5	1.30	0.00	1.30	3.70	3.00	3.00
3	4	37.1013	-94.4865	14.0	3.0	2.0	19.0	0.50	0.00	0.50	2.80	2.20	2.20
3	5	37.1016	-94.4866	13.0	1.0	1.0	15.0	0.20	0.00	0.20	2.20	1.40	1.40
3	6	37.1017	-94.4868	14.0	1.0	2.0	17.0	0.27	0.00	0.27	2.47	2.57	2.47
3	7	37.1018	-94.4871	15.0	0.0	0.0	15.0	0.45	0.00	0.45	2.35	3.25	2.35
4	1	37.1080	-94.5085	10.0	1.4	2.5	13.9	0.48	0.00	0.48	2.03	2.98	2.03
4	2	37.1081	-94.5088	13.0	0.2	1.3	14.5	0.35	0.00	0.35	1.15	1.20	1.15
4	3	37.1080	-94.5090	9.0	1.5	0.0	10.5	0.65	0.10	0.75	1.85	1.45	1.45
4	4	37.1080	-94.5092	11.5	1.3	1.0	13.8	0.30	0.15	0.45	1.40	1.40	1.40
4	5	37.1081	-94.5095	12.0	2.2	1.0	15.2	0.20	0.23	0.43	3.00	0.70	0.70
4	6	37.1081	-94.5097	11.5	2.8	0.5	14.8	0.20	0.40	0.60	3.00	1.45	1.45
4	7	37.1082	-94.5099	7.0	2.5	1.0	10.5	0.46	0.10	0.56	2.96	1.26	1.26
5	1	37.1110	-94.5225	27.5	0.5	0.5	28.5	0.32	0.30	0.62	2.22	4.32	2.22
5	2	37.1110	-94.5228	71.0	1.5	0.5	73.0	0.55	0.20	0.75	2.45	4.55	2.45
5	3	37.1111	-94.5231	27.5	2.5	2.0	32.0	2.00	0.00	2.00	4.00	5.00	4.00
5	4	37.1111	-94.5234	13.0	2.0	0.0	15.0	1.25	0.10	1.35	2.95	3.25	2.95
5	5	37.1110	-94.5237	27.5	1.0	0.0	28.5	0.25	0.05	0.30	1.45	2.45	1.45
5	6	37.1111	-94.5240	14.5	2.2	1.5	18.2	0.73	0.00	0.73	2.73	2.53	2.53
5	7	37.1113	-94.5242	16.5	0.5	1.0	18.0	1.50	0.00	1.50	3.50	3.00	3.00

Appendix A Continued.

Site	Transect	Coordinates (DD)		Width (m)			Max Depth (m)				Bank Height (m)		
		Latitude	Longitude	Active	Left offset	Right offset	Bankfull	Water	Probe	Bedrock	Left	Right	Bankfull (min)
6	1	37.1142	-94.5453	12.0	4.0	5.0	21.0	0.40	0.30	0.70	2.60	2.40	2.40
6	2	37.1142	-94.5455	9.0	2.0	2.0	13.0	0.85	0.05	0.90	1.95	2.65	1.95
6	3	37.1142	-94.5457	14.0	2.0	3.0	19.0	0.45	0.00	0.45	1.85	1.85	1.85
6	4	37.1143	-94.5459	13.5	3.0	3.0	19.5	0.45	0.00	0.45	2.85	2.15	2.15
6	5	37.1143	-94.5461	18.0	5.0	2.0	25.0	0.20	0.00	0.20	2.40	2.50	2.40
6	6	37.1144	-94.5463	14.0	6.0	3.0	23.0	0.45	0.00	0.45	2.75	2.65	2.65
6	7	37.1144	-94.5465	12.0	3.0	6.0	21.0	0.51	0.05	0.56	2.31	2.81	2.31
7	1	37.1185	-94.5578	27.0	4.0	2.0	33.0	0.26	0.60	0.86	2.46	2.46	2.46
7	2	37.1185	-94.5583	42.0	0.5	0.5	43.0	1.10	0.10	1.20	3.50	2.50	2.50
7	3	37.1187	-94.5588	42.5	1.0	0.0	43.5	0.80	0.40	1.20	2.90	3.10	2.90
7	4	37.1193	-94.5591	43.5	1.0	0.5	45.0	0.84	0.20	1.04	2.84	3.14	2.84
7	5	37.1196	-94.5595	52.0	0.0	1.5	53.5	1.40	0.00	1.40	3.70	3.70	3.70
7	6	37.1196	-94.5602	33.5	1.0	2.0	36.5	0.44	0.20	0.64	3.14	2.84	2.84
7	7	37.1195	-94.5610	40.0	3.0	0.5	43.5	0.38	0.60	0.98	3.58	3.28	3.28
8	1	37.1198	-94.5644	21.0	0.0	1.0	22.0	0.92	0.27	1.19	2.22	2.72	2.22
8	2	37.1194	-94.5646	34.5	0.0	0.0	34.5	1.10	0.00	1.10	3.10	2.80	2.80
8	3	37.1192	-94.5649	33.5	1.5	1.0	36.0	0.43	0.20	0.63	2.73	1.63	1.63
8	4	37.1192	-94.5654	30.0	1.0	2.0	33.0	0.40	0.50	0.90	2.60	2.60	2.60
8	5	37.1192	-94.5658	31.5	1.5	2.0	35.0	0.70	0.40	1.10	2.40	3.00	2.40

Appendix A Continued.

Site	Transect	Coordinates (DD)		Width (m)			Max Depth (m)				Bank Height (m)		
		Latitude	Longitude	Active	Left offset	Right offset	Bankfull	Water	Probe	Bedrock	Left	Right	Bankfull (min)
8	6	37.1191	-94.5662	13.5	0.0	2.0	15.5	1.10	0.00	1.10	2.30	3.40	2.30
8	7	37.1189	-94.5665	24.5	1.0	1.0	26.5	1.40	0.00	1.40	3.00	4.40	3.00
9	1	37.1201	-94.5774	26.5	2.3	1.2	30.0	0.65	0.00	0.65	2.75	3.45	2.75
9	2	37.1204	-94.5777	28.0	1.5	1.2	30.7	0.30	0.65	0.95	2.00	3.00	2.00
9	3	37.1205	-94.5780	38.0	1.0	0.0	39.0	1.30	0.20	1.50	2.70	4.00	2.70
9	4	37.1204	-94.5785	26.0	1.3	2.0	29.3	0.93	0.00	0.93	2.13	2.93	2.13
9	5	37.1203	-94.5788	27.0	0.0	2.5	29.5	0.60	0.10	0.70	3.00	2.00	2.00
9	6	37.1202	-94.5792	33.0	0.0	0.0	33.0	0.50	0.10	0.60	2.80	2.00	2.00
9	7	37.1202	-94.5795	37.5	0.0	1.0	38.5	0.55	0.40	0.95	2.95	1.95	1.95
10	1	37.1270	-94.6095	21.0	3.0	1.5	25.5	0.20	0.40	0.60	2.70	2.70	2.70
10	2	37.1273	-94.6097	15.0	2.0	2.0	19.0	0.75	0.20	0.95	2.45	3.75	2.45
10	3	37.1275	-94.6100	22.0	1.0	2.0	25.0	0.73	0.90	1.63	2.63	3.93	2.63
10	4	37.1275	-94.6105	51.0	1.0	4.0	56.0	0.60	0.00	0.60	2.90	2.70	2.70
10	5	37.1270	-94.6107	51.0	2.0	1.5	54.5	0.86	0.00	0.86	3.26	3.36	3.26
10	6	37.1270	-94.6112	29.0	2.0	1.5	32.5	0.75	0.00	0.75	3.35	3.15	3.15
10	7	37.1269	-94.6115	23.0	1.5	3.0	27.5	0.55	0.00	0.55	2.95	2.55	2.55
11	1	37.1284	-94.6253	25.0	2.0	2.0	29.0	0.38	0.90	1.28	2.48	3.18	2.48
11	2	37.1286	-94.6258	26.0	1.5	1.5	29.0	0.73	0.80	1.53	3.73	3.83	3.73
11	3	37.1290	-94.6259	21.0	0.5	1.0	22.5	0.20	1.10	1.30	3.00	2.40	2.40

Appendix A Continued.

Site	Transect	Coordinates (DD)		Width (m)				Max Depth (m)			Bank Height (m)		
		Latitude	Longitude	Active	Left offset	Right offset	Bankfull	Water	Probe	Bedrock	Left	Right	Bankfull (min)
11	4	37.1293	-94.6260	45.0	1.0	1.0	47.0	0.25	1.20	1.45	2.85	2.75	2.75
11	5	37.1296	-94.6262	22.0	2.0	1.5	25.5	0.43	0.50	0.93	2.83	3.83	2.83
11	6	37.1298	-94.6266	23.0	3.0	1.5	27.5	0.90	0.70	1.60	3.40	4.30	3.40
T1	1	37.1104	-94.4726	11.0	1.0	1.0	13.0	0.00	0.00	0.00	2.00	2.00	2.00
T1	2	37.1104	-94.4728	8.0	1.0	0.5	9.5	0.00	0.30	0.30	1.70	1.00	1.00
T1	3	37.1105	-94.4730	6.5	1.0	2.0	9.5	0.00	0.35	0.35	1.50	1.10	1.10
T1	4	37.1105	-94.4732	9.3	2.0	0.5	11.8	0.00	-0.05	-0.05	1.00	0.90	0.90
T1	5	37.1106	-94.4734	13.8	0.5	2.0	16.3	0.00	0.15	0.15	2.00	0.50	0.50
T1	6	37.1106	-94.4735	11.6	1.0	0.0	12.6	0.00	0.00	0.00	1.70	3.20	1.70
T1	7	37.1105	-94.4737	9.0	0.5	0.0	9.5	0.00	0.00	0.00	1.30	3.20	1.30
T2	1	37.0714	-94.4855	2.5	2.0	2.5	7.0	0.00	0.00	0.00	1.10	1.40	1.10
T2	2	37.0714	-94.4856	2.5	2.0	2.5	7.0	0.00	0.00	0.00	1.10	1.40	1.10
T2	3	37.0715	-94.4856	2.5	2.0	2.5	7.0	0.00	0.00	0.00	1.10	1.40	1.10
T2	4	37.0715	-94.4857	2.5	2.0	2.5	7.0	0.00	0.00	0.00	1.10	1.40	1.10
T2	5	37.0715	-94.4857	2.5	2.0	2.5	7.0	0.00	0.00	0.00	1.10	1.40	1.10
T2	6	37.0716	-94.4857	2.5	2.0	2.5	7.0	0.00	0.00	0.00	1.10	1.40	1.10
T2	7	37.0716	-94.4858	2.5	2.0	2.5	7.0	0.00	0.00	0.00	1.10	1.40	1.10
T3	1	37.1081	-94.5421	6.0	1.5	0.0	7.5	0.28	0.00	0.28	1.98	1.78	1.78
T3	2	37.1082	-94.5421	6.0	1.0	0.0	7.0	0.15	0.10	0.25	1.75	1.65	1.65

Appendix A Continued.

Site	Transect	Coordinates (DD)		Width (m)			Max Depth (m)				Bank Height (m)		
		Latitude	Longitude	Active	Left offset	Right offset	Bankfull	Water	Probe	Bedrock	Left	Right	Bankfull (min)
T3	3	37.1083	-94.5421	4.0	1.0	1.0	6.0	0.13	0.00	0.13	1.83	1.73	1.73
T3	4	37.1084	-94.5421	5.0	0.8	0.5	6.3	0.20	0.10	0.30	2.00	2.00	2.00
T3	5	37.1085	-94.5421	4.7	0.8	1.0	6.5	0.20	0.38	0.58	2.00	1.90	1.90
T3	6	37.1085	-94.5421	3.5	1.2	1.0	5.7	0.10	0.28	0.38	1.80	2.10	1.80
T3	7	37.1086	-94.5422	3.7	1.7	0.8	6.2	0.12	0.25	0.37	1.62	1.62	1.62

Appendix B. Geometry for Bed and Bar Deposits at Each Site and Transect.

Site	Transect	Bed Deposit						Bar Deposit					
		Width (m)	Depth (m)	Thick (m)	Area (m^2)	Void	Area-act (m^2)	Width (m)	Ht ab WS (m)	Thick (m)	Area (m^2)	Void	Area-act (m^2)
1	1	13.5	0.57	0.30	4.00	0.00	4.0	0.0	0.00	0.00	0.00	0.00	0.00
1	2	13.0	0.58	0.29	3.74	0.00	3.7	0.0	0.00	0.00	0.00	0.00	0.00
1	3	12.0	0.47	0.19	2.26	0.00	2.3	0.0	0.00	0.00	0.00	0.00	0.00
1	4	12.5	0.26	0.30	3.80	0.00	3.8	2.0	0.05	0.61	1.22	0.00	3.12
1	5	6.5	0.23	0.22	1.46	0.00	1.5	9.0	0.30	0.75	6.75	0.00	8.88
1	6	14.0	0.35	0.55	7.70	0.00	7.7	0.0	0.00	0.00	0.00	0.00	0.00
1	7	11.0	0.10	0.48	5.28	0.00	5.3	3.2	0.10	0.68	2.18	0.00	2.18
2	1	10.5	0.27	0.32	3.32	0.00	3.32	0.0	0.00	0.00	0.00	0.00	0.00
2	2	8.0	0.55	0.60	4.80	0.00	4.80	3.5	0.20	1.35	4.73	0.00	4.73
2	3	8.0	0.40	0.50	4.00	0.00	4.00	8.0	0.50	1.40	11.20	0.00	11.20
2	4	5.0	0.10	0.15	0.75	0.00	0.75	16.0	0.20	0.45	7.20	0.25	5.40
2	5	6.0	0.17	0.18	1.10	0.25	0.82	3.0	0.35	0.70	2.10	0.00	2.10
2	6	11.5	0.33	0.57	6.51	0.00	6.51	0.0	0.00	0.00	0.00	0.00	0.00
2	7	11.0	0.21	0.79	8.69	0.00	8.69	0.0	0.00	0.00	0.00	0.00	0.00
3	1	12.0	0.14	0.41	4.92	0.00	4.92	3.0	0.05	0.60	1.80	0.00	2.55
3	2	10.5	0.35	0.00	0.00	1.00	0.00	7.5	0.40	0.75	5.63	0.15	4.78
3	3	13.0	0.95	0.35	4.55	1.00	0.00	0.0	0.00	0.00	0.00	0.00	0.00
3	4	14.0	0.30	0.02	0.28	0.00	0.28	0.0	0.00	0.00	0.00	0.00	0.00

Appendix B Continued.

Site	Transect	Bed Deposit						Bar Deposit					
		Width (m)	Depth (m)	Thick (m)	Area (m^2)	Void	Area-act (m^2)	Width (m)	Ht ab WS (m)	Thick (m)	Area (m^2)	Void	Area-act (m^2)
3	5	7.0	0.20	0.00	0.00	1.00	0.00	6.0	0.20	0.40	2.40	0.30	1.68
3	6	14.0	0.15	0.02	0.28	0.00	0.28	0.0	0.00	0.00	0.00	0.00	0.00
3	7	12.0	0.10	0.35	4.20	0.00	4.20	3.0	0.30	0.75	2.25	0.00	2.25
4	1	8.4	0.28	0.20	1.70	0.00	1.70	0.0	0.00	0.00	0.00	0.00	0.00
4	2	4.0	0.20	0.15	0.62	0.10	0.55	5.0	0.10	0.45	2.25	0.00	2.25
4	3	5.5	0.45	0.30	1.66	0.25	1.25	3.5	0.20	0.95	3.33	0.00	3.33
4	4	10.5	0.15	0.30	3.13	0.00	3.13	1.0	0.10	0.55	0.55	0.00	0.55
4	5	5.0	0.18	0.25	1.27	0.00	1.27	4.0	0.20	0.63	2.52	0.00	2.52
4	6	7.5	0.12	0.48	3.57	0.00	3.57	4.0	0.20	0.80	3.20	0.00	3.20
4	7	9.0	0.36	0.20	1.76	0.00	1.76	0.0	0.00	0.00	0.00	0.00	0.00
5	1	10.5	0.17	0.45	4.68	0.00	4.68	17.0	0.71	1.33	22.54	0.00	22.54
5	2	11.0	0.31	0.44	4.84	0.00	4.84	60.0	0.90	1.65	99.00	0.00	99.00
5	3	7.5	1.00	1.00	7.50	0.30	5.25	20.0	0.60	2.60	52.00	0.30	36.40
5	4	13.0	0.86	0.49	6.42	0.00	6.42	0.0	0.00	0.00	0.00	0.00	0.00
5	5	9.5	0.19	0.14	1.36	0.00	1.36	18.0	0.26	0.56	10.05	0.00	10.05
5	6	10.5	0.43	0.30	3.19	0.50	1.60	4.0	0.40	1.13	4.52	0.50	2.26
5	7	10.5	0.10	1.40	14.70	0.00	14.70	6.0	0.20	1.70	10.20	0.00	10.20
6	1	7.5	0.21	0.49	3.71	0.50	1.85	2.5	-0.10	0.60	1.50	0.00	3.80

Appendix B Continued.

Site	Transect	Bed Deposit						Bar Deposit					
		Width (m)	Depth (m)	Thick (m)	Area (m^2)	Void	Area-act (m^2)	Width (m)	Ht ab WS (m)	Thick (m)	Area (m^2)	Void	Area-act (m^2)
6	2	9.0	0.68	0.22	2.00	0.00	2.00	0.0	0.00	0.00	0.00	0.00	0.00
6	3	14.0	0.30	0.15	2.10	0.00	2.10	0.0	0.00	0.00	0.00	0.00	0.00
6	4	9.0	0.15	0.30	2.74	0.00	2.74	3.0	-0.10	0.35	1.05	0.50	1.65
6	5	14.5	0.11	0.09	1.36	1.00	0.00	0.0	0.00	0.00	0.00	0.00	1.75
6	6	12.0	0.31	0.14	1.68	0.00	1.68	0.0	0.00	0.00	0.00	0.00	0.70
6	7	12.0	0.32	0.24	2.90	0.00	2.90	0.0	0.00	0.00	0.00	0.00	0.00
7	1	8.0	0.17	0.69	5.52	0.00	5.52	9.0	0.30	1.16	10.44	0.00	10.44
7	2	11.0	0.56	0.64	7.04	0.18	5.76	15.0	1.00	2.20	64.00	0.00	64.00
7	3	8.0	0.55	0.65	5.20	0.10	4.68	26.0	0.50	1.70	60.20	0.00	60.20
7	4	9.0	0.55	0.49	4.43	0.00	4.43	24.0	0.43	1.47	49.98	0.00	49.98
7	5	11.0	0.60	0.80	8.80	0.00	8.80	30.0	0.84	2.24	89.10	0.00	89.10
7	6	4.5	0.31	0.33	1.49	0.00	1.49	23.0	0.30	0.94	23.51	0.00	23.51
7	7	9.0	0.26	0.72	6.52	0.00	6.52	27.0	0.77	1.75	51.88	0.00	51.88
8	1	9.0	0.53	0.66	5.94	0.00	5.94	12.0	0.30	1.49	17.88	0.00	17.88
8	2	6.5	0.00	0.00	0.00	1.00	0.00	28.0	1.00	2.10	58.70	0.00	58.70
8	3	13.5	0.20	0.43	5.75	0.00	5.75	20.0	0.61	1.24	24.80	0.00	24.80
8	4	21.0	0.22	0.68	14.32	0.00	14.32	9.0	1.20	2.10	18.90	0.00	18.90
8	5	4.5	0.49	0.61	2.75	0.00	2.75	17.0	0.30	1.40	35.80	0.00	35.80

Appendix B Continued.

Site	Transect	Bed Deposit						Bar Deposit					
		Width (m)	Depth (m)	Thick (m)	Area (m^2)	Void	Area-act (m^2)	Width (m)	Ht ab WS (m)	Thick (m)	Area (m^2)	Void	Area-act (m^2)
8	6	11.0	0.51	0.59	6.53	0.18	5.35	2.5	0.15	1.25	3.13	0.00	3.13
8	7	10.0	0.57	0.83	8.30	0.20	6.64	7.0	0.10	1.50	18.75	0.00	18.75
9	1	8.5	0.51	0.14	1.2	0.00	1.19	1.8	0.40	1.05	1.89	0.00	1.89
9	2	6.0	0.18	0.77	4.6	0.00	4.63	17.0	0.46	1.41	25.80	0.00	25.80
9	3	8.0	0.80	0.70	5.6	0.00	5.60	30.0	0.74	2.24	67.20	0.00	67.20
9	4	12.0	0.27	0.66	7.9	0.00	7.94	14.0	0.35	1.28	17.92	0.00	17.92
9	5	6.0	0.35	0.35	2.1	0.00	2.08	12.0	0.40	1.10	13.20	0.00	13.20
9	6	6.0	0.31	0.29	1.8	0.00	1.76	18.0	0.58	1.18	21.20	0.00	21.20
9	7	11.0	0.24	0.48	5.3	0.00	5.31	26.5	0.47	1.42	37.725	0.00	37.73
10	1	9.0	0.13	0.47	4.23	0.00	4.23	12.0	0.15	0.75	9.00	0.00	9.00
10	2	9.0	0.30	0.65	5.85	0.00	5.85	6.0	0.25	1.20	7.20	0.00	7.20
10	3	11.0	0.30	1.33	14.63	0.00	14.63	11.0	0.40	2.03	22.33	0.00	22.33
10	4	9.0	0.45	0.15	1.35	0.00	1.35	27.0	1.80	2.40	90.30	0.00	90.30
10	5	16.0	0.75	0.11	1.76	0.00	1.76	27.0	1.90	2.76	84.20	0.00	84.20
10	6	18.0	0.60	0.15	2.70	1.00	0.00	11.0	0.50	1.25	13.75	0.00	13.75
10	7	17.0	0.45	0.10	1.70	1.00	0.00	6.0	0.30	0.85	5.10	0.00	5.10
11	1	13.0	0.14	1.14	14.77	0.00	14.77	12.0	0.40	1.68	20.16	0.00	20.16
11	2	6.0	0.46	1.07	6.42	0.33	4.28	20.0	0.35	1.88	37.60	0.00	37.60

Appendix B Continued.

Site	Transect	Bed Deposit						Bar Deposit					
		Width (m)	Depth (m)	Thick (m)	Area (m^2)	Void	Area-act (m^2)	Width (m)	Ht ab WS (m)	Thick (m)	Area (m^2)	Void	Area-act (m^2)
11	3	15.0	0.12	1.18	17.70	0.00	17.70	6.0	0.20	1.50	9.00	0.00	9.00
11	4	14.0	0.15	1.30	18.26	0.00	18.26	6.5	0.22	1.67	10.88	0.00	10.88
11	5	12.0	0.19	0.74	8.93	0.00	8.93	10.0	0.20	1.13	11.30	0.00	11.30
11	6	11.0	0.62	0.98	10.78	0.00	10.78	12.0	0.35	1.95	23.40	0.00	23.40
T1	1	2.5	0.05	0.05	0.13	0.00	0.13	8.5	0.68	0.68	5.80	0.00	5.80
T1	2	3.0	0.15	0.45	1.35	0.00	1.35	5.0	0.40	0.70	3.50	0.00	3.50
T1	3	6.5	0.25	0.60	3.90	0.00	3.90	0.0	0.00	0.00	0.00	0.00	0.00
T1	4	5.8	0.10	0.05	0.29	0.30	0.20	3.5	0.30	0.25	0.88	0.20	0.70
T1	5	6.0	0.20	0.35	2.10	0.50	1.05	6.0	0.40	0.55	4.20	0.25	3.15
T1	6	2.3	0.00	0.00	0.00	1.00	0.00	7.5	0.91	0.91	9.55	0.00	9.55
T1	7	3.0	0.00	0.00	0.00	0.00	0.00	6.0	1.03	1.03	6.15	0.00	6.15
T2	1	1.5	0.00	0.00	0.00	1.00	0.00	0.0	0.00	0.00	0.00	0.00	0.00
T2	2	2.1	0.00	0.00	0.00	1.00	0.00	0.0	0.00	0.00	0.00	0.00	0.00
T2	3	1.8	0.00	0.00	0.00	1.00	0.00	0.0	0.00	0.00	0.00	0.00	0.00
T2	4	1.2	0.00	0.00	0.00	1.00	0.00	0.0	0.00	0.00	0.00	0.00	0.00
T2	5	2.5	0.00	0.00	0.00	1.00	0.00	0.0	0.00	0.00	0.00	0.00	0.00
T2	6	2.5	0.00	0.00	0.00	1.00	0.00	0.0	0.00	0.00	0.00	0.00	0.00
T2	7	1.9	0.00	0.00	0.00	1.00	0.00	0.0	0.00	0.00	0.00	0.00	0.00

Appendix B Continued.

Site	Transect	Bed Deposit						Bar Deposit					
		Width (m)	Depth (m)	Thick (m)	Area (m^2)	Void	Area-act (m^2)	Width (m)	Ht ab WS (m)	Thick (m)	Area (m^2)	Void	Area-act (m^2)
T3	1	2.8	0.19	0.09	0.26	0.33	0.17	3.2	0.25	0.53	1.70	0.33	1.13
T3	2	2.6	0.10	0.15	0.39	0.33	0.26	3.4	0.24	0.49	1.67	0.33	1.11
T3	3	2.4	0.05	0.08	0.19	0.30	0.13	1.6	0.15	0.28	0.45	0.50	0.22
T3	4	2.8	0.13	0.17	0.48	0.40	0.29	2.2	0.15	0.45	0.99	0.40	0.59
T3	5	3.7	0.12	0.46	1.70	0.00	1.70	1.0	0.05	0.63	0.63	0.00	0.63
T3	6	3.5	0.03	0.35	1.23	0.50	0.61	0.0	0.00	0.00	0.00	0.00	0.00
T3	7	2.0	0.05	0.32	0.64	0.00	0.64	1.7	0.10	0.47	0.80	0.00	0.80

Appendix C. Total Sediment Stored in Bench and Chute Sediment. Sites Not Listed Did Not Exhibit Bench or Chute Features. Only Upper Deposit Area is Considered Bench or Chute Sediment. Lower Deposit Area is Added to the Total Bar Area. "FP" Denotes Floodplain.

Site	Transect	Feature	Total Deposit						Upper Deposit			Lower Deposit (Bar)
			Width (m)	Ht ab WS (m)	Thick (m)	Area (m^2)	Void	Area-act (m^2)	Width (m)	Fine Depth (m)	Area (m^2)	Lower-Area (Bar) (m^2)
1	1	Bench	0.0	0.00	0.00	0.00	0.00	0.00	0.0	0.00	0.00	0.00
1	2	Bench	0.0	0.00	0.00	0.00	0.00	0.00	0.0	0.00	0.00	0.00
1	3	Bench	0.0	0.00	0.00	0.00	0.00	0.00	0.0	0.00	0.00	0.00
1	4	Bench	2.5	0.70	1.26	3.15	0.00	3.15	2.5	0.50	1.25	1.90
1	5	Bench	3.9	0.81	1.26	4.93	0.00	4.93	3.9	0.72	2.80	2.13
1	6	Bench	0.0	0.00	0.00	0.00	0.00	0.00	0.0	0.00	0.00	0.00
1	7	Bench	0.0	0.00	0.00	0.00	0.00	0.00	0.0	0.00	0.00	0.00
3	1	Bench	1.5	0.25	0.80	1.20	0.00	1.20	1.5	0.30	0.45	0.75
3	2	Bench	0.0	0.00	0.00	0.00	0.00	0.00	0.0	0.00	0.00	0.00
3	3	Bench	0.0	0.00	0.00	0.00	0.00	0.00	0.0	0.00	0.00	0.00
3	4	Bench	0.0	0.00	0.00	0.00	0.00	0.00	0.0	0.00	0.00	0.00
3	5	Bench	0.0	0.00	0.00	0.00	0.00	0.00	0.0	0.00	0.00	0.00
3	6	Bench	0.0	0.00	0.00	0.00	0.00	0.00	0.0	0.00	0.00	0.00
3	7	Bench	0.0	0.00	0.00	0.00	0.00	0.00	0.0	0.00	0.00	0.00
4	1	Bench	0.0	0.00	0.00	0.00	0.00	0.00	0.0	0.00	0.00	0.00
4	2	Bench	0.0	0.00	0.00	0.00	0.00	0.00	0.0	0.00	0.00	0.00

Appendix C Continued.

Site	Transect	Feature	Total Deposit						Upper Deposit			Lower Deposit (Bar)
			Width (m)	Ht ab WS (m)	Thick (m)	Area (m^2)	Void	Area-act (m^2)	Width (m)	Fine Depth (m)	Area (m^2)	Lower-Area (Bar) (m^2)
4	3	Bench	0.0	0.00	0.00	0.00	0.00	0.00	0.0	0.00	0.00	0.00
4	4	Bench	0.0	0.00	0.00	0.00	0.00	0.00	0.0	0.00	0.00	0.00
4	5	Bench	3.0	0.80	1.25	3.75	0.00	3.75	3.0	1.25	3.75	0.00
4	6	Bench	0.0	0.00	0.00	0.00	0.00	0.00	0.0	0.00	0.00	0.00
4	7	Bench	0.0	0.00	0.00	0.00	0.00	0.00	0.0	0.00	0.00	0.00
6	1	Bench	2.0	0.60	1.30	2.60	0.00	2.60	2.0	0.15	0.30	2.30
6	2	Bench	0.0	0.00	0.00	0.00	0.00	0.00	0.0	0.00	0.00	0.00
6	3	Bench	0.0	0.00	0.00	0.00	0.00	0.00	0.0	0.00	0.00	0.00
6	4	Bench	1.5	0.60	1.05	1.58	0.00	1.58	1.5	0.30	0.45	1.13
6	5	Bench	3.5	0.80	1.00	3.50	0.00	3.50	3.5	0.50	1.75	1.75
6	6	Bench	2.0	0.80	1.25	2.50	0.00	2.50	2.0	0.90	1.80	0.70
6	7	Bench	0.0	0.00	0.00	0.00	0.00	0.00	0.0	0.00	0.00	0.00
7	1	Bench	0.0	0.00	0.00	0.00	0.00	0.00	0.0	0.00	0.00	0.00
7	2	Bench	13.0	1.20	2.40	31.20	0.00	31.20	13.0	0.20	2.60	28.60
7	3	Bench	5.5	1.20	2.40	13.20	0.00	13.20	5.5	0.50	2.75	10.45
7	4	Bench	8.5	1.10	2.14	18.19	0.00	18.19	8.5	0.50	4.25	13.94
7	5	Bench	8.0	1.50	2.90	23.20	0.00	23.20	8.0	0.60	4.80	18.40

Appendix C Continued.

Site	Transect	Feature	Total Deposit						Upper Deposit			Lower Deposit (Bar)
			Width (m)	Ht ab WS (m)	Thick (m)	Area (m^2)	Void	Area-act (m^2)	Width (m)	Fine Depth (m)	Area (m^2)	Lower-Area (Bar) (m^2)
7	6	Bench	3.5	0.80	1.44	5.04	0.00	5.04	3.5	0.90	3.15	1.89
7	7	Bench	4.0	1.40	2.38	9.52	0.00	9.52	4.0	1.20	4.80	4.72
7	1	Chute	0.0	0.00	0.00	0.00	0.00	0.00	0.0	0.00	0.00	0.00
7	2	Chute	3.0	0.80	2.00	6.00	0.00	6.00	3.0	1.20	3.60	2.40
7	3	Chute	3.0	1.40	2.60	7.80	0.00	7.80	3.0	0.75	2.25	5.55
7	4	Chute	2.0	0.40	1.44	2.88	0.00	2.88	2.0	1.10	2.20	0.68
7	5	Chute	3.0	0.40	1.80	5.40	0.00	5.40	3.0	0.60	1.80	3.60
7	6	Chute	2.5	0.60	1.24	3.10	0.00	3.10	2.5	1.24	3.10	0.00
7	7	Chute	0.0	0.00	0.00	0.00	0.00	0.00	0.0	0.00	0.00	0.00
8	1	Bench	0.0	0.00	0.00	0.00	0.00	0.00	0.0	0.00	0.00	0.00
8	2	Bench	0.0	0.00	0.00	0.00	0.00	0.00	0.0	0.00	0.00	0.00
8	3	Bench	0.0	0.00	0.00	0.00	0.00	0.00	0.0	0.00	0.00	0.00
8	4	Bench	0.0	0.00	0.00	0.00	0.00	0.00	0.0	0.00	0.00	0.00
8	5	Bench	10.0	0.50	1.60	16.00	0.00	16.00	10.0	0.40	4.00	12.00
8	6	Bench	0.0	0.00	0.00	0.00	0.00	0.00	0.0	0.00	0.00	0.00
8	7	Bench	7.5	0.90	2.30	17.25	0.00	17.25	7.5	1.20	9.00	8.25
9	1	Chute	0.0	0.00	0.00	0.00	0.00	0.00	0.0	0.00	0.00	0.00

Appendix C Continued.

Site	Transect	Feature	Total Deposit						Upper Deposit			Lower Deposit (Bar)
			Width (m)	Ht ab WS (m)	Thick (m)	Area (m^2)	Void	Area-act (m^2)	Width (m)	Fine Depth (m)	Area (m^2)	Lower-Area (Bar) (m^2)
9	2	Chute	5.0	0.60	1.55	7.75	0.00	7.75	5.0	1.20	6.00	1.75
9	3	Chute	0.0	0.00	0.00	0.00	0.00	0.00	0.0	0.00	0.00	0.00
9	4	Chute	0.0	0.00	0.00	0.00	0.00	0.00	0.0	0.00	0.00	0.00
9	5	Chute	9.0	-0.25	0.45	4.05	0.00	4.05	9.0	0.45	4.05	0.00
9	6	Chute	9.0	0.20	0.80	7.20	0.00	7.20	9.0	0.80	7.20	0.00
9	7	Chute	0.0	0.00	0.00	0.00	0.00	0.00	0.0	0.00	0.00	0.00
10	1	Bench	0.0	0.00	0.00	0.00	0.00	0.00	0.0	0.00	0.00	0.00
10	2	Bench	0.0	0.00	0.00	0.00	0.00	0.00	0.0	0.00	0.00	0.00
10	3	Bench	0.0	0.00	0.00	0.00	0.00	0.00	0.0	0.00	0.00	0.00
10	4	Bench	15.0	1.40	2.00	30.00	0.00	30.00	15.0	0.30	4.50	25.50
10	5	Bench	0.0	0.00	0.00	0.00	0.00	0.00	0.0	0.00	0.00	0.00
10	6	Bench	0.0	0.00	0.00	0.00	0.00	0.00	0.0	0.00	0.00	0.00
10	7	Bench	0.0	0.00	0.00	0.00	0.00	0.00	0.0	0.00	0.00	0.00
10	1	Chute	0.0	0.00	0.00	0.00	0.00	0.00	0.0	0.00	0.00	0.00
10	2	Chute	0.0	0.00	0.00	0.00	0.00	0.00	0.0	0.00	0.00	0.00
10	3	Chute	0.0	0.00	0.00	0.00	0.00	0.00	0.0	0.00	0.00	0.00
10	4	Chute	0.0	0.00	0.00	0.00	0.00	0.00	0.0	0.00	0.00	0.00

Appendix C Continued.

Site	Transect	Feature	Total Deposit						Upper Deposit			Lower Deposit (Bar)
			Width (m)	Ht ab WS (m)	Thick (m)	Area (m^2)	Void	Area-act (m^2)	Width (m)	Fine Depth (m)	Area (m^2)	Lower-Area (Bar) (m^2)
10	5	Bench	0.0	0.00	0.00	0.00	0.00	0.00	0.0	0.00	0.00	0.00
10	6	Bench	0.0	0.00	0.00	0.00	0.00	0.00	0.0	0.00	0.00	0.00
10	7	Bench	0.0	0.00	0.00	0.00	0.00	0.00	0.0	0.00	0.00	0.00
10	1	Chute	0.0	0.00	0.00	0.00	0.00	0.00	0.0	0.00	0.00	0.00
10	2	Chute	0.0	0.00	0.00	0.00	0.00	0.00	0.0	0.00	0.00	0.00
10	3	Chute	0.0	0.00	0.00	0.00	0.00	0.00	0.0	0.00	0.00	0.00
10	4	Chute	0.0	0.00	0.00	0.00	0.00	0.00	0.0	0.00	0.00	0.00
10	5	Chute	8.0	1.45	2.31	18.48	0.00	18.48	8.0	1.10	8.80	9.68
10	6	Chute	0.0	0.00	0.00	0.00	0.00	0.00	0.0	0.00	0.00	0.00
10	7	Chute	0.0	0.00	0.00	0.00	0.00	0.00	0.0	0.00	0.00	0.00
11	1	Bench	0.0	0.00	0.00	0.00	0.00	0.00	0.0	0.00	0.00	0.00
11	2	Bench	0.0	0.00	0.00	0.00	0.00	0.00	0.0	0.00	0.00	0.00
11	3	Bench	0.0	0.00	0.00	0.00	0.00	0.00	0.0	0.00	0.00	0.00
11	4	Bench	2.0	0.40	1.85	3.70	0.00	3.70	2.0	1.85	3.70	0.00
11	5	Bench	0.0	0.00	0.00	0.00	0.00	0.00	0.0	0.00	0.00	0.00
11	6	Bench	0.0	0.00	0.00	0.00	0.00	0.00	0.0	0.00	0.00	0.00
T1	1	Bench	0.0	0.00	0.00	0.00	0.00	0.00	0.0	0.00	0.00	0.00

Appendix C Continued.

Site	Transect	Feature	Total Deposit						Upper Deposit			Lower Deposit (Bar)
			Width (m)	Ht ab WS (m)	Thick (m)	Area (m^2)	Void	Area-act (m^2)	Width (m)	Fine Depth (m)	Area (m^2)	Lower-Area (Bar) (m^2)
T1	2	Bench	0.0	0.00	0.00	0.00	0.00	0.00	0.0	0.00	0.00	0.00
T1	3	Bench	0.0	0.00	0.00	0.00	0.00	0.00	0.0	0.00	0.00	0.00
T1	4	Bench	0.0	0.00	0.00	0.00	0.00	0.00	0.0	0.00	0.00	0.00
T1	5	Bench	1.8	0.60	0.75	1.35	0.00	1.35	1.8	0.25	0.45	0.90
T1	6	Bench	1.8	1.60	1.60	2.88	0.00	2.88	1.8	0.10	0.18	2.70
T1	7	Bench	0.0	0.00	0.00	0.00	0.00	0.00	0.0	0.00	0.00	0.00
T2	1	Bench	1.0	0.25	0.25	0.25	0.00	0.25	1.0	0.25	0.25	0.00
T2	2	Bench	0.4	0.18	0.18	0.07	0.00	0.07	0.4	0.18	0.07	0.00
T2	3	Bench	0.7	0.26	0.26	0.18	0.00	0.18	0.7	0.26	0.18	0.00
T2	4	Bench	1.4	0.22	0.22	0.30	0.00	0.30	1.4	0.22	0.30	0.00
T2	5	Bench	0.0	0.00	0.00	0.00	0.00	0.00	0.0	0.00	0.00	0.00
T2	6	Bench	0.0	0.00	0.00	0.00	0.00	0.00	0.0	0.00	0.00	0.00
T2	7	Bench	0.6	0.22	0.22	0.13	0.00	0.13	0.6	0.22	0.13	0.00

Appendix D. The Description, Location, and Calibrated Elemental Concentration of Each Sample. "ND" Denotes Not Detected.

					Coordinates (DD)		Concentration (ppm)					
Sample	Site	Transect	Unit	Date	Lat	Long	Pb	Zn	Fe	Mn	Ca	Cd
1	4	TS6	Bed	7/14/20	37.10812	-94.50967	589	3,613	14,010	739	17,447	34
2	4	TS6	Bar	7/14/20	37.10812	-94.50967	284	2,013	15,298	753	17,650	4
3	4	TS5	Bench	7/14/20	37.10807	-94.50945	397	3,375	16,532	673	5,630	28
4	4	TS5	Bench	7/14/20	37.10807	-94.50945	385	3,520	17,506	954	26,336	40
5	4	TS5	Bar	7/14/20	37.10807	-94.50945	274	3,156	16,780	1,477	26,476	28
6	4	TS4	Bed	7/14/20	37.10804	-94.50922	227	3,077	19,398	967	10,685	41
7	4	TS2.5	Bar	7/14/20	37.10803	-94.50889	236	1,416	20,057	706	13,997	8
8	4	TS2	Bed	7/14/20	37.10806	-94.50878	184	1,385	16,934	1,127	20,064	5
9	T3	TS5	Bar	7/14/20	37.10844	-94.54205	353	4,787	13,365	463	114,956	42
10	T3	TS5	Bed	7/14/20	37.10843	-94.54207	211	4,146	5,513	841	115,129	32
11	T3	TS4	Bed	7/14/20	37.10831	-94.54206	139	3,219	4,003	465	144,477	38
12	T3	TS4	Bar	7/14/20	37.10831	-94.54204	545	9,496	18,739	1,518	104,486	77
13	T3	TS1	Bed	7/14/20	37.10797	-94.54208	427	5,445	20,693	1,672	63,789	16
14	T3	TS1	Bar	7/14/20	37.10798	-94.54204	606	13,202	17,535	1,504	83,342	62
15	9	TS1	Bar	7/15/20	37.12008	-94.57732	395	7,659	16,142	988	34,269	49
16	9	TS1	Bed	7/15/20	37.12007	-94.57742	384	3,845	22,880	760	35,176	48
17	9	TS4	Bar	7/15/20	37.12038	-94.57841	214	2,664	9,925	417	39,714	16
18	9	TS4	Bed	7/15/20	37.12042	-94.57845	651	7,025	20,688	1,223	33,549	55
19	9	TS6	Bar	7/15/20	37.12027	-94.57924	365	6,428	25,392	945	51,351	64

Appendix D Continued.

					Coordinates (DD)		Concentration (ppm)					
Sample	Site	Transect	Unit	Date	Lat	Long	Pb	Zn	Fe	Mn	Ca	Cd
20	9	TS6	Bar	7/15/20	37.12033	-94.57925	388	5,835	14,994	483	51,435	49
21	9	TS7	Bar	7/15/20	37.12030	-94.57950	370	6,012	13,350	639	58,526	40
22	9	TS7	Bed	7/15/20	37.12025	-94.57954	596	5,550	15,152	930	39,403	38
23	9	TS7	Bed	7/15/20	37.12033	-94.57948	356	3,240	18,602	2,186	21,280	18
24	5	TS2	Bar	7/15/20	37.11104	-94.52274	431	2,827	16,888	626	33,023	26
25	5	TS2	Bar	7/15/20	37.11089	-94.52277	719	4,568	23,572	656	48,285	22
26	5	TS2	Bed	7/15/20	37.11112	-94.52276	523	4,442	17,692	895	33,190	37
27	5	TS3	Bar	7/15/20	37.11106	-94.52306	676	6,744	22,345	904	35,955	37
28	5	TS4	Bed	7/15/20	37.11108	-94.52343	185	2,099	17,282	763	38,601	ND
29	5	TS7	Bed	7/15/20	37.11128	-94.52425	486	2,233	36,415	1,223	10,001	28
30	1	TS4	Bed	8/03/20	37.09027	-94.46148	110	1,649	40,960	968	7,136	13
31	1	TS5	Bar	8/03/20	37.09033	-94.46173	123	1,696	23,739	1,148	8,236	9
32	1	TS5	Bench	8/03/20	37.09037	-94.46172	130	1,382	24,480	1,068	2,548	6
33	1	TS5	Bench	8/03/20	37.09039	-94.46170	183	1,573	17,623	931	4,022	6
34	1	TS7	Bar	8/03/20	37.09047	-94.46234	219	1,128	19,089	421	2,462	ND
35	1	TS7	Bed	8/03/20	37.09045	-94.46235	325	2,259	25,875	1,351	5,635	10
36	1	TS4	Bench	8/03/20	37.09031	-94.46146	180	1,615	18,774	760	5,753	16
37	1	TS5.5	FP	8/03/20	37.09044	-94.46184	18	110	11,804	232	ND	0
38	1	TS5	FP	8/03/20	37.09026	-94.46169	444	3,433	15,483	555	1,828	36
39	1	TS5	FP	8/03/20	37.09026	-94.46169	691	4,931	18,148	133	129	53

Appendix D Continued.

					Coordinates (DD)		Concentration (ppm)					
Sample	Site	Transect	Unit	Date	Lat	Long	Pb	Zn	Fe	Mn	Ca	Cd
40	1	TS5	FP	8/03/20	37.09026	-94.46169	2,504	5,685	20,557	106	365	55
41	T1	TS4	Bar	8/03/20	37.11057	-94.47317	282	5,719	27,0414	8,978	843	47
42	T1	TS4	Bed	8/03/20	37.11052	-94.47319	58	3,111	55,831	2,332	3,349	36
43	T1	TS1	Bar	8/03/20	37.11038	-94.47263	261	4,461	128,085	4,392	11,795	54
44	T1	TS1	Bar	8/03/20	37.11042	-94.47263	294	6,123	178,220	6,887	1,136	50
45	T1	TS5	Bench	8/03/20	37.11060	-94.47338	225	4,019	27,126	1,715	6,474	43
46	T1	TS6	Bar	8/03/20	37.11052	-94.47353	288	5,927	118,189	10,790	4,811	68
47	T1	TS6	Bar	8/03/20	37.11050	-94.47353	227	4,061	112,266	6,466	3,549	54
48	T1	TS3	FP	8/03/20	37.11032	-94.47309	111	800	17,041	1,214	1,424	3
49	T1	TS1	FP	8/03/20	37.11027	-94.47263	37	236	13,636	607	266	ND
50	8	TS1	Bed	8/03/20	37.11975	-94.56441	306	1,742	17,315	792	22,834	ND
51	8	TS1	Bar	8/03/20	37.11976	-94.56454	438	7,329	30,097	1,154	56,704	29
52	8	TS4	Bar	8/03/20	37.11935	-94.56538	540	11,676	24,760	694	53,182	55
53	8	TS4	Bed	8/03/20	37.11924	-94.56538	304	5,545	22,858	905	59,314	30
54	8	TS3	FP	8/03/20	37.11926	-94.56477	1,791	12,822	24,792	652	27,910	106
55	8	TS3	FP	8/03/20	37.11926	-94.56477	3,620	7,888	21,319	603	3,823	84
56	8	TS3	FP	8/03/20	37.11927	-94.56477	7,618	5,088	21,504	341	2,738	46
57	8	TS4	FP	8/03/20	37.11915	-94.56551	2,054	14,442	19,122	538	67,826	167
58	8	TS7	Bench	8/03/20	37.11880	-94.56635	905	5,811	18,831	859	39,830	47
59	8	TS7	Bar	8/03/20	37.11885	-94.56643	290	4,648	15,422	656	55,439	26

Appendix D Continued.

					Coordinates (DD)		Concentration (ppm)					
Sample	Site	Transect	Unit	Date	Lat	Long	Pb	Zn	Fe	Mn	Ca	Cd
62	3	TS1	Bed	8/03/20	37.10088	-94.48582	114	2,226	32,226	1,844	58,350	5
63	3	TS2	Bar	8/03/20	37.10096	-94.48609	153	2,110	22,836	1,361	14,510	7
64	3	TS7.5	Bar	8/03/20	37.10170	-94.48719	146	2,117	21,095	1,035	13,593	4
65	3	TS7.5	Bar	8/03/20	37.10171	-94.48716	186	1,915	23,857	944	15,990	7
66	3	TS2.5	Bar	8/03/20	37.10106	-94.48624	106	1,437	24,899	787	23,390	11
101	6	TS7	Bed	8/04/20	37.11442	-94.54646	502	5,530	14,066	595	83,833	51
102	6	TS6	Bench	8/04/20	37.11441	-94.54629	1,128	6,042	18,243	1,403	30,385	58
103	6	TS4	Bench	8/04/20	37.11437	-94.54586	1,765	8,822	21,393	746	43,046	67
104	6	TS3	Bed	8/04/20	37.11425	-94.54568	271	2,157	18,608	621	94,341	25
105	7	TS7	Bench	8/04/20	37.11966	-94.56087	1,234	7,255	19,064	1,023	44,476	68
106	7	TS7	Bar	8/04/20	37.11956	-94.56094	270	2,760	11,112	912	42,072	15
107	7	TS7	Bar	8/04/20	37.11961	-94.56091	393	3,909	12,299	426	70,174	30
108	7	TS7	Bed	8/04/20	37.11949	-94.56098	374	8,503	24,420	855	74,210	73
110	7	TS4	Bed	8/04/20	37.11927	-94.55910	461	1,822	20,733	761	24,545	16
111	7	TS4	Chute	8/04/20	37.11911	-94.55939	882	7,686	15,842	714	47,936	51
112	7	TS4	Bench	8/04/20	37.11906	-94.55944	806	7,108	16,667	828	54,076	70
113	7	TS4	Bar	8/04/20	37.11915	-94.55933	571	4,459	21,382	813	40,326	47
114	7	TS4	Bar	8/04/20	37.11921	-94.55925	670	5,838	18,282	1,109	38,714	55
140	10	TS1	Bar	9/24/20	37.12696	-94.60951	387	8,045	20,113	1,224	39,269	39
141	10	TS2	Bar	9/24/20	37.12726	-94.60976	300	3,561	11,444	645	58,770	21

Appendix D Continued.

					Coordinates (DD)		Concentration (ppm)					
Sample	Site	Transect	Unit	Date	Lat	Long	Pb	Zn	Fe	Mn	Ca	Cd
142	10	TS6	Bed	9/24/20	37.12693	-94.61121	164	3,669	13,323	434	59,343	19
143	10	TS5	Chute	9/24/20	37.12711	-94.61080	290	7,938	10,110	543	64,310	33
144	10	TS4	Bar	9/24/20	37.12736	-94.61034	344	6,204	16,309	568	37,349	43
145	10	TS4	Bed	9/24/20	37.12748	-94.61047	378	6,563	15,068	722	36,642	40
146	10	TS4	Bench	9/24/20	37.12722	-94.61024	694	5,736	16,276	706	43,339	55
160	11	TS6	Bar	9/24/20	37.12995	-94.62656	395	4,359	12,546	606	57,273	39
162	11	TS2	Bed	9/24/20	37.12861	-94.62575	261	2,461	12,003	722	52,488	13
163	11	TS2	Bed	9/24/20	37.12862	-94.62573	210	2,827	7,786	934	6,124	17
164	11	TS1	Bed	9/24/20	37.12839	-94.62536	277	3,226	11,692	741	32,635	23
165	11	TS3	FP	9/24/20	37.12901	-94.62582	3,277	4,791	18,922	529	2,448	59
166	11	TS3	FP	9/24/20	37.12901	-94.62581	2,566	10,501	31,585	540	2,673	90
167	11	TS3	FP	9/24/20	37.12901	-94.62580	1,607	21,795	18,506	456	96,681	300
168	11	TS3	FP	9/24/20	37.12901	-94.62579	1,630	17,429	28,210	679	17,427	140
169	11	TS3	FP	9/24/20	37.12901	-94.62578	2,426	21,618	33,843	479	56,391	231
170	11	TS3	FP	9/24/20	37.12901	-94.62578	936	8,223	18,774	862	32,966	60
171	2	TS7	Bed	9/25/20	37.09496	-94.47171	181	3,710	27,377	275	16,678	13
172	2	TS4	Bar	9/25/20	37.09490	-94.47099	181	2,955	21,899	1,717	16,687	7
173	2	TS3	Bed	9/25/20	37.09499	-94.47088	174	2,378	18,814	1,523	57,500	17
174	2	TS3	Bar	9/25/20	37.09497	-94.47082	167	1,646	34,015	688	6,191	22
176	2	TS2	Bar	9/25/20	37.09499	-94.47057	139	1,209	18,086	625	10,539	2

Appendix D Continued.

					Coordinates (DD)		Concentration (ppm)					
Sample	Site	Transect	Unit	Date	Lat	Long	Pb	Zn	Fe	Mn	Ca	Cd
177	2	TS3	Bench	9/25/20	37.09495	-94.47079	67	1,837	12,084	562	2,619	28
178	2	TS2	Bench	9/25/20	37.09496	-94.47059	275	1,224	21,371	419	2,816	ND
303	9	TS6	FP	9/25/20	37.12067	-94.57795	1,409	12,362	23,266	679	25,458	98
306	7	TS4	FP	9/25/20	37.11931	-94.55903	1,413	13,942	18,937	468	54,999	110
308	7	TS4	FP	9/25/20	37.11931	-94.55903	1,101	17,235	19,468	662	30,721	104
309	4	T2	FP	9/25/20	37.10799	-94.50883	42	292	15,145	216	3,211	ND
310	9	TS6	FP	9/25/20	37.12006	-94.57923	90	4,161	14,698	760	5,074	51
311	4	T2	FP	9/25/20	37.10799	-94.50883	174	1,169	11,664	649	4,944	1
312	7	TS4	FP	9/25/20	37.11931	-94.55904	1,028	5,744	15,452	692	5,666	73
313	7	TS4	FP	9/25/20	37.11931	-94.55903	112	614	19,170	516	7,006	2
314	9	TS6	FP	9/25/20	37.12006	-94.57923	59	500	14,688	347	4,445	ND
317	B3	N/A	FP	9/25/20	37.01940	-94.38802	54	489	12,751	497	4,8117	ND
318	B3	N/A	FP	9/25/20	37.01947	-94.38799	53	312	10,491	696	6,934	ND
320	B2	N/A	FP	9/25/20	37.06850	-94.38971	73	162	25,715	1,118	1,586	ND
321	B2	N/A	FP	9/25/20	37.06854	-94.38958	40	245	15,934	752	3,796	ND
401	B2	N/A	Bed	9/25/20	37.06852	-94.38966	82	348	119,202	8,040	ND	ND
402	T2	TS1	Bench	9/25/20	37.07140	-94.48554	158	1,671	34,729	1,963	80,948	3
404	T2	TS2	Bench	9/25/20	37.07141	-94.48560	95	1,536	23,184	765	121,509	10
405	B1	N/A	Bar	9/25/20	37.06831	-94.37081	72	133	61,531	1,865	1,312	ND
407	B1	N/A	FP	9/25/20	37.06832	-94.37070	19	58	14,148	332	361	ND

Appendix D Continued.

					Coordinates (DD)		Concentration (ppm)					
Sample	Site	Transect	Unit	Date	Lat	Long	Pb	Zn	Fe	Mn	Ca	Cd
408	T2	TS3	Bench	9/25/20	37.07147	-94.48563	154	1,371	22,867	837	70,632	1
409	B1	N/A	Bed	9/25/20	37.06831	-94.37076	92	144	45,183	2,720	13,252	ND
410	T2	TS7	Bench	9/25/20	37.07158	-94.48579	115	12,124	37,524	765	138,715	35

Appendix E. Lead and Zinc Concentrations in the 8 – 16 mm Size Fraction from Five Bars in Turkey Creek (Ferguson, 2021). Samples Were Collected Below the Armor Layer at the Upstream (Head), Middle (Mid), and Downstream (Tail) Sections on Both the Right and Left Side of the Bar.

Sample ID	Site	Bar Unit	Pb (ppm)	Zn (ppm)
1HLB	4	Head	66	769
1HRB	4	Head	107	527
1MLB	4	Mid	33	600
1MRB	4	Mid	792	1,039
1TLB	4	Tail	47	367
1TRB	4	Tail	38	498
2HLB	9	Head	184	959
2HRB	9	Head	134	987
2MLB	9	Mid	199	665
2MRB	9	Mid	51	680
2TLB	9	Tail	94	906
2TRB	9	Tail	24	720
3HLB	5	Head	98	747
3HRB	5	Head	76	737
3MLB	5	Mid	37	398
3MRB	5	Mid	60	681
3TLB	5	Tail	79	292
3TRB	5	Tail	218	3,177
4HLB	7	Head	190	443

Appendix E Continued.

Sample ID	Site	Bar Unit	Pb (ppm)	Zn (ppm)
4HRB	7	Head	136	985
4MLB	7	Mid	159	30,577
4MRB	7	Mid	187	908
4TLB	7	Tail	214	980
4TRB	7	Tail	119	1,070
5HLB	11	Head	146	859
5HRB	11	Head	377	1,549
5MLB	11	Mid	63	829
5MRB	11	Mid	95	728
5TLB	11	Tail	68	872
5TRB	11	Tail	152	1,495

Appendix F. Total Longitudinal Mass Storage of Sediment for Coarse and Fine Size Fractions in Bed and Bar Deposits throughout Turkey Creek.

Site	Total Storage (Mg/m)	Bed Storage (Mg/m)						Bar Storage (Mg/m)					
		Total	<0.25mm	0.25 mm - 2 mm	2 - 8 mm	8 - 16 mm	> 16 mm	Total	<0.25 mm	0.25 mm - 2 mm	2 - 8 mm	8 - 16 mm	> 16 mm
1	14.3	8.8	0.1	0.4	2.6	2.9	2.8	4.4	0.1	0.4	1.8	1.0	1.2
2	15.9	8.8	0.1	1.6	2.8	2.1	2.3	7.1	0.2	1.6	1.7	1.4	2.3
3	6.4	3.0	0.0	0.2	1.1	1.1	0.5	3.4	0.1	0.5	1.1	0.8	0.9
4	8.9	4.1	0.0	0.2	1.0	0.9	2.0	3.7	0.1	0.2	0.8	0.8	1.8
5	66.9	11.9	0.2	1.9	0.7	5.1	4.0	55.1	1.3	9.1	16.4	11.1	17.2
6	5.2	4.1	0.0	0.6	1.3	1.3	0.8	0.0	0.0	0.0	0.0	0.0	0.0
7	128.1	11.3	0.0	2.1	4.0	2.1	3.1	107.1	3.2	13.4	36.2	21.2	33.1
8	70.3	12.4	0.1	2.2	5.0	2.7	2.4	54.3	0.6	9.4	18.2	9.9	16.2
9	70.1	8.9	0.1	0.3	1.9	2.4	4.2	56.6	1.2	8.7	14.0	16.1	16.6
10	84.0	8.5	0.2	1.1	4.2	1.2	1.7	71.5	0.7	7.8	25.6	19.8	17.6
11	67.2	27.1	0.1	2.0	7.5	5.9	11.6	40.2	1.0	5.5	15.8	11.5	6.3
T1	10.9	1.9	0.2	1.0	0.6	0.1	0.1	8.8	0.0	1.7	3.6	2.0	1.5
T2	0.3	0.0	0.0	0.0	0.0	0.0	0.0	0.0	0.0	0.0	0.0	0.0	0.0
T3	2.5	1.2	0.0	0.2	0.6	0.2	0.1	1.3	0.1	0.4	0.5	0.2	0.2

Appendix G. Total Longitudinal Mass Storage of Sediment for Various Size Fractions in Bench and Chute Deposits throughout Turkey Creek. The Chute at Site 9 Was Excluded Since It Was Not Sampled.

Site	Bench Storage (Mg/m)				Chute Storage (Mg/m)			
	Total	< 2 mm	2-16 mm	> 16 mm	Total	< 2 mm	2-16 mm	> 16 mm
1	1.2	0.7	0.4	0.1	0.0	0.0	0.0	0.0
2	0.0	0.0	0.0	0.0	0.0	0.0	0.0	0.0
3	0.0	0.0	0.0	0.0	0.0	0.0	0.0	0.0
4	1.1	0.4	0.4	0.3	0.0	0.0	0.0	0.0
5	0.0	0.0	0.0	0.0	0.0	0.0	0.0	0.0
6	1.2	1.2	0.0	0.0	0.0	0.0	0.0	0.0
7	6.1	5.8	0.4	0.0	3.5	3.5	0.0	0.0
8	3.5	3.5	0.0	0.0	0.0	0.0	0.0	0.0
9	0.0	0.0	0.0	0.0	4.7	N/A	N/A	N/A
10	1.2	1.2	0.0	0.0	2.7	0.6	1.6	0.4
11	0.0	0.0	0.0	0.0	0.0	0.0	0.0	0.0
T1	0.2	0.2	0.0	0.0	0.0	0.0	0.0	0.0
T2	0.3	0.2	0.1	0.0	0.0	0.0	0.0	0.0
T3	0.0	0.0	0.0	0.0	0.0	0.0	0.0	0.0